



**US Army Corps
of Engineers®**
Engineer Research and
Development Center

ERDC
INNOVATIVE SOLUTIONS
for a safer, better world

Performance of Geogrid-Stabilized Flexible Pavements

Gregory J. Norwood and Jeb S. Tingle

July 2014



The US Army Engineer Research and Development Center (ERDC) solves the nation's toughest engineering and environmental challenges. ERDC develops innovative solutions in civil and military engineering, geospatial sciences, water resources, and environmental sciences for the Army, the Department of Defense, civilian agencies, and our nation's public good. Find out more at www.erdcd.usace.army.mil.

To search for other technical reports published by ERDC, visit the ERDC online library at <http://acwc.sdp.sirsi.net/client/default>.

Performance of Geogrid-Stabilized Flexible Pavements

Gregory J. Norwood and Jeb S. Tingle

*Geotechnical and Structures Laboratory
US Army Engineer Research and Development Center
3909 Halls Ferry Road
Vicksburg, MS 39180-6199*

Final report

Approved for public release; distribution is unlimited.

Prepared for Tensar International Corporation
Alpharetta, GA

Abstract

The US Army Engineer Research and Development Center (ERDC) constructed a full-scale test section to evaluate the performance of geogrid-stabilized thin highway pavements. The test section included two representative highway pavements composed of hot-mix asphalt concrete (HMA) over a base course of crushed limestone and a 6 CBR clay subgrade. One highway lane was surfaced with 3-in. HMA and a 6-in. crushed limestone base course stabilized with geogrid. The second highway lane was surfaced with 4 in. of HMA and an unstabilized, 8-in. crushed limestone base course. Each test lane contained a suite of instrumentation consisting of strain gauges, earth pressure cells, moisture probes, pore water pressure transducers, and temperature probes. The geogrid was also instrumented with strain gauges in an attempt to determine the strain on the geogrid during testing. Each test lane was trafficked with simulated truck traffic to evaluate the rutting performance of the different pavement sections. This report summarizes the material characterization, pavement construction, instrumentation response, and performance response of the two test items.

DISCLAIMER: The contents of this report are not to be used for advertising, publication, or promotional purposes. Citation of trade names does not constitute an official endorsement or approval of the use of such commercial products. All product names and trademarks cited are the property of their respective owners. The findings of this report are not to be construed as an official Department of the Army position unless so designated by other authorized documents.

DESTROY THIS REPORT WHEN NO LONGER NEEDED. DO NOT RETURN IT TO THE ORIGINATOR.

Contents

Abstract	ii
Figures and Tables	v
Preface	vii
Unit Conversion Factors	viii
1 Introduction	1
1.1 Background.....	1
1.2 Objective	1
1.3 Scope	1
2 Test Plan and Layout	3
3 Materials	5
3.1 Subgrade.....	5
3.2 Base course	5
3.3 Asphalt	8
4 Instrumentation	11
4.1 Earth Pressure Cells	11
4.2 Asphalt strain gauges.....	12
4.3 Geogrid strain gauges	13
4.4 Single-depth deflectometers.....	16
5 Pavement Characterization	17
5.1 As-built properties	17
5.2 Dynamic cone penetrometer.....	18
5.3 Falling weight deflectometer	18
6 Traffic Testing	22
7 Results	24
7.1 Surface deformations.....	24
7.2 Falling weight deflectometer.....	27
7.3 Earth pressure cells	28
7.4 Single-depth deflectometers.....	31
7.5 Geogrid strain gauges	34
7.6 Asphalt strain gauges.....	35
8 Post-test Forensics	40
9 Conclusions and Recommendations	44

References	46
Appendix A: Earth Pressure Cell Responses	47
Appendix B: Single-Depth Deflectometer Responses	61
Appendix C: Geogrid Strain Response	75
Appendix D: Asphalt Strain Response	82
Report Documentation Page	

Figures and Tables

Figures

Figure 1. Test-section profile view.	3
Figure 2. Test-section material gradations.	6
Figure 3. Subgrade compaction before final grading.....	6
Figure 4. Crushed limestone base-course material being placed.....	7
Figure 5. Base-course compaction.	7
Figure 6. Test section during application of first HMA layer.	10
Figure 7. Instrumentation layout for typical test item.	11
Figure 8. Installation of an earth pressure cell.	12
Figure 9. Installation of asphalt strain gauge.....	13
Figure 10. Geogrid strain gauges.....	14
Figure 11. Strain gauges installed on the geogrid.....	14
Figure 12. Location of strain gauges on geogrid.	15
Figure 13. Installation of geogrid strain gauges in the test section.	15
Figure 14. Installed SDD.	16
Figure 15. Historical moisture content/strength relationship for Vicksburg Buckshot Clay.	18
Figure 16. As-built DCP results for Item 1 station 37.5.	19
Figure 17. As-built DCP results for Item 2 station 25.	20
Figure 18. FWD testing inside HVS.	21
Figure 19. As-built ISM values for Items 1 and 2.....	21
Figure 20. Verifying the applied load on the HVS dual-wheel tandem axle configuration.	22
Figure 21. Traffic pattern applied during trafficking.....	23
Figure 22. Measurement of rut depth.....	24
Figure 23. Average maximum rut depth.	25
Figure 24. Item 2 temperature change during HVS malfunction.	26
Figure 25. Permanent surface deformation.....	26
Figure 26. ISM changes during trafficking.	28
Figure 27. EPC response during 10 min of trafficking after 13,000 passes.	30
Figure 28. Change in EPC reading for base course during trafficking.....	31
Figure 29. Change in EPC readings for subgrade during trafficking.....	32
Figure 30. SDD peak values for 10-min test after 832 ESALs (416 passes).	33
Figure 31. SDD peak value changes during trafficking.	34
Figure 32. Geogrid strain values for 10-min test after 104,000 ESALs (52,000 passes).....	36
Figure 33. Geogrid strain gauge peak changes during trafficking.....	37
Figure 34. Asphalt strain gauge values for 10-min test after 26,000ESALs (13,000 passes).	38

Figure 35. ASG peak tensile strain value changes during trafficking.....	39
Figure 36. Item 1 excavated trench.....	41
Figure 37. Item 1 post-traffic layer thicknesses.	41
Figure 38. Excavated geogrid in Item 2.....	42
Figure 39. Item 2 excavated trench.....	42
Figure 40. Item 2 post-traffic layer thicknesses.	43

Tables

Table 1. Test-section HMA properties.....	9
Table 2. Asphalt Institute recommended values.	9
Table 3. As-built test-section properties.	17
Table 4. Maximum rut depth measurements.....	27
Table 5. Permanent surface deformation measurements.....	27
Table 6. Installation depths of installed EPCs.	28
Table 7. Measured vs. predicted stresses.	32
Table 8. Post-test test-section properties.....	40

Preface

The work was performed by the Airfields and Pavements Branch (GM-A) of the Engineering Systems Division (GM), US Army Engineer Research and Development Center, Geotechnical and Structures Laboratory (ERDC-GSL). At the time of publication, Dr. Gary L. Anderton was Chief, CEERD-GM-A; Dr. Larry N. Lynch was Chief, CEERD-GM; and Dr. David A. Horner, CEERD-GV-T, was the Technical Director for Force Projection and Maneuver Support. The Deputy Director of ERDC-GSL was Dr. William P. Grogan, and the Director was Dr. David W. Pittman.

COL Jeffrey R. Eckstein was the Commander of ERDC, and Dr. Jeffery P. Holland was the Director.

Unit Conversion Factors

Multiply	By	To Obtain
cubic feet	0.02831685	cubic meters
cubic inches	1.6387064 E-05	cubic meters
cubic yards	0.7645549	cubic meters
degrees Fahrenheit	$(F-32)/1.8$	degrees Celsius
feet	0.3048	meters
gallons (US liquid)	3.785412 E-03	cubic meters
inches	0.0254	meters
miles per hour	0.44704	meters per second
pounds (force)	4.448222	newtons
pounds (force) per foot	14.59390	newtons per meter
pounds (force) per inch	175.1268	newtons per meter
pounds (force) per square foot	47.88026	pascals
pounds (force) per square inch	6.894757	kilopascals
pounds (mass)	0.45359237	kilograms
pounds (mass) per cubic foot	16.01846	kilograms per cubic meter
pounds (mass) per cubic inch	2.757990 E+04	kilograms per cubic meter
pounds (mass) per square foot	4.882428	kilograms per square meter
pounds (mass) per square yard	0.542492	kilograms per square meter
tons (force)	8,896.443	newtons
yards	0.9144	meters

1 Introduction

1.1 Background

Transportation professionals are presented with the challenge of building and maintaining expanding infrastructure systems under the constraints of shrinking budgets. The competing demands of minimizing costs and maximizing performance are a key issue for designers and maintainers at the federal, state and local levels. As raw material costs continue to increase, this challenge has intensified. In particular, rising crude oil costs have served to highlight these issues during the design of flexible pavements. The inclusion of geosynthetics in flexible pavement structures for base reinforcement has long been accepted as a means of reducing costs and/or extending pavement service life. As new products enter the market, designers are forced to speculate concerning the performance benefits of these products when specifying them.

1.2 Objective

The objective of this effort was to construct and traffic a full-scale test section with varying structural components over a firm subgrade to provide performance data for comparing the effectiveness of Tensar's triaxial geogrid to an unstabilized flexible pavement design. A secondary objective was to develop performance data for the verification of mechanistic performance models for Tensar's geogrid reinforcement products currently on the market.

1.3 Scope

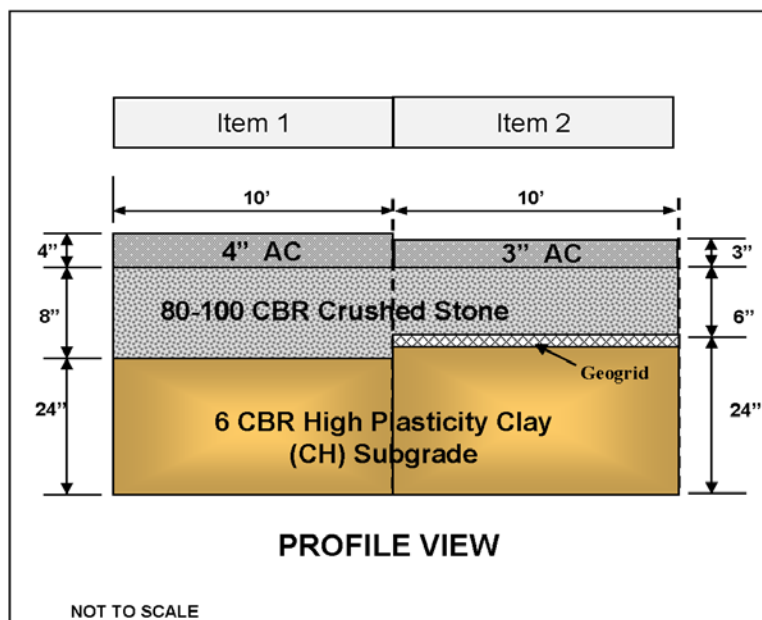
The scope of this project included the construction and trafficking of a full-scale test section comprised of two individual test items, one having a geogrid-stabilized base course. The US Army Engineer Research and Development Center (ERDC) constructed the full-scale test section as designed by Tensar under shelter in its Hangar 4 Pavement Test Facility. During construction, quality control data were collected periodically to verify layer properties and to ensure that the project objectives were accomplished. Each test item was trafficked with ERDC's Heavy Vehicle Simulator (HVS). Pavement performance data were collected at selected intervals during trafficking for use in comparing the performance of the test item with the geogrid-stabilized base course to the test item with an

unstabilized base course. In addition, instrumentation response data were collected and reported to support the verification of mechanistic pavement performance models.

2 Test Plan and Layout

The structural design of the test section was developed by Tensar Corporation. Tensar designed two unique pavement structures to quantify the benefit associated with the use of a geogrid in a flexible pavement structure over a firm subgrade. A profile view of the test section is shown in Figure 1. Each test item consisted of a 10-ft-wide by 50-ft-long testing area. The subgrade for both test items was constructed with 24 in. of high-plasticity clay (CH) placed to achieve the target California Bearing Ratio (CBR) value of 6%. A CBR of 6% was selected to provide a test section with medium subgrade strength. Item 1 was constructed with an 8-in.-thick unstabilized aggregate base course consisting of a crushed limestone flexible base meeting TXDOT Grade 2 Type A specifications. Item 1 was surfaced with a 4-in. hot-mix asphalt (HMA) concrete layer. Item 2 was constructed with a 6-in.-thick flexible base course of the same material, stabilized by placing a triaxial geogrid at the base-subgrade interface. Item 2 was surfaced with a 3-in. HMA layer. The two test items were constructed simultaneously to minimize variability and ensure consistency between the two pavement structures. All construction and traffic testing occurred under ERDC's Hangar 4 pavement testing facility, which minimized the potential for moisture variations due to environmental factors.

Figure 1. Test-section profile view.



The structural design of the test section was developed by Tensar Corporation following the guidelines set forth in the AASHTO 1993 design guide (AASHTO 1993) and their SpectraPave4Pro™ software. The unstabilized control item was developed using the tools and tables provided in the second edition of Pavement Analysis and Design (Huang 2004). The designed structural number for the unstabilized item is 2.88. The geogrid-stabilized item was assigned a structural number of 2.92. SpectraPave4Pro assigns the geogrid-stabilized layer a layer coefficient of 0.267 for use in calculating the total structural number of the geogrid-stabilized item. For further information on the design structural number of the geogrid-stabilized layer, please reference Tensar's SpectraPave4-Pro™ software.

Each test item contained a suite of instrumentation consisting of asphalt strain gauges, earth pressure cells, single-depth deflectometers, moisture probes, pore water pressure transducers, and temperature probes. The geogrid was also instrumented with strain gauges in an attempt to determine the strain mobilized by the geogrid during testing.

The test items were trafficked with ERDC's Heavy Vehicle Simulator (HVS) simulating normal highway loadings. The configuration used for testing consisted of a tandem-axle dual wheel gear loaded to a nominal load of 20,000 lb. Tire pressures were maintained at 120 psi throughout testing. The equivalent axle load factor for this configuration is 2.08. Therefore, one pass of the HVS was equal to 2.08 equivalent standard axle loads (ESALs).

3 Materials

Description and characterization of the materials used during construction of the test sections are presented in this chapter. Field and laboratory tests were conducted on the subgrade, base, and surface layers of each test item. The results of these tests are also summarized in this chapter.

3.1 Subgrade

A locally available high plasticity clay (CH) was used to construct the test-section subgrade. The CH material consisted of 95.1% fines passing the No. 200 sieve as shown in Figure 2. As determined by ASTM D4318-10, the liquid limit, plastic limit, and plasticity index were 73%, 24%, and 49%, respectively. According to the Unified Soil Classification System (USCS), the soil was classified as a high-plasticity clay (CH) and an A-7-6 according to the AASHTO classification system. The subgrade material was processed to a uniform moisture content of 31% and compacted in 6-in. lifts with a large pneumatic-tired roller. Each subgrade lift was compacted to its maximum density at the target moisture content to achieve the design 6% CBR subgrade strength. The target moisture content of 31% was selected based upon the relationship between moisture content and CBR when compacted using modified proctor compaction effort. The in situ dry density after compaction was 88.4 pcf at the target moisture content of 31%. Figure 3 shows a layer of the subgrade material being compacted before final grading.

3.2 Base course

Crushed limestone was used to construct the flexible aggregate base course. The gradation for the crushed limestone is also shown in Figure 2. ASTM procedure D2487-11 was used to determine that the base course was comprised of 46.4% gravel, 43.6% sand, and 10.0% non-plastic fines passing the No. 200 sieve. The coefficient of curvature (C_c) was calculated as 9.08, and the coefficient of uniformity (C_u) was 80.09. The crushed limestone aggregate base was classified as a poorly-graded gravel with silt and sand (GP-GM) according to the USCS, an A-1-a according to the AASHTO procedure, and a Type A Grade 2 flexible base according to the TxDOT Standard Specifications for Construction and Maintenance of Highways, Streets, and Bridges. Modified proctor compaction tests were performed in accordance with ASTM D1557-11 Method C Modified. The maximum dry density was 144.7 pcf at an optimum moisture content of 4.9%.

Figure 2. Test-section material gradations.

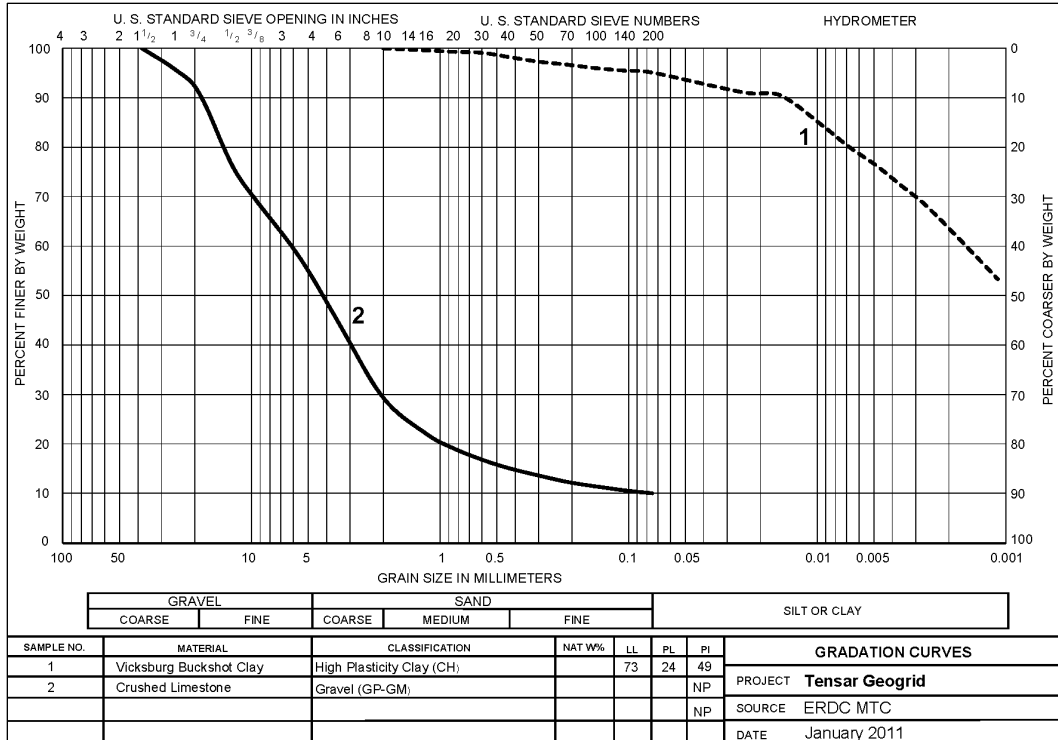


Figure 3. Subgrade compaction before final grading.



The crushed limestone material was placed in 8- to 10-in. lifts and compacted using a large vibratory steel-wheel roller. Figure 4 shows the crushed limestone material being dumped in place, while Figure 5 shows the material being compacted.

Figure 4. Crushed limestone base-course material being placed.



Figure 5. Base-course compaction.



3.3 Asphalt

The HMA used as a surface course for this testing was representative of local highway mix for Mississippi. This mix is a 9.5 mm nominal maximum aggregate size (NMAS) surface mix. Gradation and pertinent laboratory characteristics of the HMA are shown in Table 1. Table 2 represents the Asphalt Institute recommended values for Superpave mix design for anticipated traffic levels of 300,000 to 3,000,000 ESALs. Placement of the HMA is shown in Figure 6.

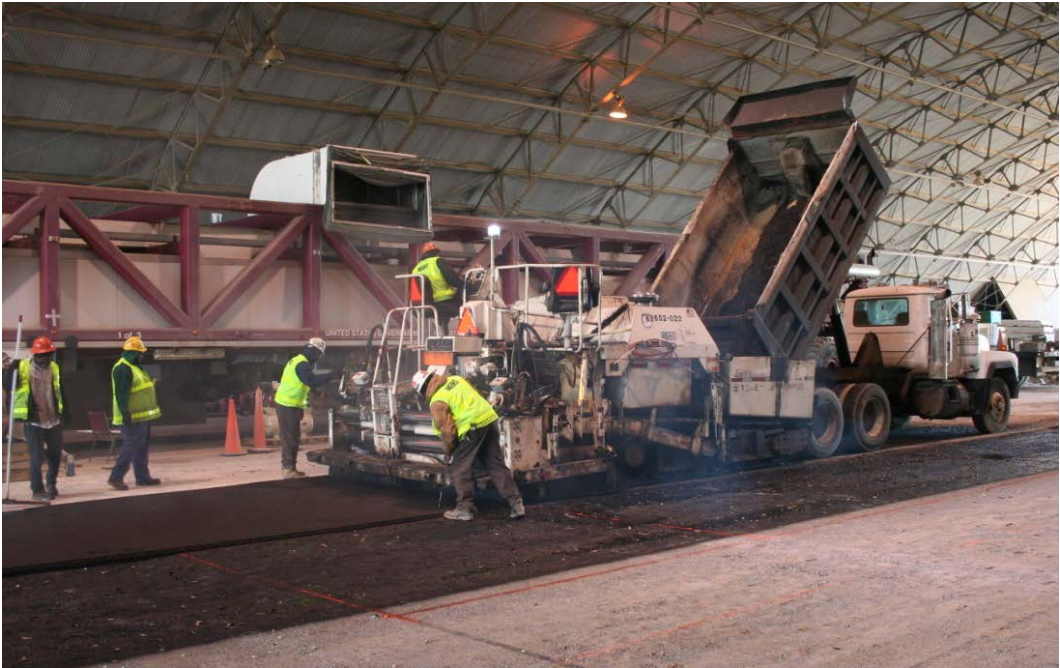
Table 1. Test-section HMA properties.

Hot-Mix Asphalt Properties		
N _d		75
Binder Grade		PG 67-22
Mixing Temp (C)		310
Compaction Temp (C)		292
Percent Passing	1.0 in. (25.0 mm)	100
	3/4 in. (19.0 mm)	100
	1/2 in. (12.5 mm)	100
	3/8 in. (9.5 mm)	95
	#4 (4.75 mm)	54
	#8 (2.36 mm)	34
	#16 (1.18 mm)	27
	#30 (0.60 mm)	20
	#50 (0.30 mm)	7
	#100 (0.15 mm)	5
	#200 (0.075 mm)	3.8
RAP (%)		15
RAP AC (%)		5.5
G _{sb}		2.6
G _{sa}		2.682
Abs (%)		1.18
P _b (%)		5.7
G _{mm}		2.429
G _{se}		2.643
VMA		15.4
VFA		74
P ₂₀₀ /P _{be}		0.76

Table 2. Asphalt Institute recommended values.

Recommended Values	
Superpave Parameter	Asphalt Institute
N _d	75
VMA	15.0 minimum
VFA	65 - 78
P ₂₀₀ /P _{be}	0.6 - 1.2

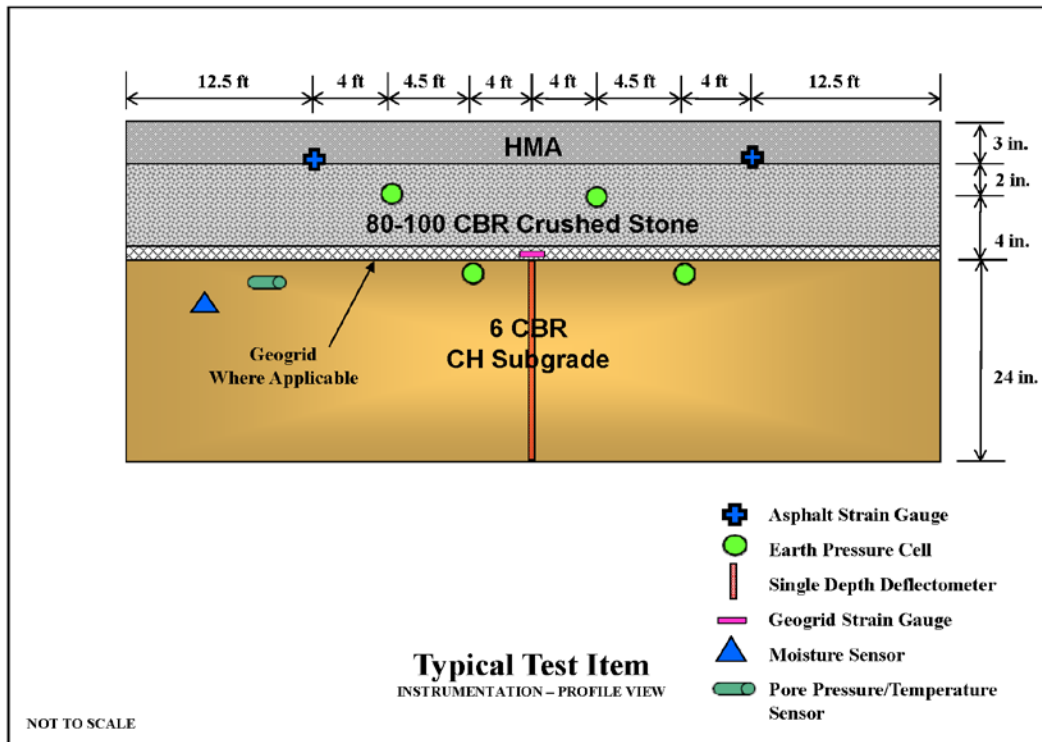
Figure 6. Test section during application of first HMA layer.



4 Instrumentation

To monitor and characterize pavement response during traffic testing, the test section was fully instrumented. Sensors were placed in the subgrade, base course, and HMA surface course. Additionally, the geogrid in Item 2 was instrumented to measure that material response as well. Instrumentation used to capture the dynamic response of the pavement included earth pressure cells (EPCs), single-depth deflectometers (SDDs), asphalt strain gauges (ASGs), and geogrid strain gauges (GGs). Environmental parameters were measured and monitored using pore water pressure sensors (including temperature) and moisture sensors. Figure 7 shows the profile view of the typical instrumentation for a traffic lane.

Figure 7. Instrumentation layout for typical test item.



4.1 Earth Pressure Cells

Vertical stresses in the base course and subgrade were measured using 9-in.-diam EPCs. EPCs provide a quantitative measurement of the vertical distribution of the stresses within each traffic lane during testing. For this study, Geokon EPCs were installed. Cells with a maximum pressure range

of 100 psi were installed in the subgrade, and 200-psi EPCs were installed in the base course. Figure 8 shows an EPC being installed 2 in. below the surface of the subgrade at the interface with the base course.

Figure 8. Installation of an earth pressure cell.



4.2 Asphalt strain gauges

Tensile strain at the bottom of an HMA layer provides a quantitative measure of the pavement response during trafficking. Increases in permanent, or plastic, strain lead to pavement failure. For this study, strain at the bottom of the HMA surface was measured using dynamic asphalt strain gauges (ASGs) in both the transverse and longitudinal directions. The strain at this location can be used to estimate the fatigue life of the HMA surface layer of the pavement. The ASGs were manufactured by Applied Geomechanics and are capable of measuring a range of $\pm 3,000$ microstrain. The gauges were placed on the surface of the base course, and HMA from the asphalt paver was placed as cover over each of the gauges immediately prior to paving of the entire test section. This process is shown in Figure 9.

Figure 9. Installation of asphalt strain gauge.



4.3 Geogrid strain gauges

One of the primary mechanisms by which geogrid purportedly works is through lateral restraint of the base course. In order for the geogrid to properly perform, a certain amount of strain must be mobilized in the geogrid, essentially locking the geogrid and aggregate into a stiff sublayer at the bottom of the base course. Strain measurements along the geogrid provide a means of quantifying the mobilization of the geogrid.

Strain gauges were attached to the individual ribs (in between the nodes of a single rib) of the geogrid. Vishay Micro-Measurements EP-08-230DS-120 gauges, shown in Figure 10, were installed on the geogrid. The strain gauges were covered with Aqua-Seal to prevent moisture damage. Finally, an epoxy coat was applied to provide additional protection from aggregate damage to the strain gauges. Figure 11 shows the installed gauges.

Gauges were applied to the individual ribs (in between the nodes of a single rib) of the geogrids. The strain gauges were located at the positions indicated in Figure 12. Wiring was laid in a trench in the subgrade below the geogrid to prevent damage during base-course installation. The wooden supports were removed, and the strain gauges were covered with a thin layer of sand to minimize damage due to large aggregates during base-course construction as shown in Figure 13.

Figure 10. Geogrid strain gauges.



Figure 11. Strain gauges installed on the geogrid.

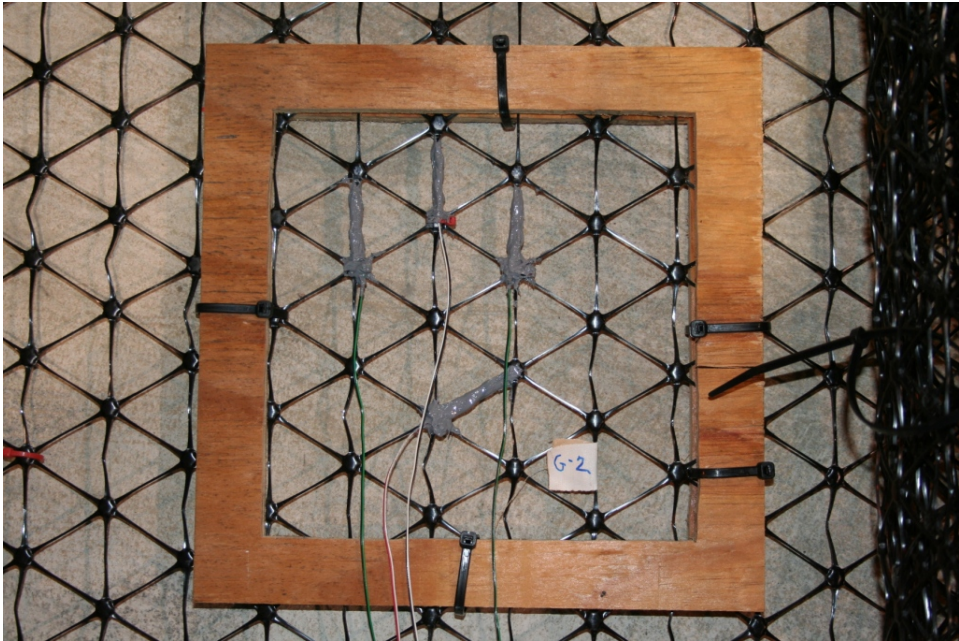


Figure 12. Location of strain gauges on geogrid.

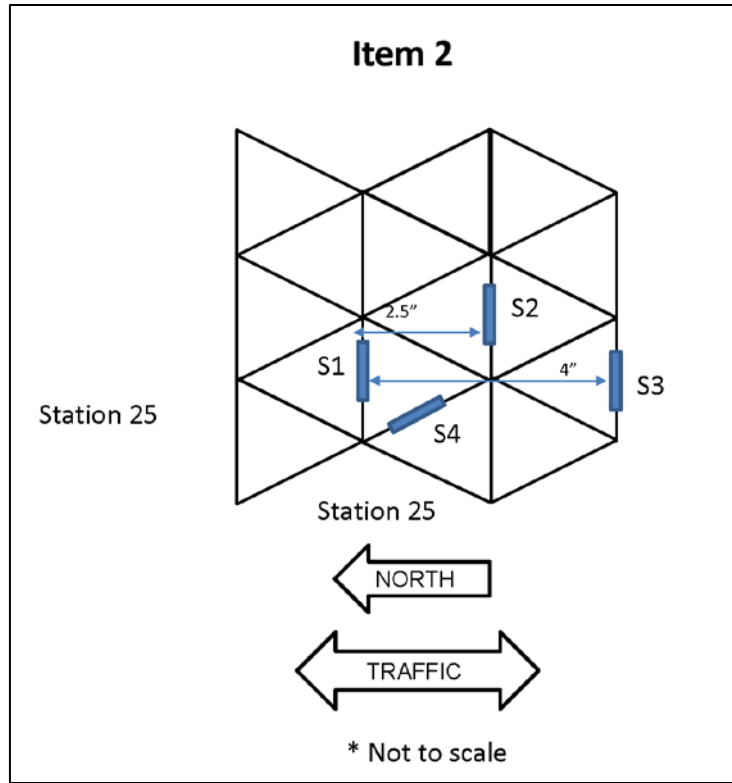


Figure 13. Installation of geogrid strain gauges in the test section.



4.4 Single-depth deflectometers

Measurements of deformations in the subgrade are used to quantify the stabilization benefits of a geogrid as well as assisting with the validation of the failure mechanism within the pavement structure. Potential reductions in vertical stresses at the subgrade should also be reflected as reductions in the deformation. In theory for pavements with similar structural components, the geogrid-stabilized pavement should show lower deflections than the unstabilized pavement at a given traffic level.

Vertical deflections in the subgrade were measured using single-depth deflectometers (SDDs). One SDD was placed in the middle of each test item along the centerline of traffic. The SDD was placed such that the shaft was anchored at a depth of 9 ft. from the top of the subgrade. A linear velocity displacement transducer (LVDT) with a range of ± 2 in. was placed in the housing such that it was in contact with both the anchor rod and the surface plate as shown in Figure 14. Thus, the LVDT measured movement of the plate 2 in. below the base-subgrade interface relative to the control point located at a depth of 9 ft.

Figure 14. Installed SDD.



5 Pavement Characterization

5.1 As-built properties

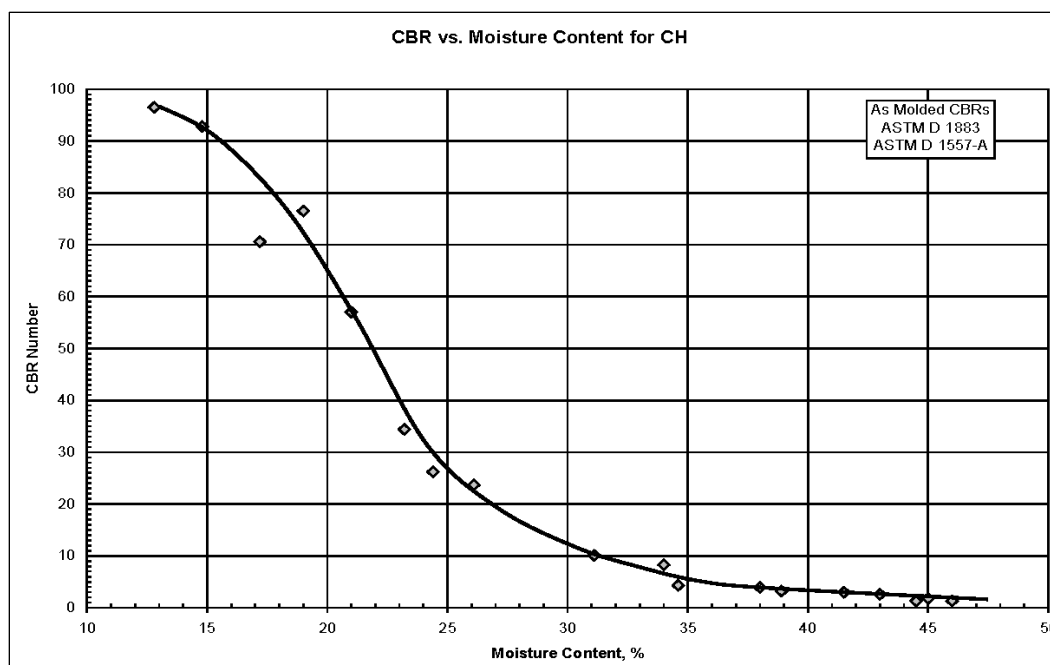
The test items were characterized by performing a series of tests on the as-constructed pavement. During test-section construction, the dry density and moisture content were measured for each pavement layer using a nuclear moisture-density device method outlined by ASTM D6938-10. Values from these tests were used to verify the uniformity of each of the pavement layers during construction as well as for comparative purposes between layers. Field in-place CBR tests were performed according to ASTM D4429-09a. As-built properties of the base and subgrade are summarized in Table 3.

Table 3. As-built test-section properties.

Test	Item 1	Item 2
	4-in. Nominal AC Unstabilized Base	3-in. Nominal AC Stabilized Base
CH Subgrade Properties		
Wet Density (pcf)	116.9	116.2
Dry Density (pcf)	88.9	88.4
Moisture (%)	30.0	31.4
Oven-Dried Moisture (%)	34.1	32.8
CBR In-Place (%)	5.9	6.3
Crushed Limestone Base Properties		
Wet Density (pcf)	143.0	141.3
Dry Density (pcf)	138.1	136.3
Moisture (%)	3.6	3.7
Oven-Dried Moisture (%)	2.4	2.3
CBR In-Place (%)	95.3	100+
Thickness (in.)	7.7	6.2

The measured oven-dried moisture content for both items is consistent with the historical values for 6 CBR Vicksburg Buckshot Clay. Figure 15 displays historical CBR vs. moisture content relationship for the Vicksburg Buckshot Clay. Values from the field in-place CBR tests show subgrade strengths ranging from 5.9 to 6.3%.

Figure 15. Historical moisture content/strength relationship for Vicksburg Buckshot Clay.



5.2 Dynamic cone penetrometer

A series of Dynamic Cone Penetrometer (DCP) tests were performed to further characterize the strength of the unbound pavement layers. DCP tests were performed after construction of the base and subgrade layers, following the procedures described by ASTM D 6951-09. Measured values of the DCP index (millimeters of penetration per hammer blow) were converted to CBR strength using the relationship developed by Webster et al. (1992, 1994). As-built DCP results are shown for Item 1 Station 37.5 in Figure 16 and Item 2 Station 25 in Figure 17. The DCP tests were conducted immediately after the base course was placed and compacted, not allowing time for the base course to “set-up” or harden to the full 100 CBR. The field CBR values were conducted several days later, which allowed the base course time to harden and is reflected in the results previously presented in Table 3.

5.3 Falling weight deflectometer

Falling Weight Deflectometer (FWD) tests were performed on the surface of both test items after construction as shown in Figure 18. Results from the FWD tests were evaluated in terms of the Impulse Stiffness Modulus (ISM). The ISM is the ratio of the applied load to the measured plate deflection. Higher ISM values represent a stiff pavement while low ISM

values represent a weak pavement. As-built ISM values for Items 1 and 2 are presented in Figure 19. The average ISM values for Items 1 and 2 were 521 and 354 kips/in., respectively. The increased stiffness of Item 1 compared to Item 2 is partially due to the extra 2 in. of base course and extra 1 in. of HMA of Item 1.

Figure 16. As-built DCP results for Item 1 station 37.5.

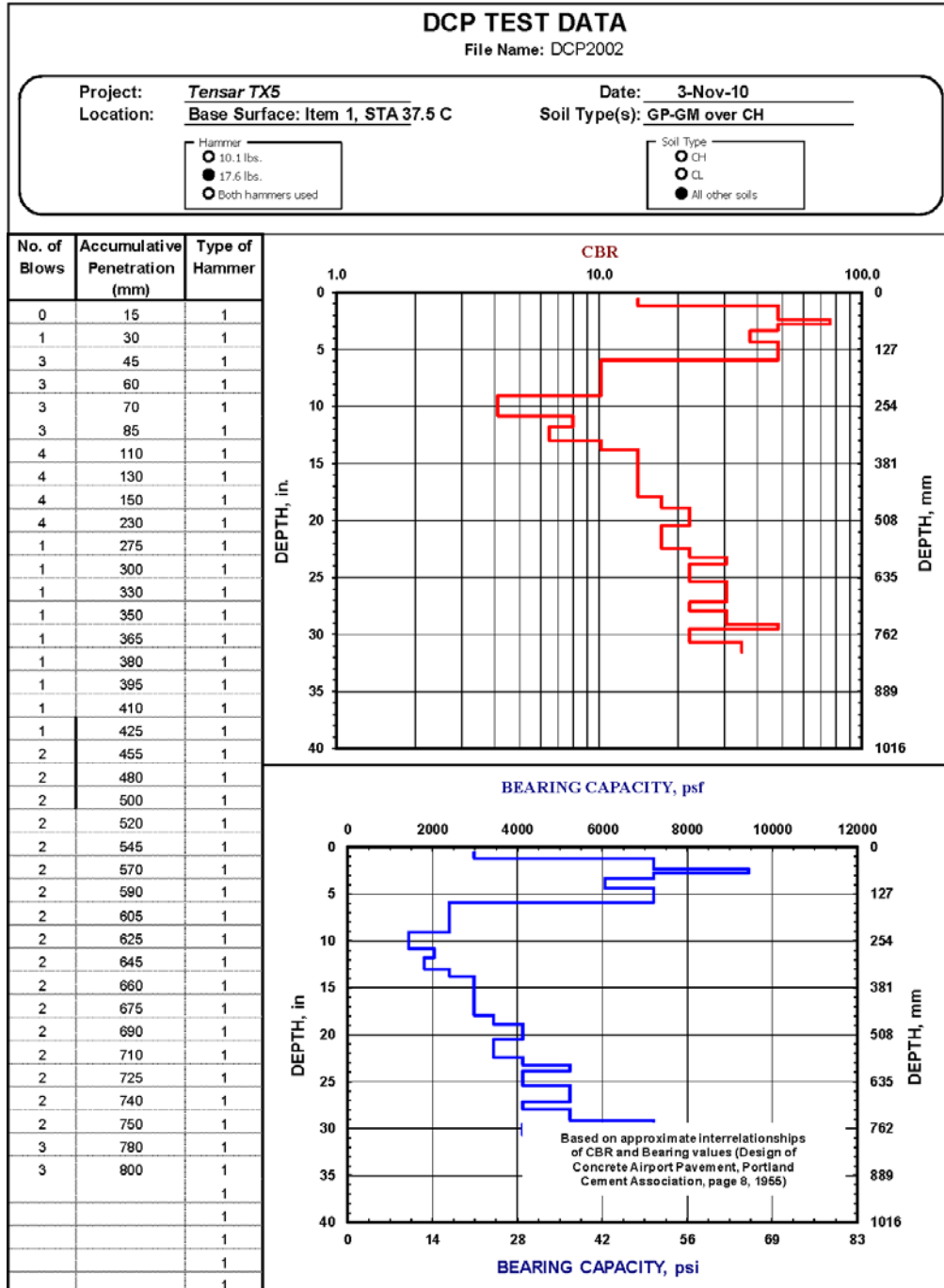
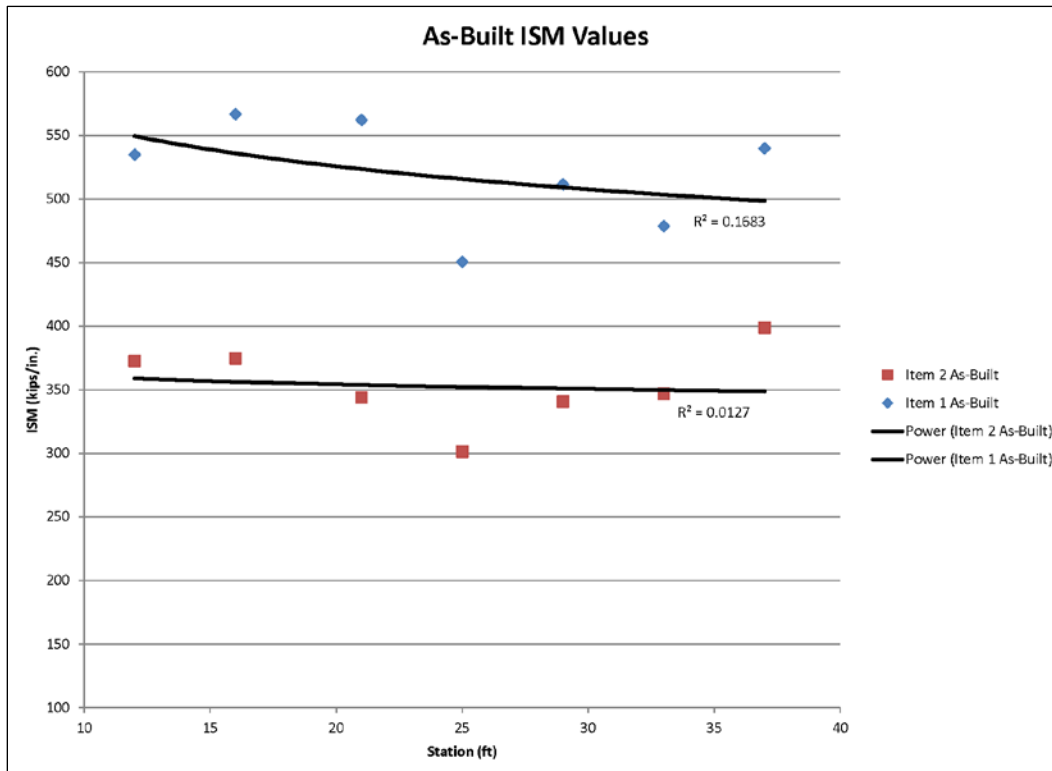


Figure 18. FWD testing inside HVS.



Figure 19. As-built ISM values for Items 1 and 2.



6 Traffic Testing

Accelerated traffic testing of Items 1 and 2 was carried out using the ERDC HVS. A dual-wheel tandem axle configuration was used to apply the traffic to the test items. Figure 20 shows the wheel configuration used during testing. The dual-wheel tandem axle was subjected to a nominal load of 20,000 lb. Wheel loads were verified prior to testing by concurrently weighing each axle with portable aircraft wheel scales. Tire pressures were maintained at 120 psi throughout testing of both test items. The equivalent axle load factor for this configuration is 2.08. Therefore, one pass of the HVS is equal to 2.08 equivalent standard axle loads (ESALs). To minimize the effect of temperature on rutting results, testing on each item was conducted at a constant pavement temperature of 77°F.

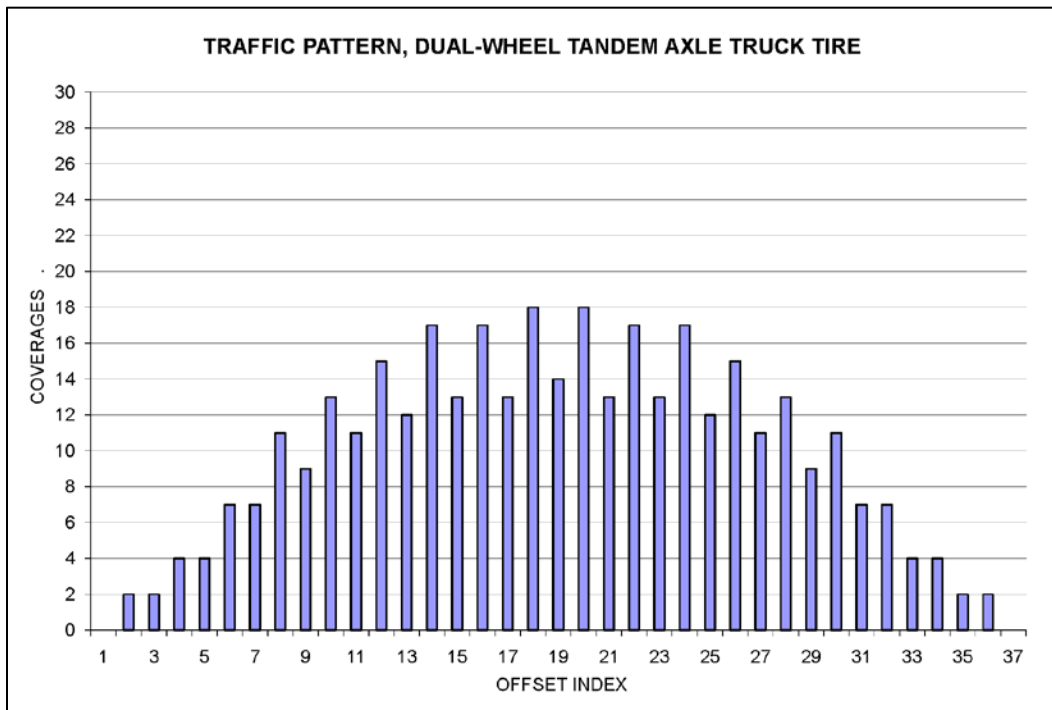
Figure 20. Verifying the applied load on the HVS dual-wheel tandem axle configuration.



Each test item was subjected to a uniformly distributed bi-directional traffic pattern displayed in Figure 21. The lateral offset indices refer to 1-in. increments along which the wheel travels longitudinally. Thus, the extent of the lateral wander associated of this traffic pattern is approximately 3 ft. A 3-ft-wide wander pattern was utilized to mimic previous studies (Timm and Priest, 2005) as well as duplicate what has been observed in other test sections (Tingle and Jersey, 2007). Traffic loading was applied over the full 50-ft length of each test section. Periodic interruptions were made during

trafficking to collect pavement performance data and instrumentation response data. Data collection and instrumentation response recordings were performed at predetermined stations located within the inner 40 ft of the test section to avoid potential end effects created when the load changes direction. The failure criterion for both items was defined as a 1-in. surface rut, including any upheaval along the edges of the traffic lane.

Figure 21. Traffic pattern applied during trafficking.



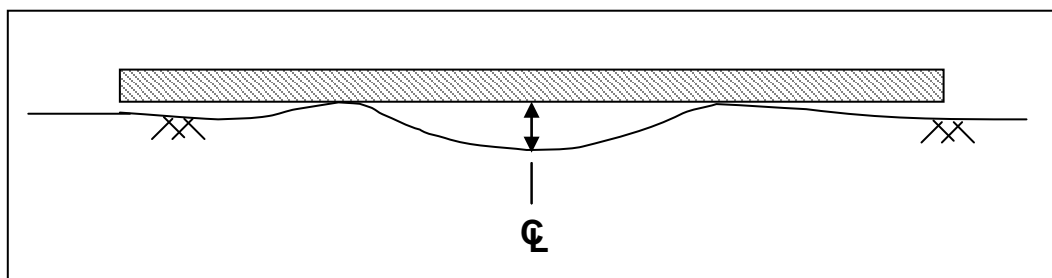
7 Results

Failure of a flexible pavement test item is typically defined as 1 in. of rutting for accelerated pavement testing. This failure definition is based around the concept of pavement serviceability and the fact that pavement serviceability begins to decrease exponentially in flexible pavement systems after 1 in. of rutting.

7.1 Surface deformations

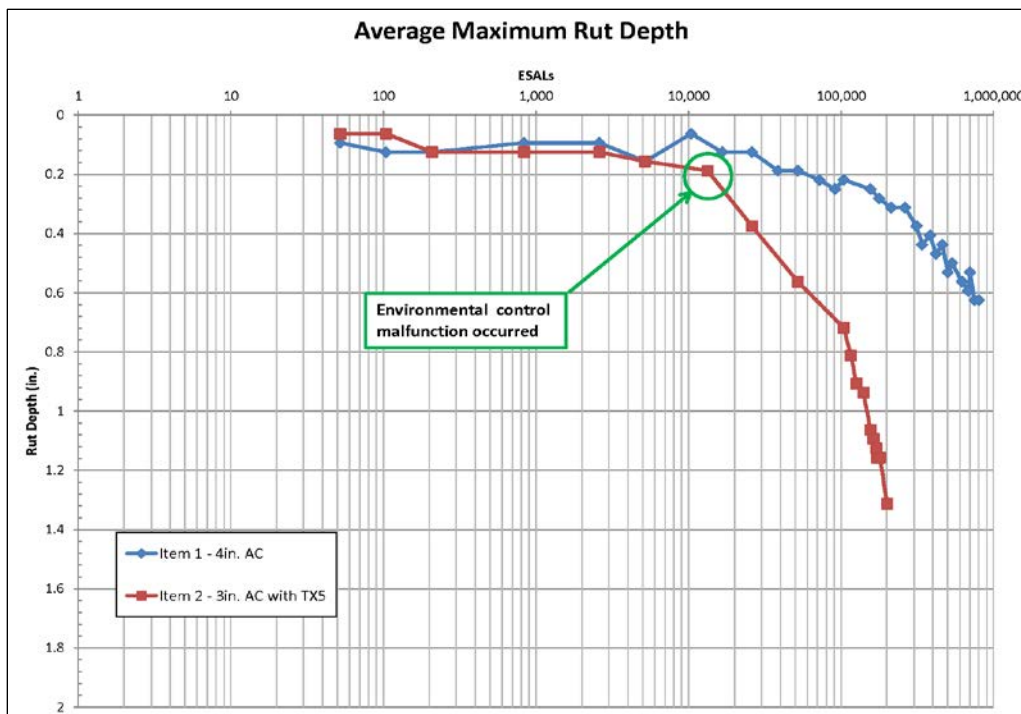
Surface deformation and rut depth measurements were recorded at predetermined traffic intervals throughout the testing period. Surface deformation measurements represent the change in the centerline profile of the traffic lane. Surface deformation measurements were taken using a rod and level. Rut depth measurements were taken by placing a metal straight edge across the traffic lane at selected stations and measuring the maximum rut depth. The maximum rut depth includes the permanent surface deformation as well as any upheaval along the edge of the traffic pattern. Figure 22 displays a schematic of the maximum rut measurement concept.

Figure 22. Measurement of rut depth.



The reported maximum rut depths presented in Figure 23 represent maximum rut depth of 50% of the traffic lane. Maximum rut measurements were taken at stations 12.5, 25, and 37.5 of the traffic lanes. The average of the maximum rut depth measurements was reported. Surface deformation measurements are presented in Figure 25. The reported surface deformation for each pass was calculated by averaging rod and level measurements taken at 1-ft increments along the full length of the traffic lanes. Measurements located at the ends were excluded due to exaggerated rutting caused by the change of direction of the HVS carriage.

Figure 23. Average maximum rut depth.



Both lanes performed equally until approximately 13,000 ESALs. It should be noted that after the data collection point of 13,000 ESALs on Item 2, the HVS-A environmental control system malfunctioned. After the malfunction, the top of the pavement temperature increased to above 100°F, the middle of the pavement reached 91°F and the bottom of the pavement reached 86°F before the problem was discovered and trafficking was stopped. Figure 24 is a plot of the pavement temperature for Item 2 during the incident. The environmental system was repaired and trafficking resumed. As seen in the rut and deformation plots, Item 2 began to deteriorate after this data collection point. While Item 2 was tested to 200,000 ESALs, the data beyond 15,000 ESALs should not be used for comparative purposes because of the damage incurred during the elevated temperatures while Item 1 was maintained at a constant temperature of 77°F during testing. Permanent deformation measurements serve as a better performance measure in this case because it eliminates the majority of the effect from the induced rutting on Item 2 as a result of the elevated temperatures. Figure 25 displays how the geogrid-stabilized Item 2 performed equally to the thicker unstabilized item even after the environmental control malfunction occurred. A summary of the comparable rut depth measurements is displayed in Table 4. Only values before the environment control system malfunctioned are displayed in Table 4. Permanent deformations measurements are displayed in Table 5 and are shown for all traffic levels to display the equal performance of the two test items.

Figure 24. Item 2 temperature change during HVS malfunction.

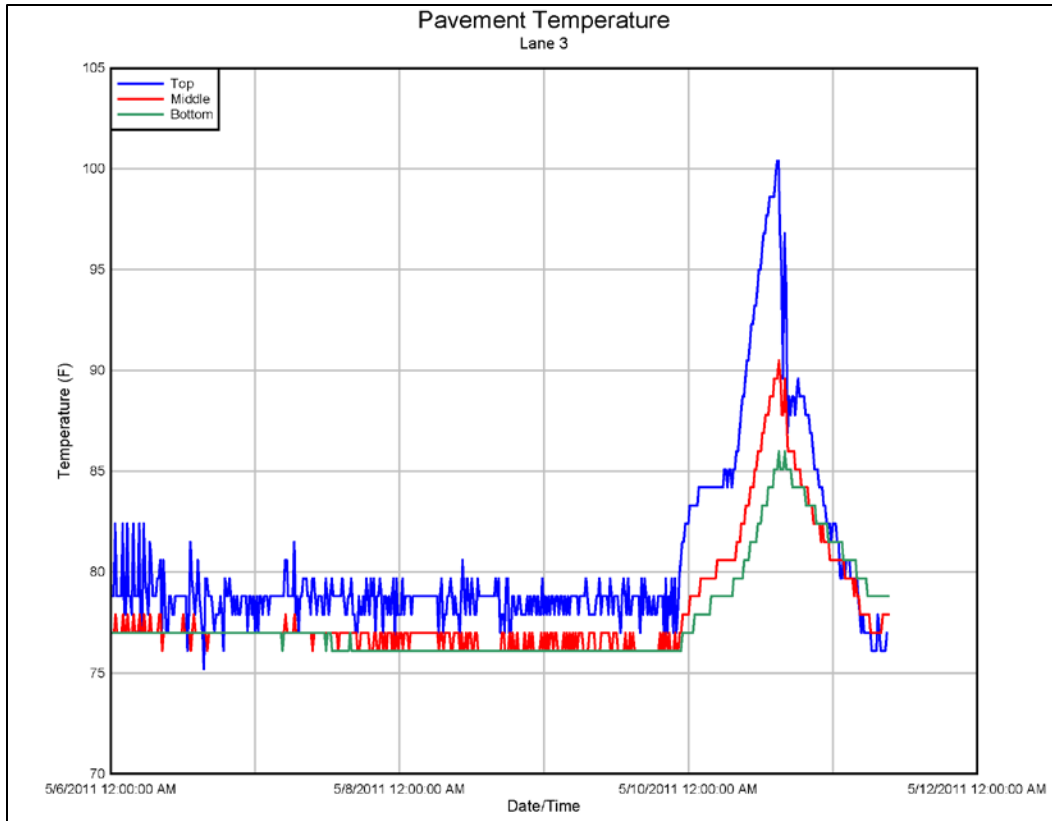


Figure 25. Permanent surface deformation.

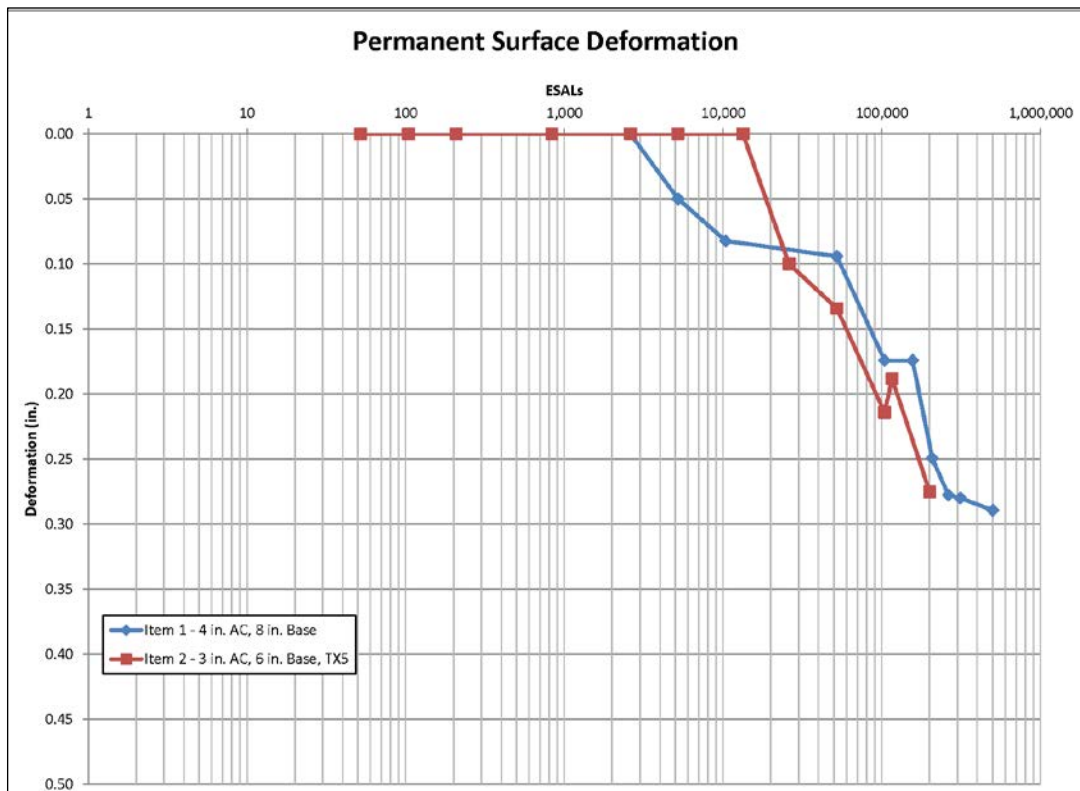


Table 4. Maximum rut depth measurements.

Test Item	Pavement Structure	ESALs					
		52	832	2600	5200	13,312	16,600
Item 1	4-in. HMA 8-in. Base Unstabilized	0.01	0.13	0.13	0.14	NA	0.14
Item 2	3-in. HMA 6-in. Base Stabilized	0.06	0.13	0.13	0.16	0.18	NA

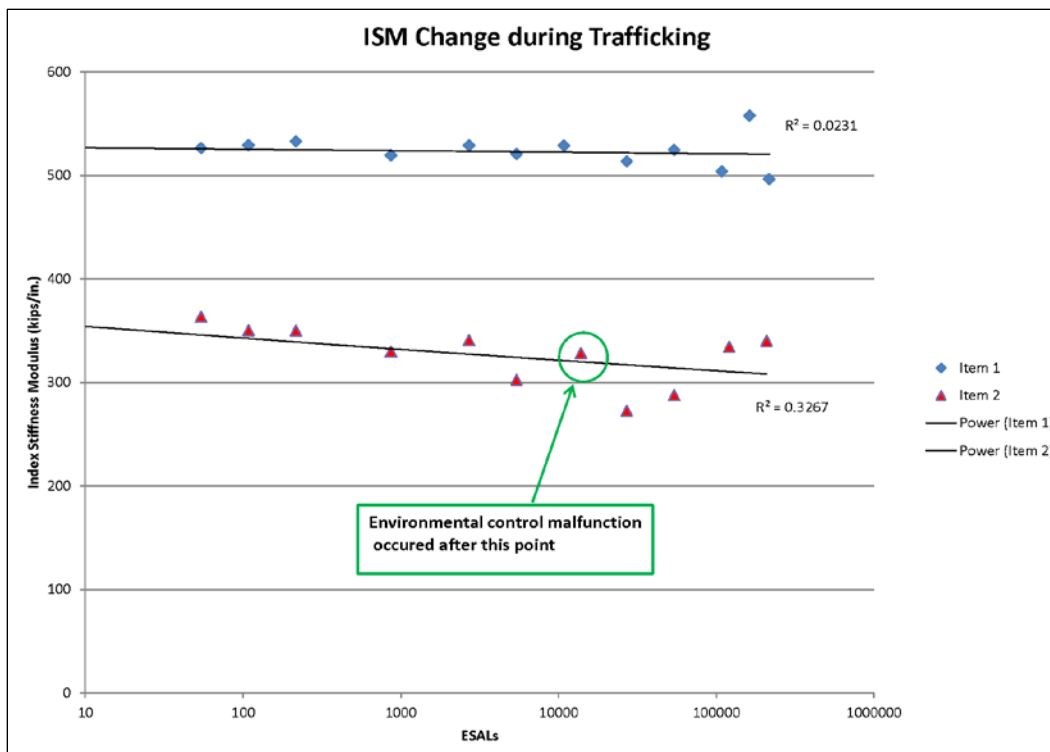
Table 5. Permanent surface deformation measurements.

Test Item	Pavement Structure	ESALs						
		832	5200	52,000	104,000	200,000	500,000	800,000
Item 1	4-in. HMA 8-in. Base Unstabilized	0.00	0.05	0.09	0.17	0.25	0.29	0.29
Item 2	3-in. HMA 6-in. Base Stabilized	0.00	0.00	0.13	0.21	0.28	NA	NA

7.2 Falling weight deflectometer

FWD data were analyzed to characterize each test item in terms of pavement structure stiffness. The ISM, which is a normalization of the applied load divided by the resulting load plate deflection, was the basis for comparison. FWD data were collected at seven separate stations along each test item at certain traffic intervals. The data locations were kept consistent throughout testing and were located at Stations 12.5, 17, 21, 25, 29, 33, and 37.5. Average ISM values for the as-built Item 1 and Item 2 were 521 and 354 kips/in., respectively. Changes in ISM values and the effect of trafficking on each test item are summarized in Figure 26. After the completion of testing, the ISM value for Item 1 was 497 kips/in. representing a decrease of 24 kips/in. The final ISM value for Item 2 was 340 kips/in. representing a decrease of 14 kips/in. Trend lines are presented for visual purposes rather than for predictive purposes. As shown, the beginning and ending ISM values for Item 2 had little change indicating no damage to the base course over the testing duration, which was verified with post-test forensics. These values further validate the reasoning to not use rut depth as a performance measure for this evaluation due to the temperature effects on the pavement causing premature rutting in the surface course only.

Figure 26. ISM changes during trafficking.



7.3 Earth pressure cells

Earth pressure cells were installed in the subgrade and base course of both test items. Table 6 summarizes the installation depths and locations of the EPCs installed in Items 1 and 2. EPC1 and EPC2 were installed in the subgrade while EPC3 and EPC4 were installed in the base course. Installation depths in Table 6 are from the surface of the HMA. Readings were taken at specified traffic intervals and when there was a noticeable change in rutting. Raw EPC data are located in Appendix A.

Table 6. Installation depths of installed EPCs.

Item	EPC	Location	Station	Instrumentation Depth (in.)
1	EPC1	Subgrade	21	10.8
1	EPC2	Subgrade	33.5	10.8
1	EPC3	Base	16.5	5.0
1	EPC4	Base	29	4.3
2	EPC1	Subgrade	21	14.2
2	EPC2	Subgrade	33.5	14.2
2	EPC3	Base	16.5	6.1
2	EPC4	Base	29	5.9

In order to average out the wander of the HVS and any misalignments due to construction, pressure readings were recorded for approximately 10 min of traffic after each designated data collection point. The peak values from the 10 min of EPC readings were chosen to represent the maximum pressure reading at that specific traffic interval. Taking the maximum value from more than 10 min of trafficking helped ensure that the maximum value was recorded when the HVS wheel load was directly over the installed pressure cell. This helped to alleviate any impact on the recorded values that might have resulted from installation and alignment differences in the pressure cells between test items. Figure 27 is an example of the EPC response during a 10-min traffic test. The peak values for each EPC during the 10 min of trafficking are shown in the top right corner of the figure.

The peak EPC values from the 10-min tests were collected after each data collection point for gauges installed in both the base course and the subgrade. The changes in the EPC peak values for gauges installed in the base course of both Item 1 and Item 2 during trafficking are shown in Figure 28. Changes in the EPC peak values for gauges installed in the subgrade of both Item 1 and Item 2 are shown in Figure 29.

For this study, predicted stresses within the pavement structure were calculated using the Pavement Engineering Utility version 7 (PSEVEN). PSEVEN is a software tool developed at the ERDC for the analysis, design and evaluation of pavement structures. This tool implements pavement criteria and procedures contained in Department of Defense Unified Facilities Criteria (UFC) 3-260-02. PSEVEN can be used for the analysis of flexible, rigid, unsurfaced, and mat-surfaced pavements. Required pavement thicknesses, allowable loads and allowable passes are computed for one or more ground vehicles and aircraft. PSEVEN is able to use vehicle geometrical and load data from the standard database supplied with the pavement engineering and design software package PCASE 2.09. Custom vehicles can be created and managed to add vehicles not included in the standard vehicles database. PSEVEN can also be used to design and analyze pavements using the layered elastic theory. Other features of PSEVEN include: frost calculations, minimum thickness of asphalt surfaces, and Aircraft Classification Numbers.

Figure 27. EPC response during 10 min of trafficking after 13,000 passes.

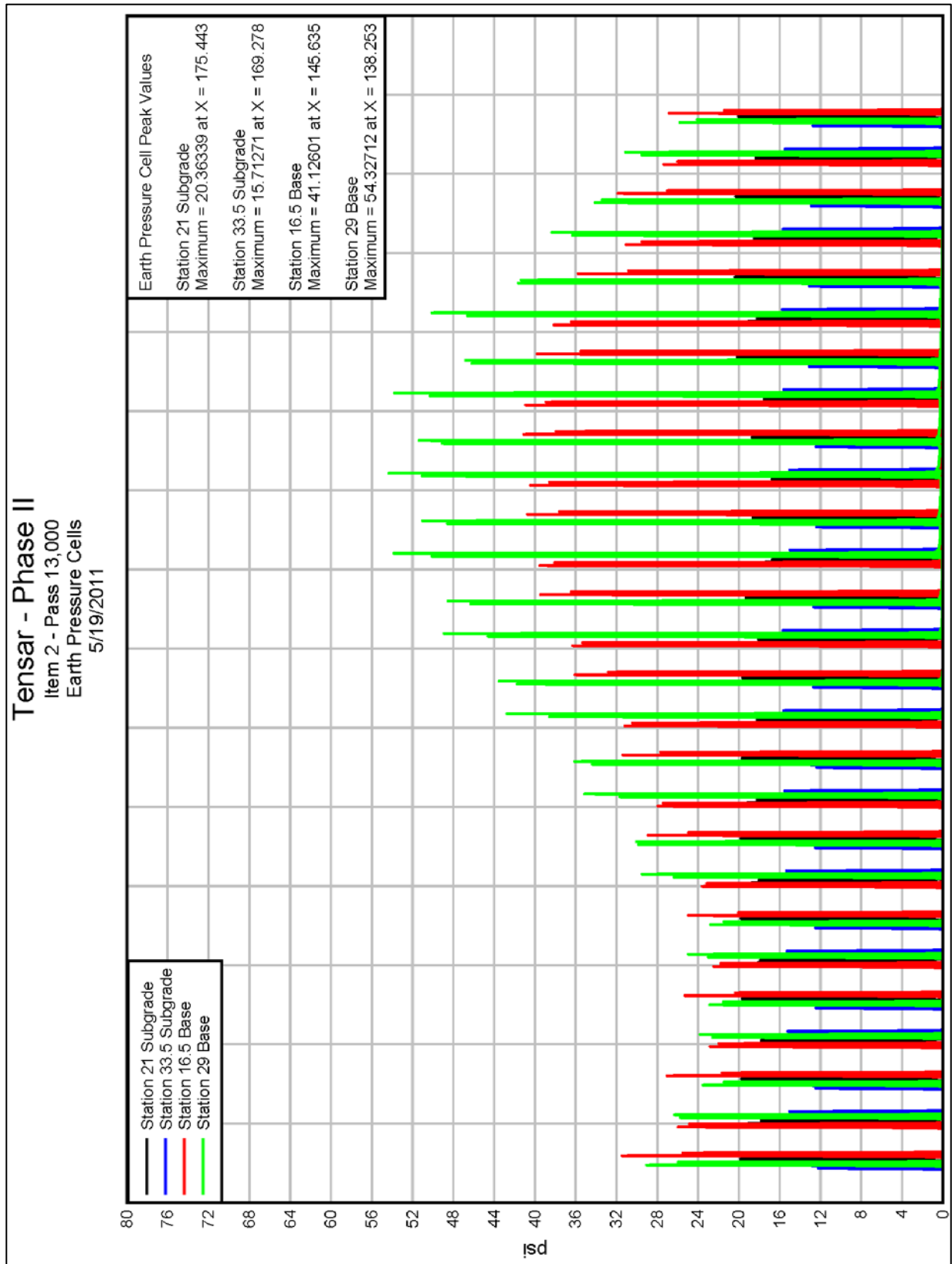


Figure 28. Change in EPC reading for base course during trafficking.

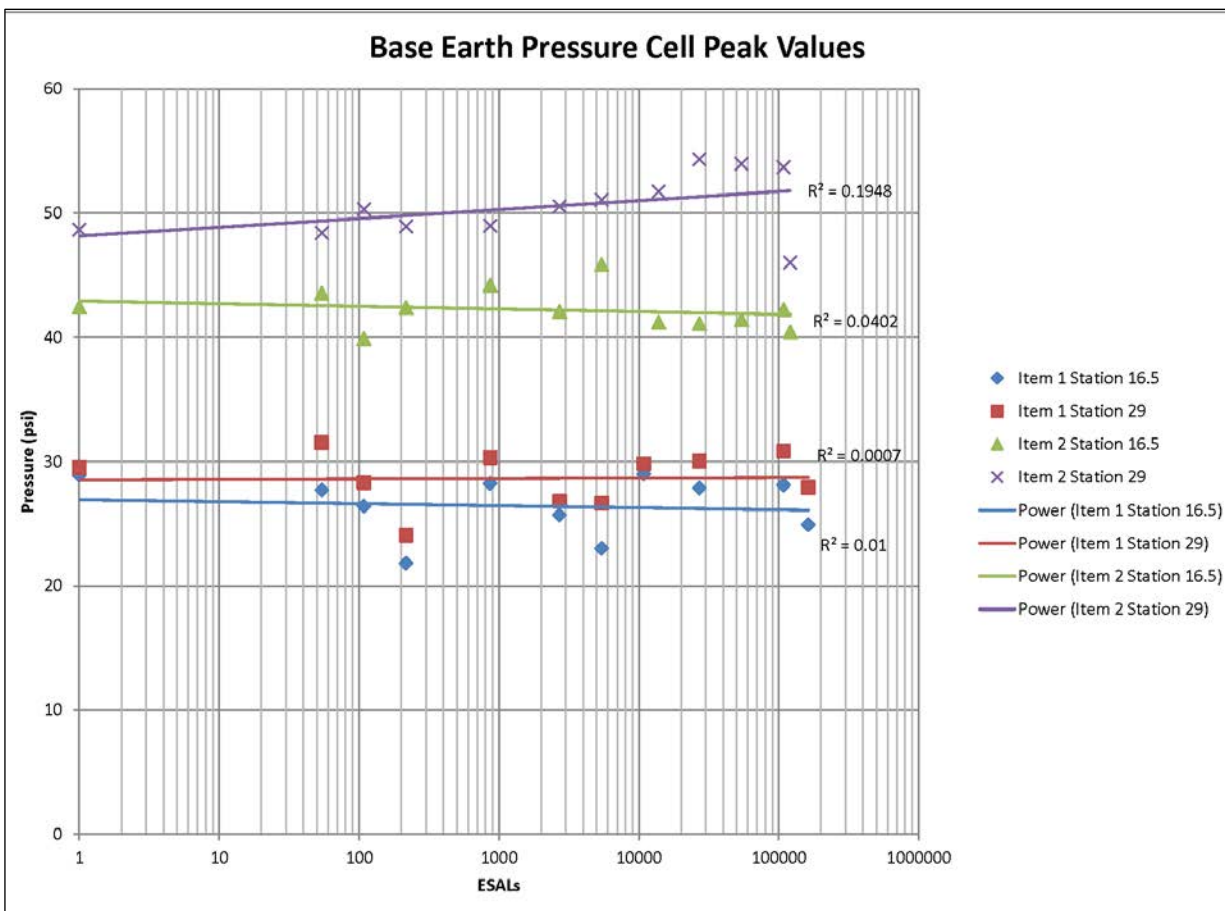


Table 7 summarizes the data calculated using PSEVEN as well as the measured responses from the EPCs installed in the test section. The values used for the measured response were recorded at the beginning of the traffic testing before any damage to the test section had occurred. As-built values were used for the thickness of the base course at the location of the EPC reading as well as the depth at which the EPC was installed in each item.

7.4 Single-depth deflectometers

Single-depth deflectometers were installed in each test item at approximately Station 25. The installed gauges have a measurement range of ± 2 in. Gauges were installed at the top of the subgrade and recorded measurements give an estimate of the deflections experienced by the subgrade. Raw SDD data is located in Appendix B.

Figure 29. Change in EPC readings for subgrade during trafficking.

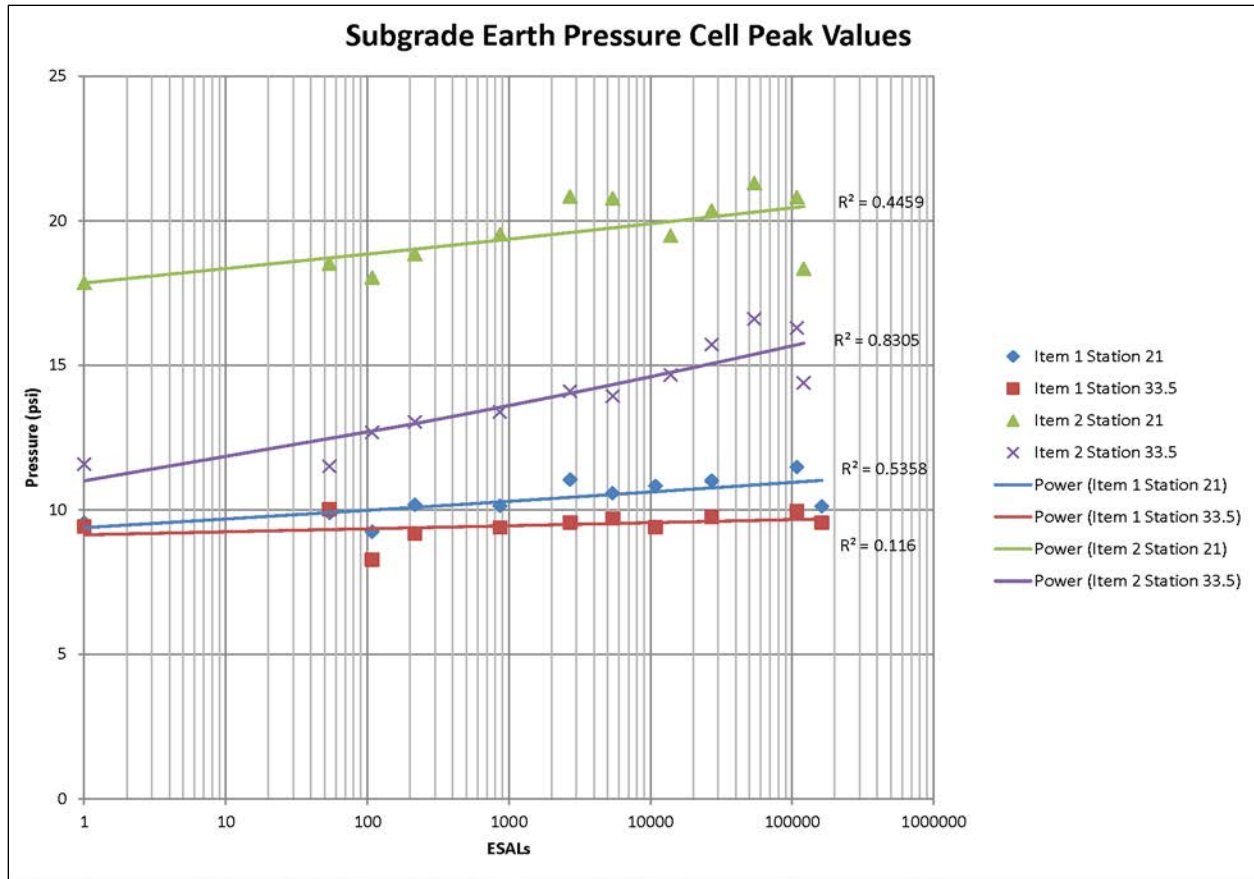
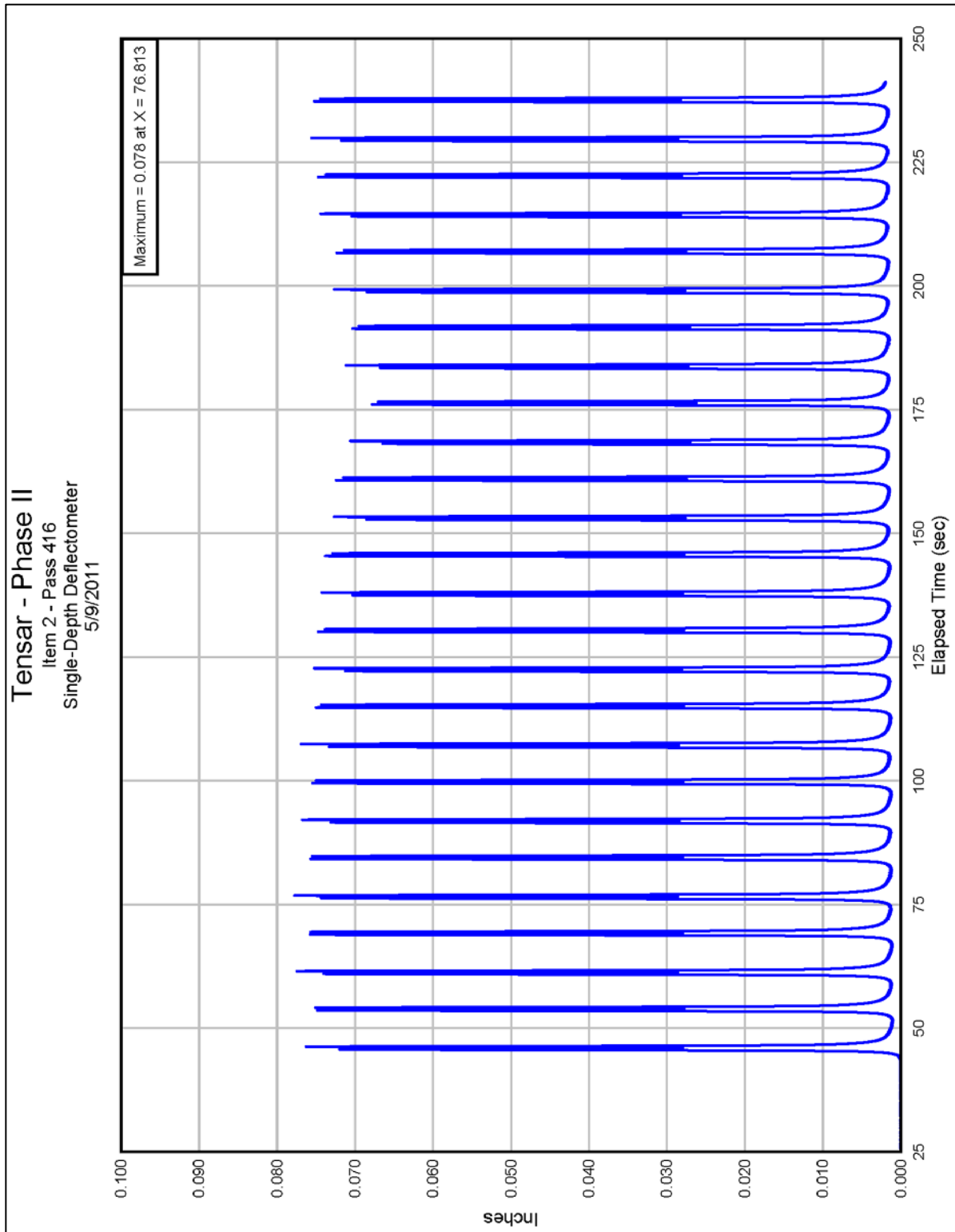


Table 7. Measured vs. predicted stresses.

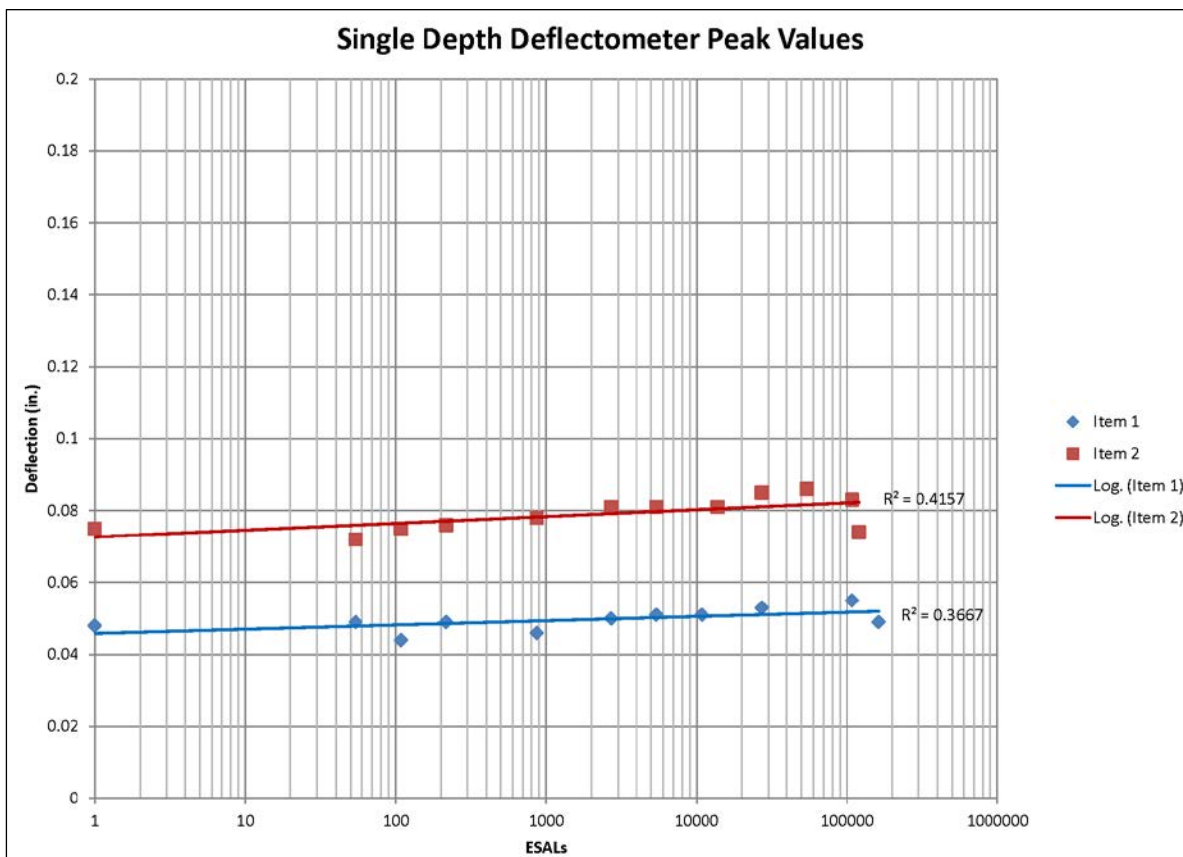
Location			As- built HMA Thickness (in.)	As- built Base Course Thickness (in.)	EPC Depth from Surface (in.)	PSEVEN Predicted Stress (psi)	Measured Stress (psi)	Measured vs. PSEVEN (psi)
Item 1	Station 21	Subgrade	4.2	7.7	10.8	14.2	9.6	-4.6
Item 1	Station 33.5	Subgrade	3.5	7.9	10.8	14.2	9.4	-4.8
Item 1	Station 16.5	Base	3.9	7.8	5.0	45.1	28.9	-16.2
Item 1	Station 29	Base	4.0	7.7	4.3	53.6	29.5	-24.0
Item 2	Station 21	Subgrade	2.5	6.4	14.2	9.1	17.9	8.8
Item 2	Station 33.5	Subgrade	2.5	5.9	14.2	9.1	11.6	2.5
Item 2	Station 16.5	Base	3.0	6.2	6.1	34.9	42.4	7.5
Item 2	Station 29	Base	2.4	6.2	5.8	37.4	48.5	11.1

As with the EPC measurements, the deflections reported are the peak values from the 10 min of data collected after a predetermined traffic level was reached. Figure 30 is a representative plot of the 10-min SDD data



that was collected and used to derive the peak value changes over time. SDD peak value changes during trafficking are shown in Figure 31.

Figure 31. SDD peak value changes during trafficking.



Deflections for the geogrid-stabilized Item 2 were higher than the deflections for the unstabilized Item 1. This response was anticipated especially at the initial onset of trafficking due to the thickness of the HMA and base-course layers on Item 2 being less than Item 1.

7.5 Geogrid strain gauges

Measurement of strain in the geogrid is an important parameter that can be used to compare geogrids to one another as well as help develop predictive numerical models of pavements stabilized using geogrids. More importantly strain gauges on the geogrids show the mobilization of the tensile strength of the geogrid under loading. For this testing, geogrid strain gauges were installed in several locations on the geogrid, as previously shown in Figure 12. The base course creates a harsh, unfavorable environment for the installation of strain gauges; therefore, the survival rate of the geogrid strain gauges is low. After installation, only one of the three gauges was functioning correctly. The surviving gauge was labeled as S1 in Figure 12 and

was perpendicular to the direction of traffic. Raw geogrid strain gauge data is located in Appendix C.

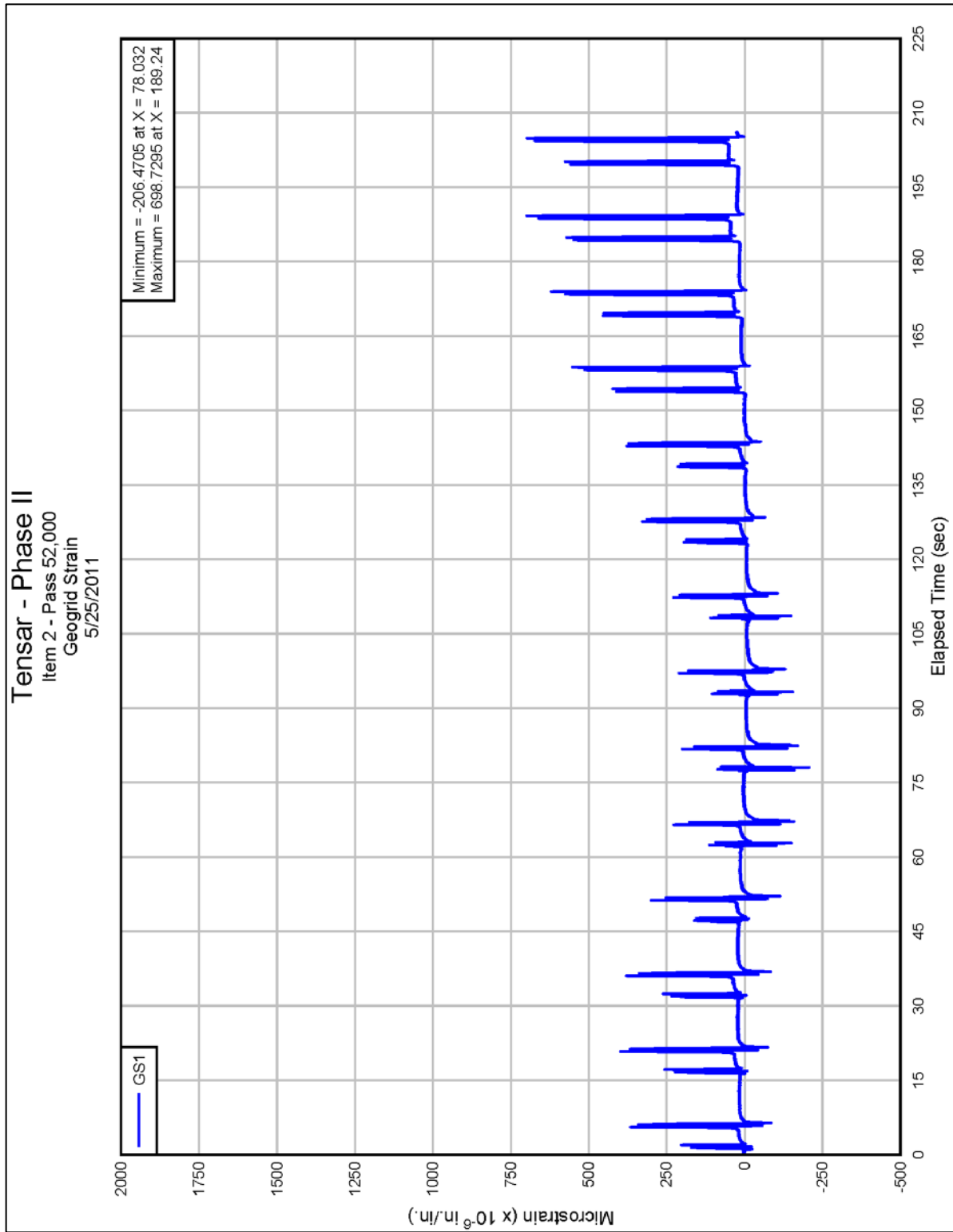
At the onset of testing, instrumentation response was recorded after predetermined traffic intervals. As testing progressed, response was also recorded after any significant change in pavement rutting in addition to the recording at specified traffic intervals. Also, as with the previously discussed instrumentation, instrumentation response was recorded for 10-min intervals after each data collection point. Figure 32 displays a typical plot of the geogrid strain gauge response for the 10-min collection period. Positive strain readings are indicative of tension and negative readings indicate compression. Figure 33 displays the peak values of each gauge and how these values changed during trafficking.

7.6 Asphalt strain gauges

Asphalt strain gauges (ASGs) were installed at Stations 12.5 and 37.5 for this study. Two strain gauges were placed at each station with one measuring the transverse direction and the other measuring the longitudinal direction. As with the previous trafficking data, at the onset of testing, instrumentation response was recorded after predetermined traffic intervals. As testing progressed, response was also recorded after any significant change in pavement rutting in addition to the recording at specified traffic intervals. Instrumentation response was recorded for 10-min intervals after each data collection point. Raw ASG data are located in Appendix D.

After installation and construction were complete, it was determined that all the ASGs for the unstabilized Item 1 were functioning properly and only the ASGs at Station 37.5 for the stabilized Item 2 were functioning properly. Figure 34 displays a typical plot of the ASG response for the 10-min collection period. Peak tensile strain values were selected from the 10-min test data. Figure 35 displays the peak tensile strain values for each location and how these values changed during trafficking.

As displayed in Figure 35, the strain at the bottom of the asphalt layer increased immediately after the environmental chamber malfunction. The peak strain readings for Item 2 increased 12% from 614 microstrain before the event to 686 microstrain after the event. For comparative purposes, the change in max tensile strain for Item 1 for the same traffic interval was essentially zero with an actual -1.8% decrease. These readings further rein-



force the conclusion that the rutting in Item 2 was due to the elevated temperatures experienced during the equipment malfunction.

Figure 33. Geogrid strain gauge peak changes during trafficking.

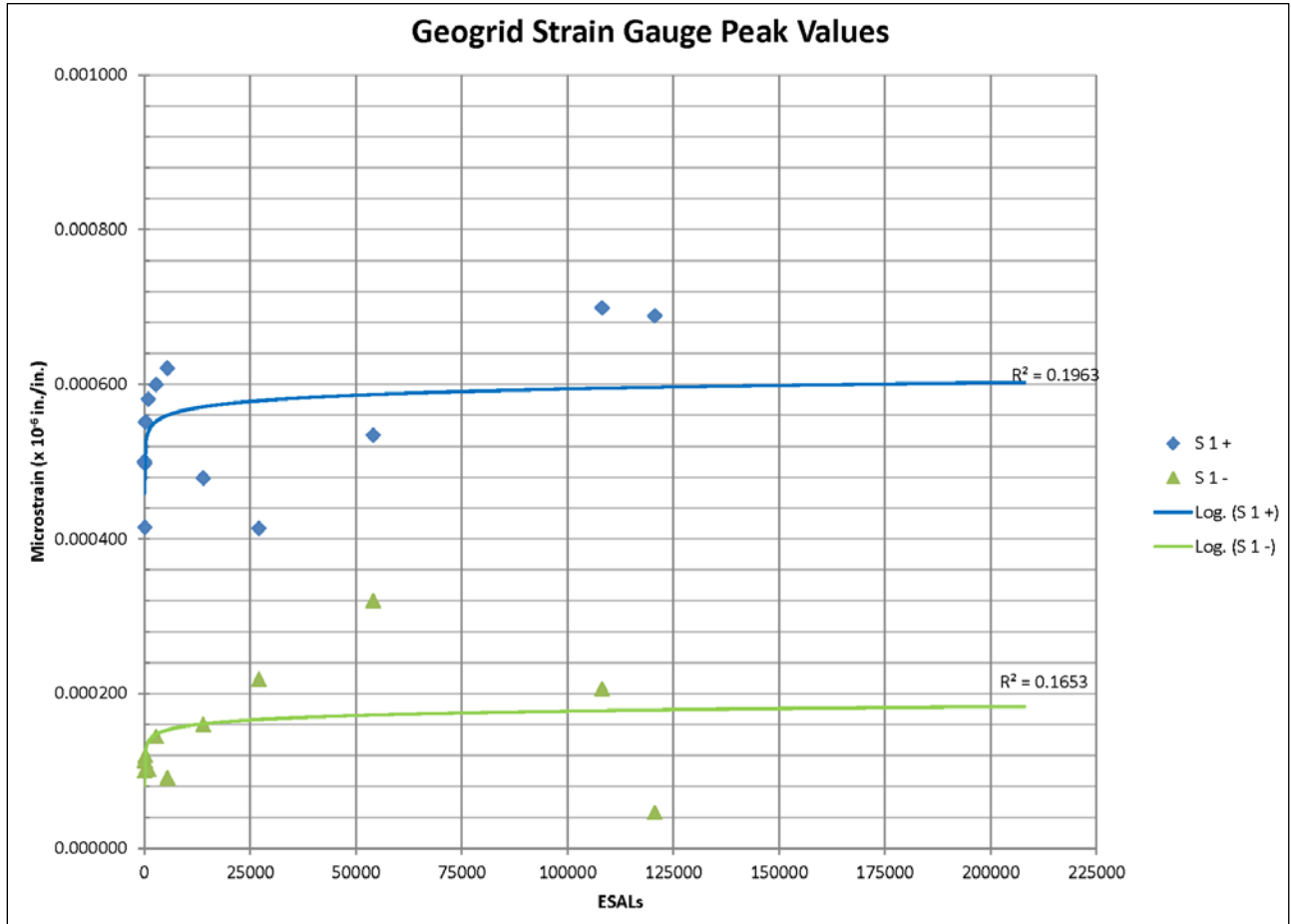


Figure 34. Asphalt strain gauge values for 10-min test after 26,000ESALS (13,000 passes).

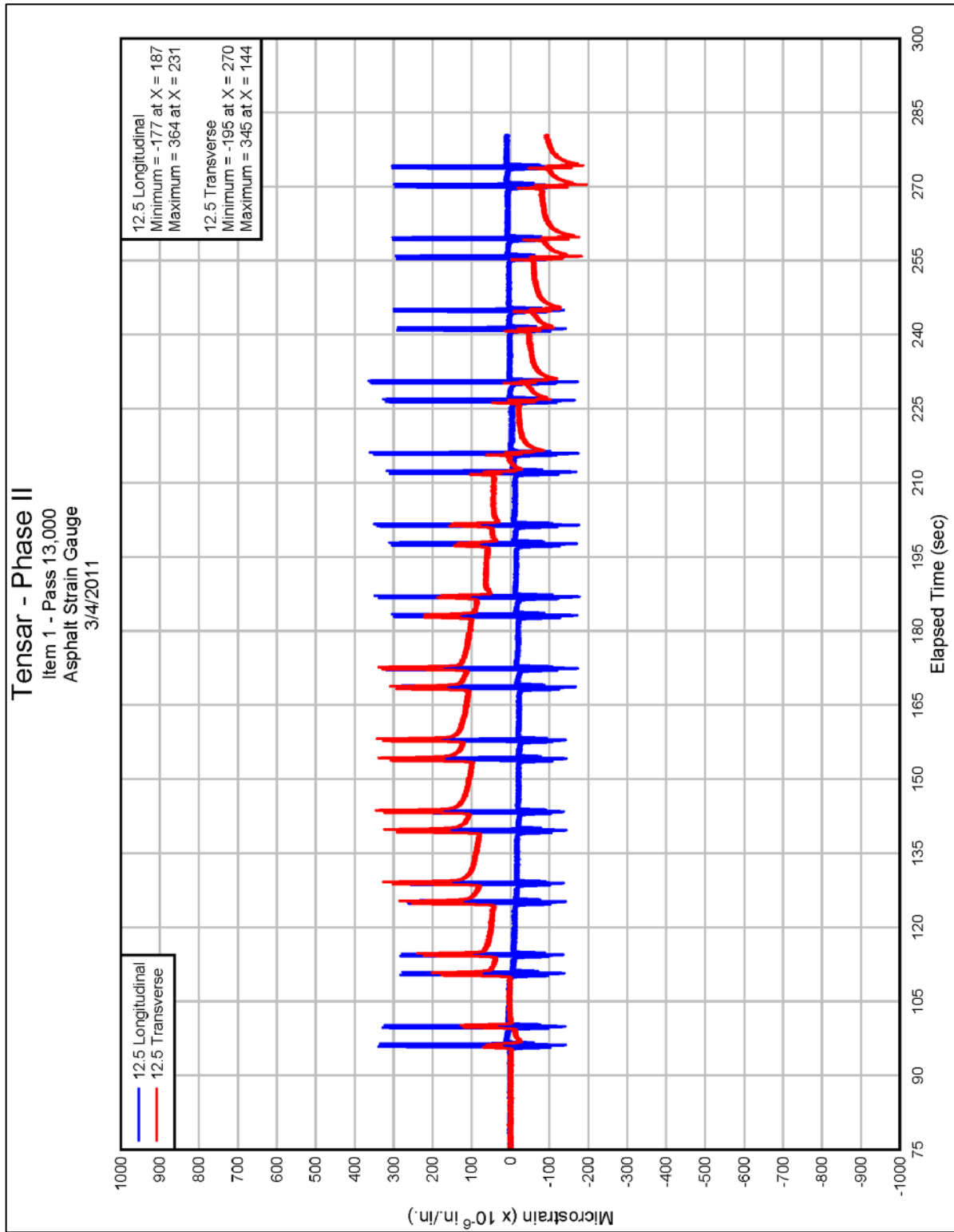
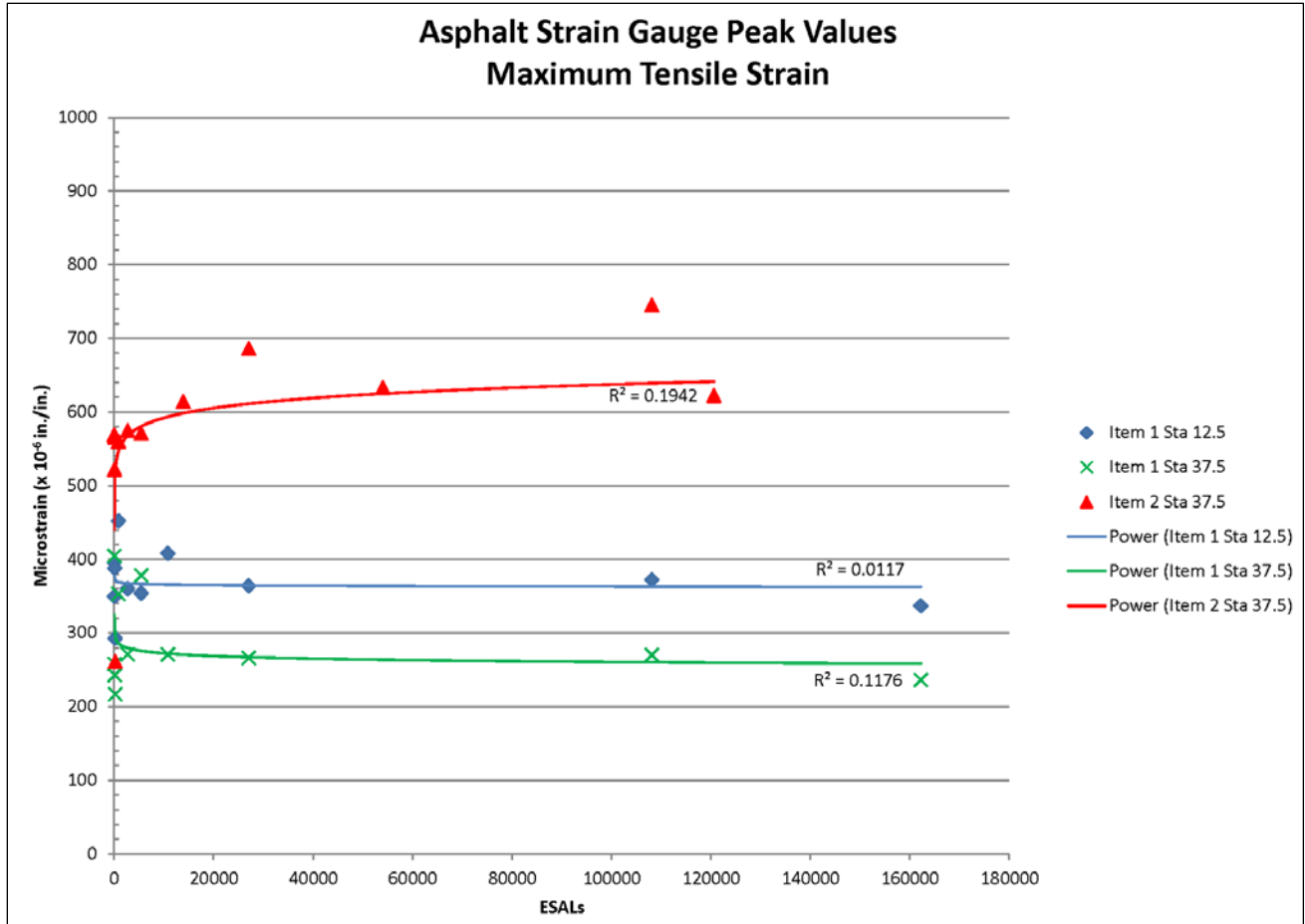


Figure 35. ASG peak tensile strain value changes during trafficking.



8 Post-test Forensics

Upon conclusion of traffic testing, each lane was trenched in two locations to further investigate the method of pavement failure. Trench locations were based on location of maximum and minimum rutting in each lane. Each trench was approximately 3 ft in width and started with excavation of the HMA surface. Measurements of layer thickness were recorded at each location. Additionally, in-field CBR tests, nuclear density measurements, and moisture contents were conducted on each layer within the wheel path and outside the wheel path. Results from the tests are displayed in Table 8. The post-test densities for the CH subgrade material show minor changes of -0.3 and 0.8 pcf for Items 1 and 2, respectively.

Table 8. Post-test test-section properties.

Test	Item 1	Item 2
	4-in. Nominal AC Unstabilized Base	3-in. Nominal AC Stabilized Base
CH Subgrade Properties		
Wet Density (pcf)	113.9	115.8
Dry Density (pcf)	88.6	89.2
Moisture (%)	28.1	30.2
Oven-Dried Moisture (%)	30.1	29.6
CBR In-Place (%)	11.0	9.5

Due to the disturbance of the base course when removing the HMA layer, CBR tests were not conducted on the top layer of the base course. The granular material was loose from the excavation, and results from any attempted CBR tests would have been unreliable. Care was taken when excavating the base course to avoid damage to the geogrid before inspection. Inspection of the trenches in Items 1 and 2 confirmed there was no failure in the subgrade for either Item. Figures 36 and 39 show the excavated trenches of both test items at the completion of post-traffic testing. Figures 37 and 40 are graphical depictions of the individual layer thicknesses post excavation. From Figures 36 and 39 it can be seen there was no damage to the subgrade layer in Item 1 and Item 2. Visual observation indicates failure occurred mostly in the HMA of Item 2. The damage in the base-course layer of Item 2 is more than likely a result of the reduced thickness in the HMA layer caused by shear flow of the asphalt

during the temperature spike from the environmental chamber failure. Figure 38 shows the geogrid upon excavation of the overlying base-course material in Item 2. From Figure 38, the indentions in the subgrade are indicative of good aggregate strike-through and therefore good aggregate interlock with the geogrid.

Figure 36. Item 1 excavated trench.



Figure 37. Item 1 post-traffic layer thicknesses.

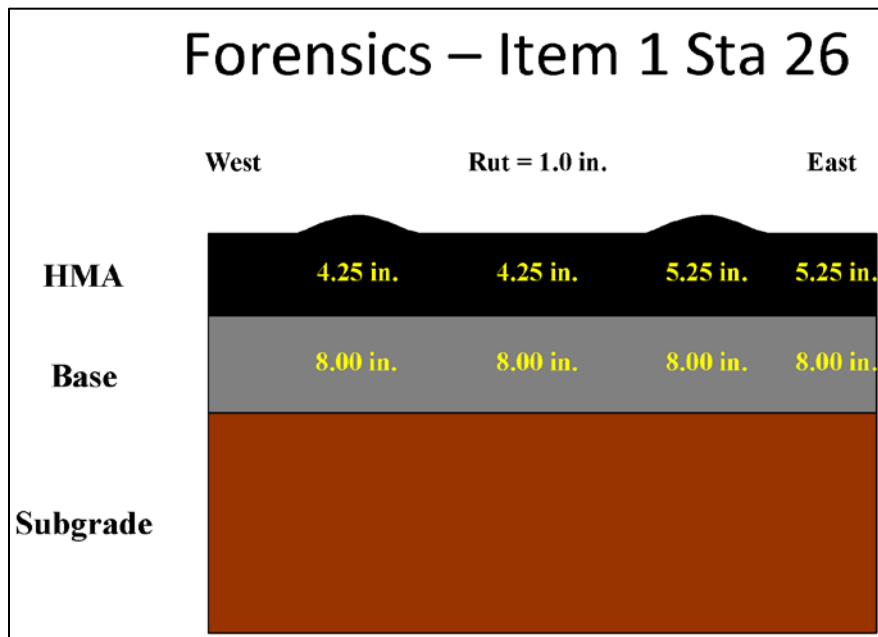


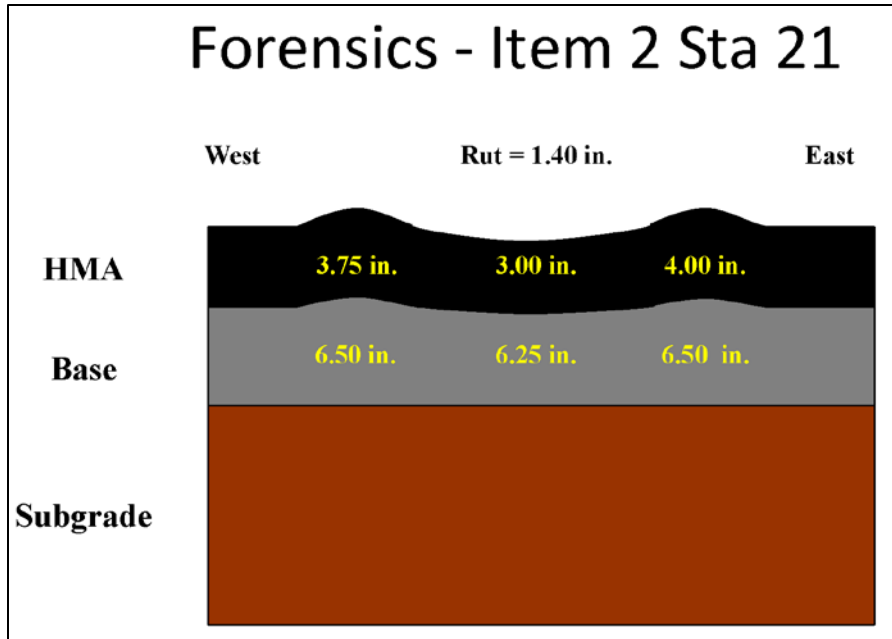
Figure 38. Excavated geogrid in Item 2.



Figure 39. Item 2 excavated trench.



Figure 40. Item 2 post-traffic layer thicknesses.



9 Conclusions and Recommendations

In this study, a full-scale test section was constructed and trafficked to evaluate the performance of geogrid-stabilized roads. Several conclusions and recommendations were generated after analysis of the construction and traffic data. The following conclusions are a result of the study:

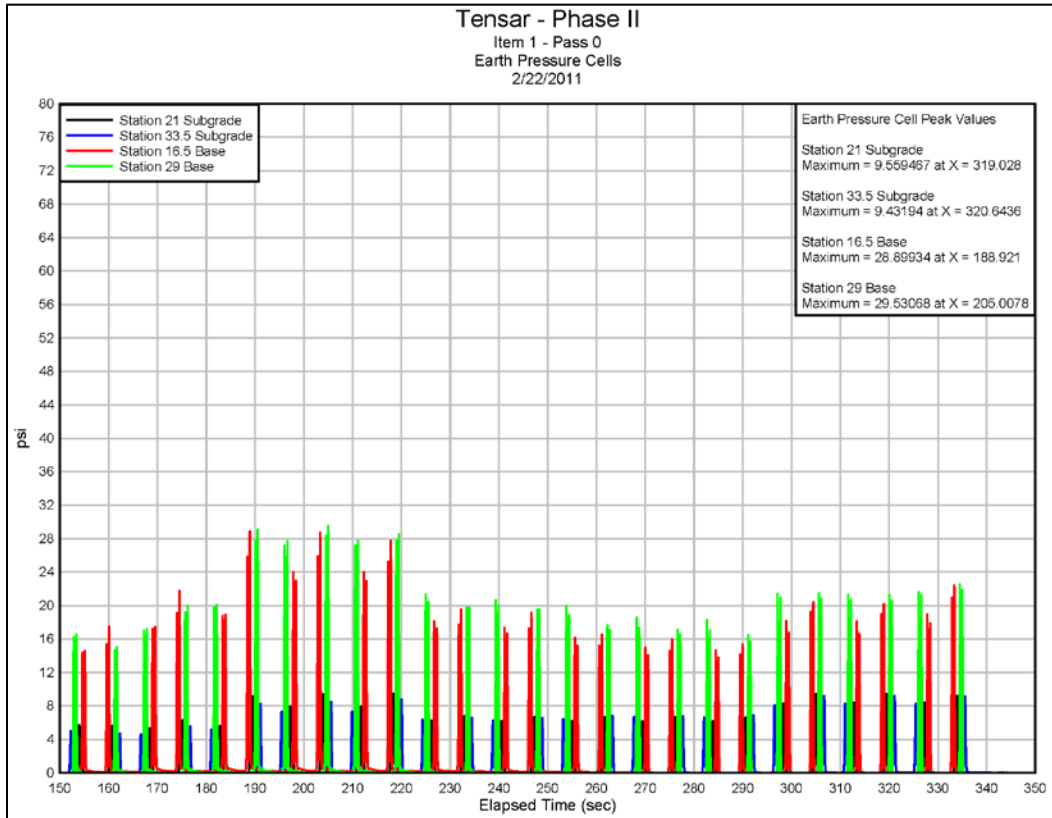
1. The pavement test items were constructed in a uniform manner with minor variability between test items. The uniformity of construction allows meaningful comparisons between test items.
2. The geogrid-stabilized pavement section performed equally as well as the thicker unstabilized pavement section up until the point the environmental chamber of the HVS malfunctioned causing a significant temperature spike during trafficking of the geogrid-stabilized Item 2. Rutting data after this event should not be used as a performance measurement to compare the geogrid-stabilized section vs. the unstabilized section. Rutting of Item 2 after this event can be attributed to plastic flow of the HMA layer and this is confirmed by the lack of rutting in the base course and subgrade layers of Item 2 during post-test excavation.
3. Measured deflections were higher for the geogrid-stabilized Item 2 but this did not appear to influence the shearing of the subgrade in Item 2.
4. The measured deflections in both items increased initially at approximately the same rate. During later stages of trafficking, measured deflections for both the geogrid-stabilized and the unstabilized items leveled off and showed little to no increase with subsequent passes.
5. Post-test forensics showed no evidence of shearing in the base course of Item 1 and very little in the base course of Item 2. Shearing and therefore rutting in the base course of Item 2 can be attributed to the temperature spike causing a reduced thickness in the HMA layer.
6. Post-test forensics showed no evidence of shearing in the subgrade of either Item 1 or Item 2.
7. Post-test forensics showed a slight change in the test-section subgrade over time. The subgrade strength of the unstabilized Item 1 increased to a CBR of 11, whereas Item 2 had less of an increase with a post-test CBR of 9.5. The additional strength gain of Item 1 provided an additional benefit to the unstabilized item when compared to the geogrid-stabilized item.

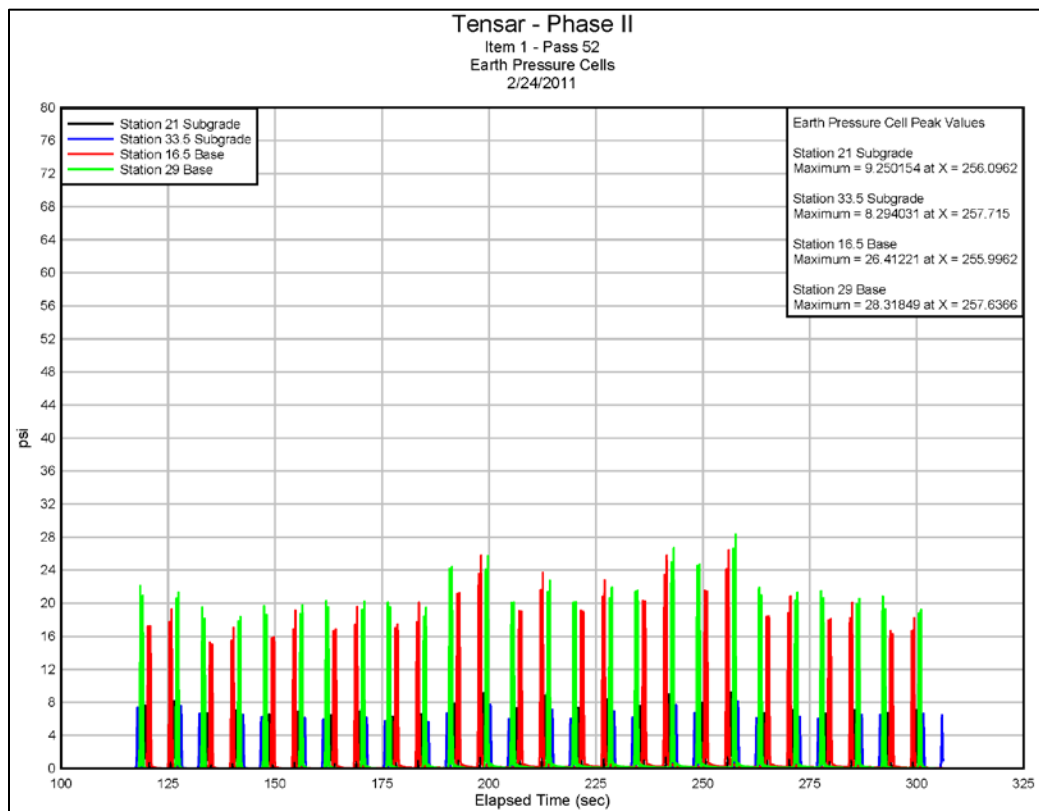
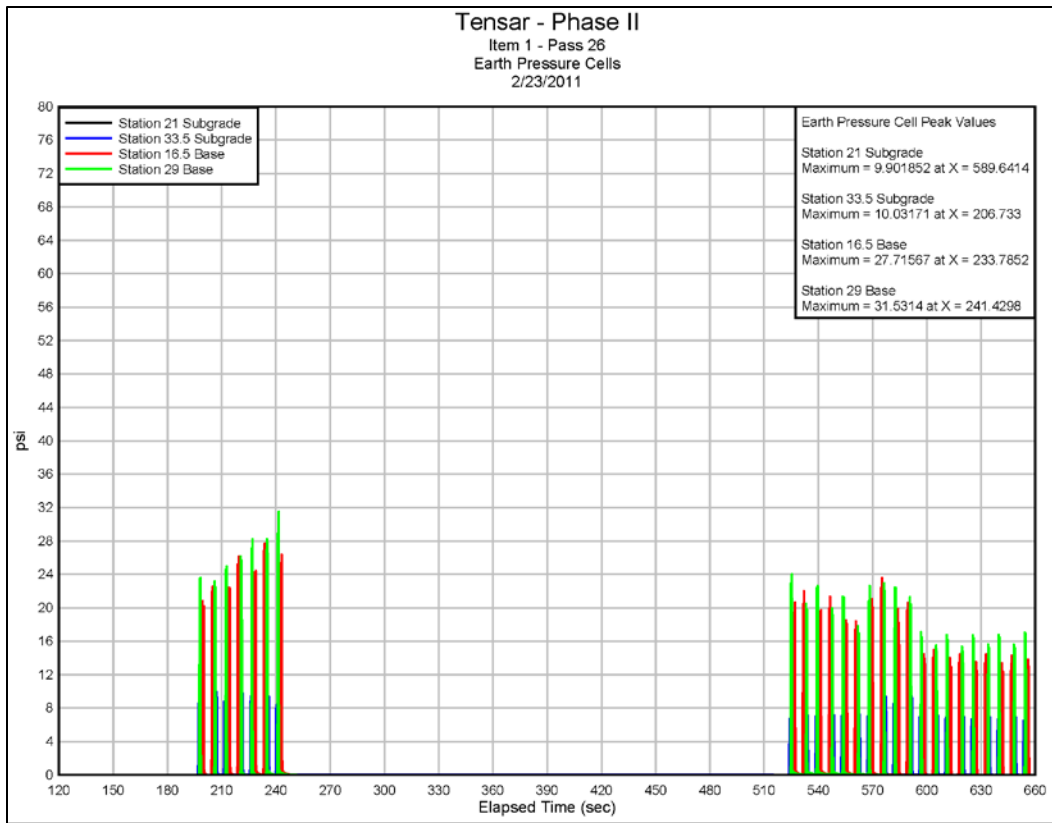
8. Further investigation into the geogrid strain responses is needed. Tensile strain responses increased during the temperature spike and decreased immediately afterwards only to increase again as trafficking progressed.

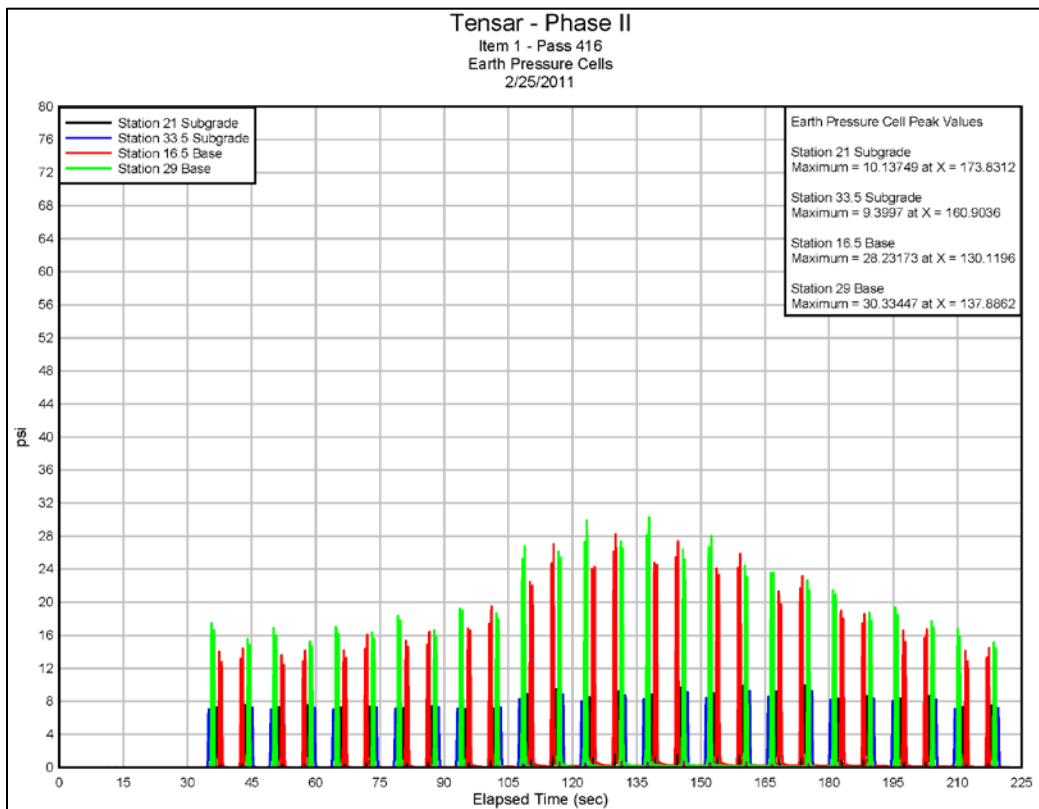
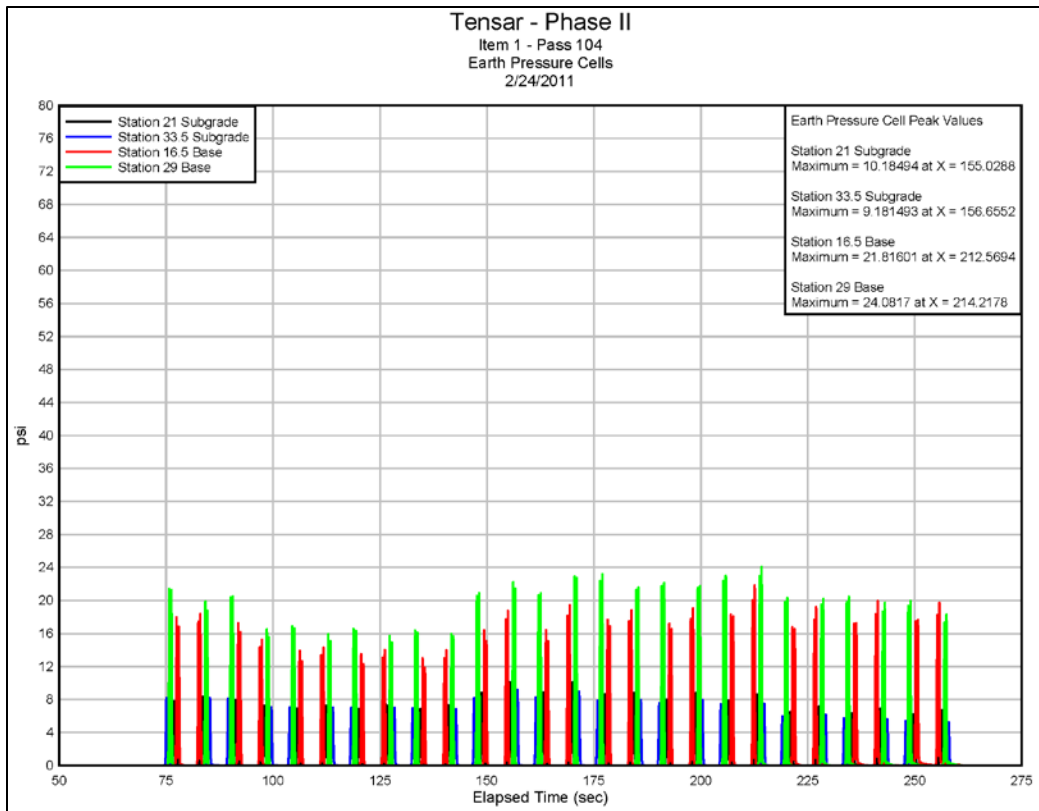
References

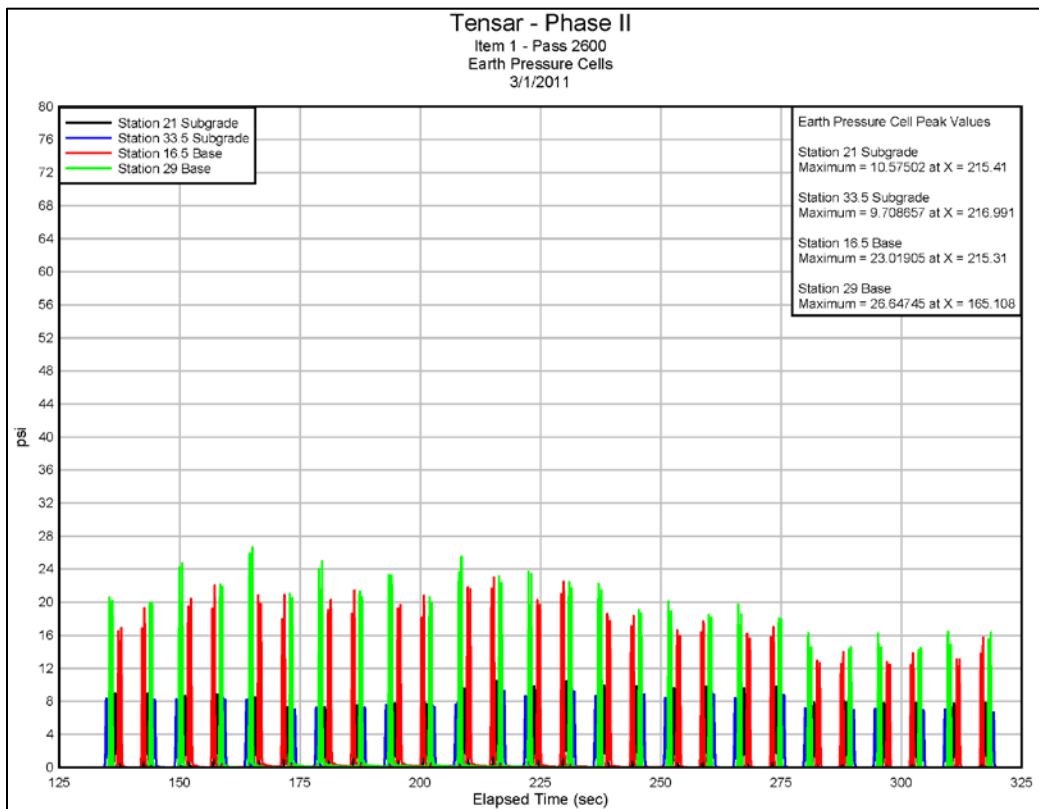
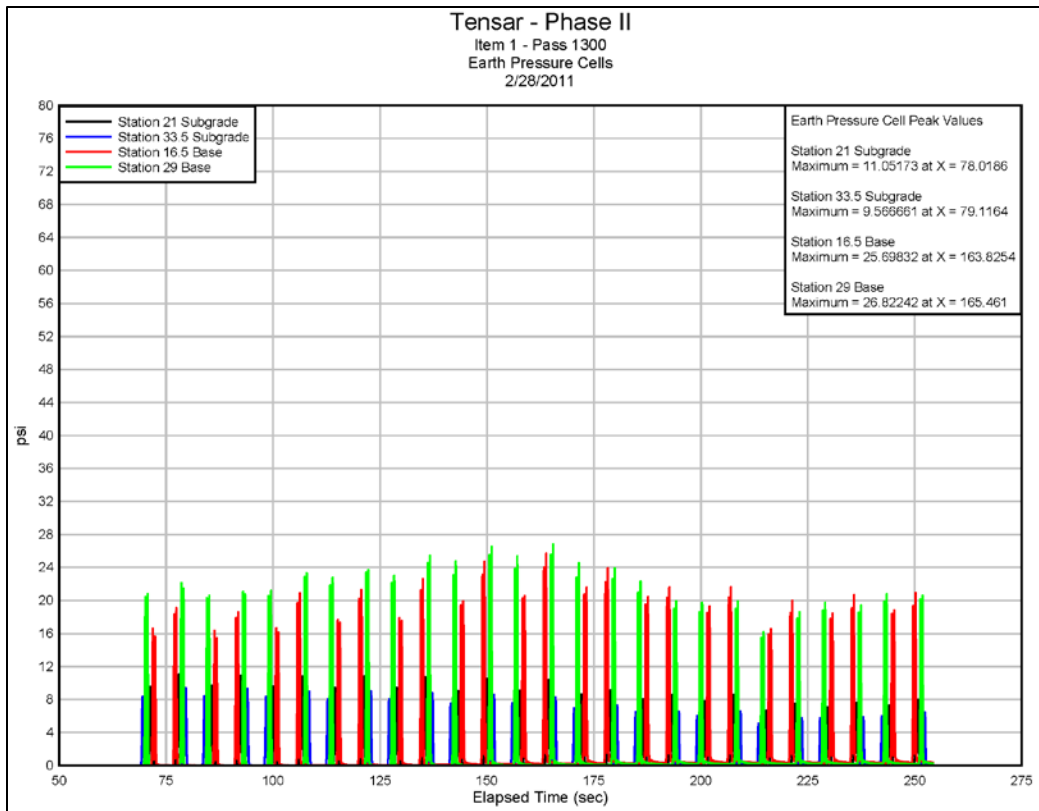
- AASHTO. 1993. *Guide for design of pavement structures*. Washington DC: Association of American Highway and Transportation Officials.
- AASHTO. 2006. *Standard method of test for sieve analysis of fine and coarse aggregates*. AASHTO T027-06. Washington, DC: Association of American Highway and Transportation Officials.
- ASTM. 2009. *Standard test method for CBR (California Bearing Ratio) of soils in place*. Designation: D4429-09a. West Conshohocken, PA: American Society for Testing and Materials.
- ASTM. 2009. *Standard test method for use of the dynamic cone penetrometer in shallow pavement applications*. Designation: D6951-09. West Conshohocken, PA: American Society for Testing and Materials.
- ASTM. 2010. *Standard test methods for in-place density and water content of soil-aggregate by nuclear methods (shallow depth)*. Designation: D6938-10. West Conshohocken, PA: American Society for Testing and Materials.
- ASTM. 2010. *Standard test methods for liquid limit, plastic limit, and plasticity index of soils*. Designation: D4318-10. West Conshohocken, PA: American Society for Testing and Materials.
- ASTM. 2011. *Standard test methods for classification of soils for engineering purposes (Unified Soil Classification System)*. Designation: D2487-11. West Conshohocken, PA: American Society for Testing and Materials.
- ASTM. 2001. *Standard test methods for laboratory compaction characteristics of soil using modified effort*. Designation: D1557-11. West Conshohocken, PA: American Society for Testing and Materials.
- Huang, Y. H. 2004. *Pavement analysis and design*. 2nd ed. Upper Saddle River, NJ: Prentice Hall.
- Timm, D. H., and A. L. Priest. 2005. *Wheel wander at the NCAT test track*. NCAT Report 05-02. Auburn, AL: National Center for Asphalt Technology.
- Tingle, J. S., and S. R. Jersey. 2007. Empirical design methods for geosynthetic-stabilized low-volume roads. *Transportation Research Record 1989*:91-101.
- Webster, S. L., R. W. Brown, and J. R. Porter. 1994. *Force projection site evaluation using the electrical cone penetrometer (ECP) and the dynamic cone penetrometer (DCP)*. Technical Report GL-94-17. Vicksburg, MS: US Army Waterways Experiment Station.
- Webster, S. L., R. H. Grau, and T. P. Williams. 1992. *Description and application of dual-mass dynamic cone penetrometer*. Instruction Report GL-92-3. Vicksburg, MS: US Army Waterways Experiment Station.

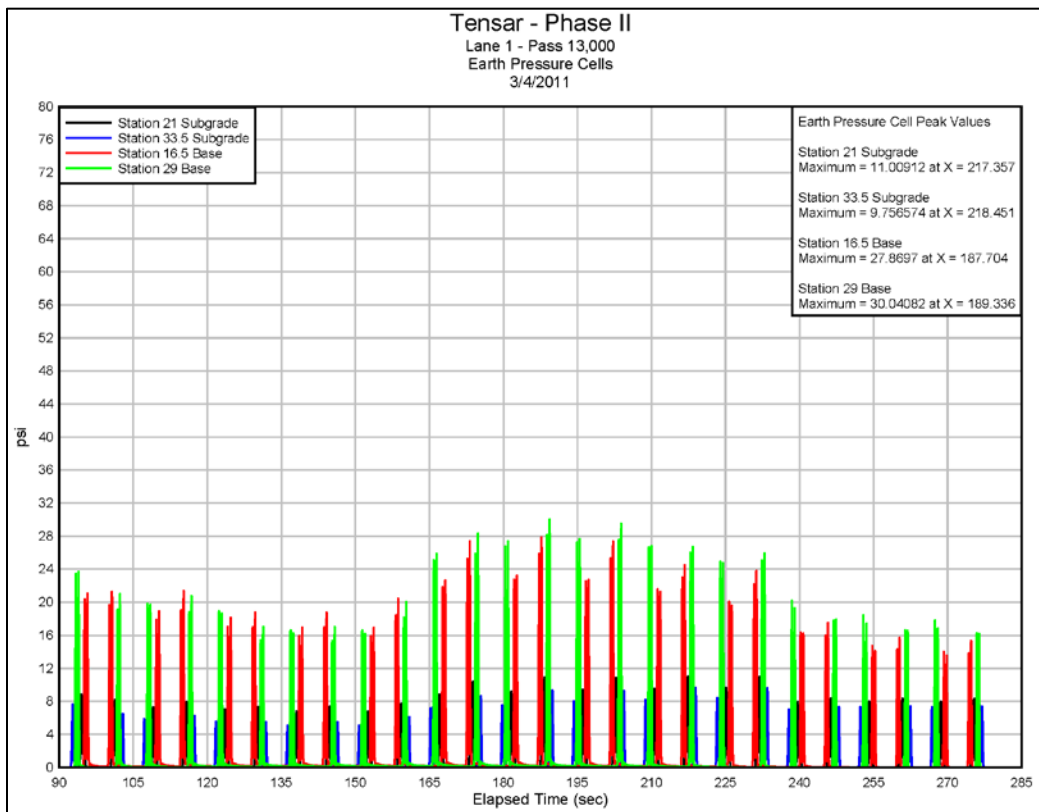
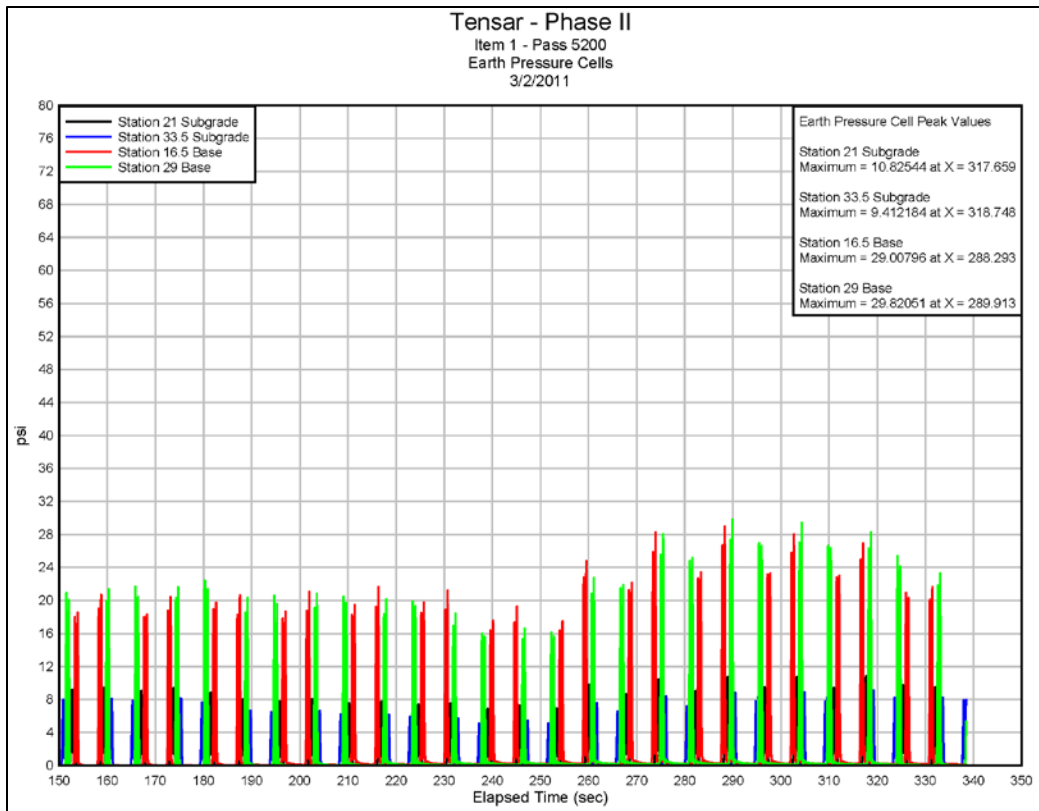
Appendix A: Earth Pressure Cell Responses

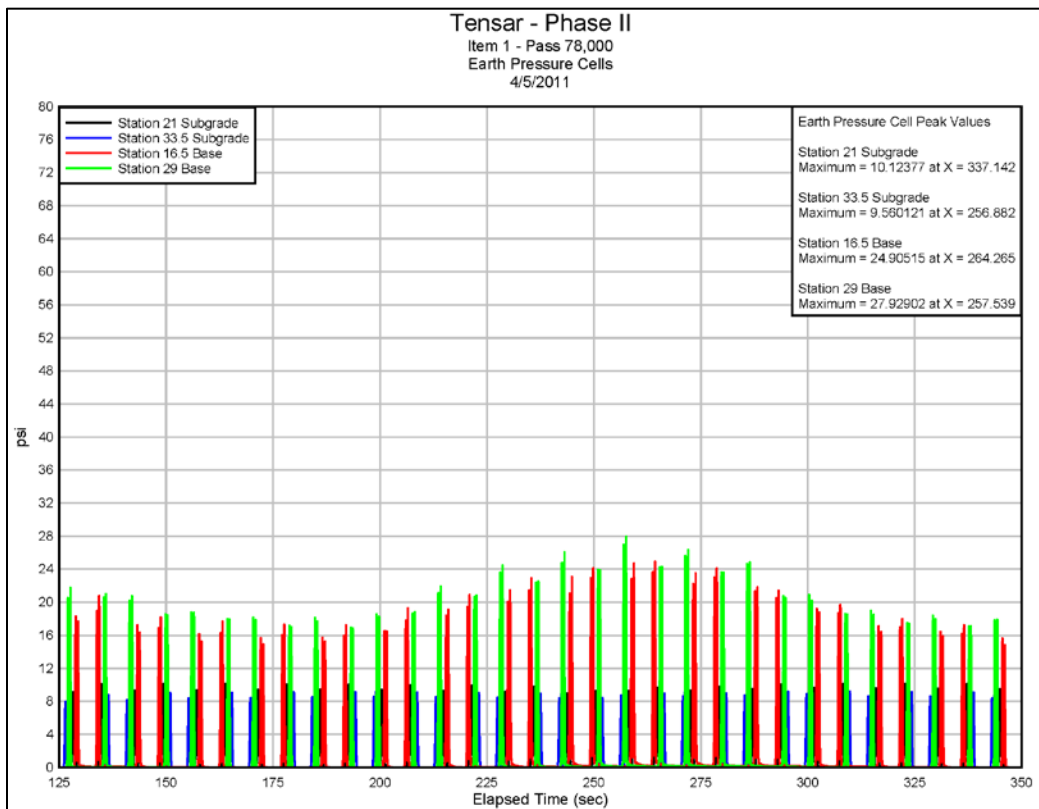
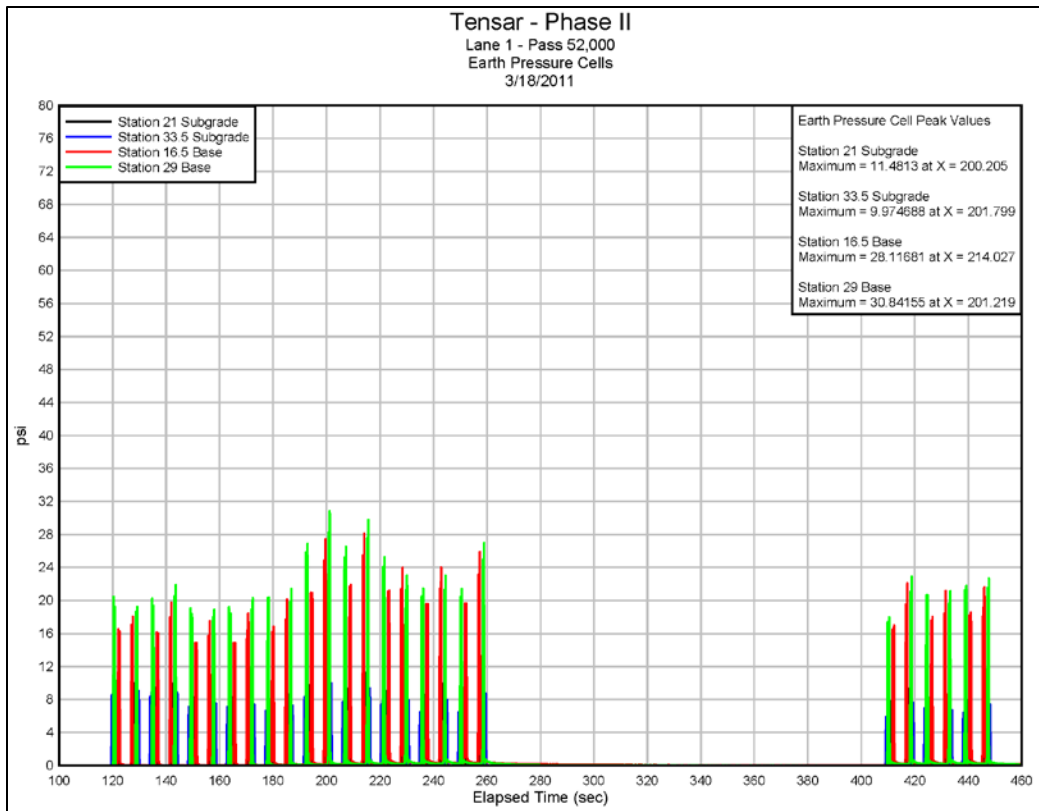


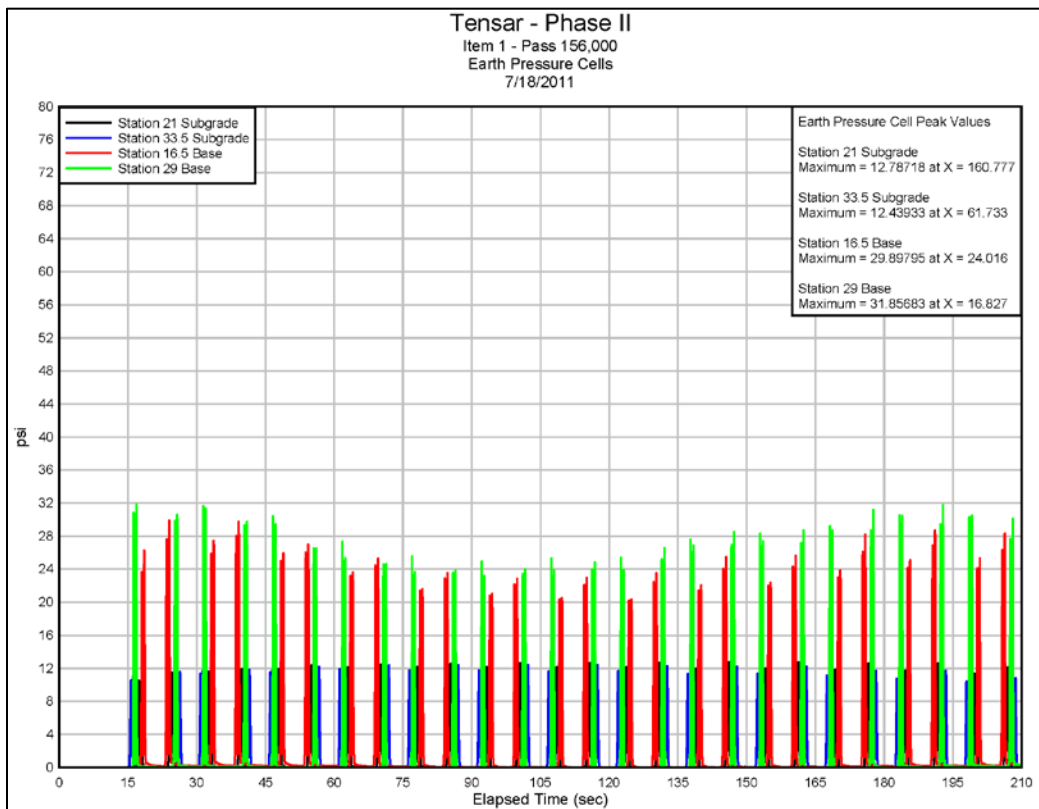
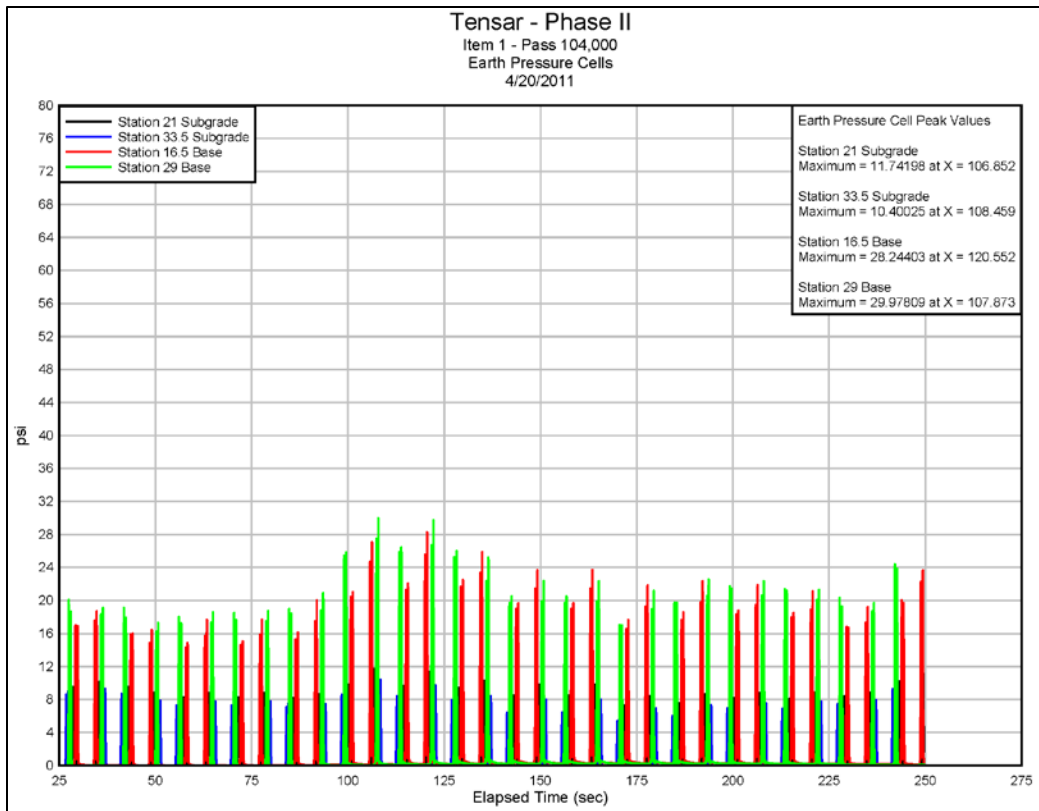


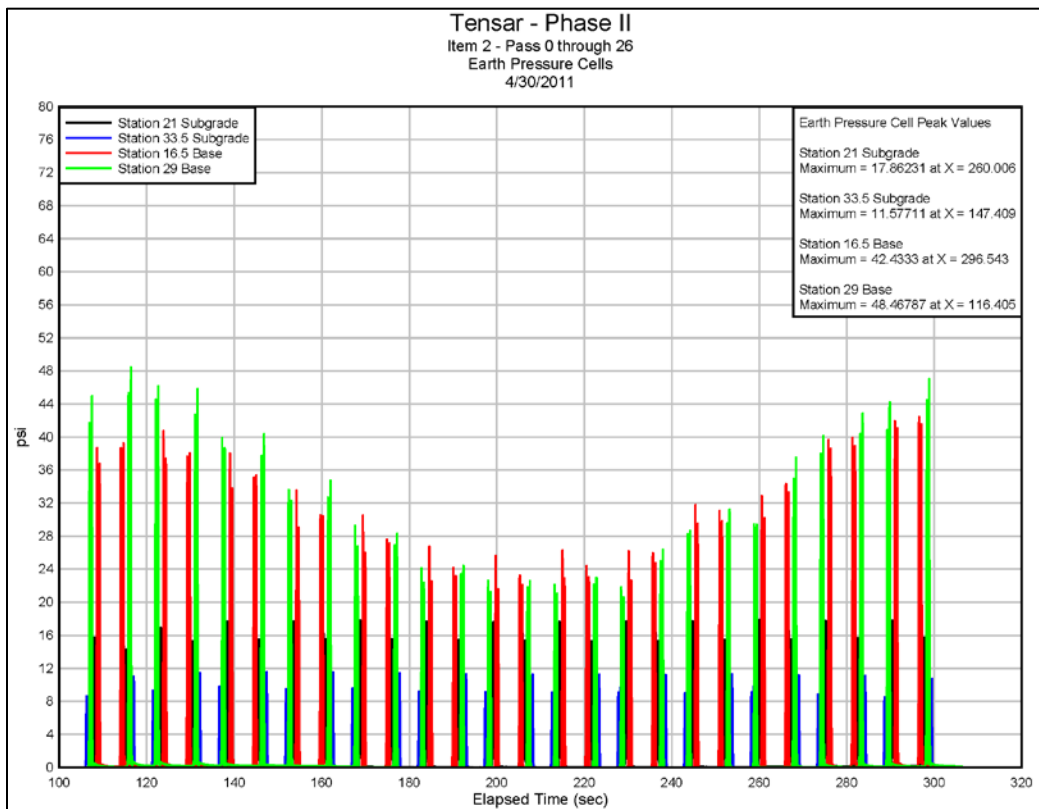
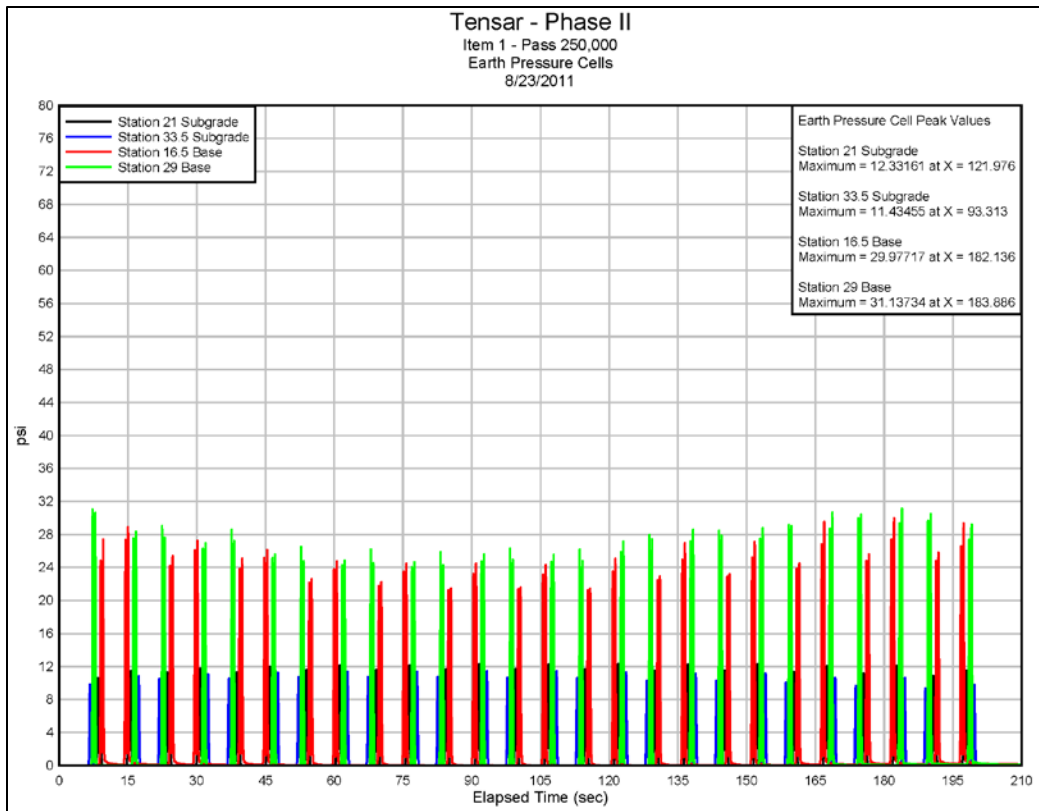


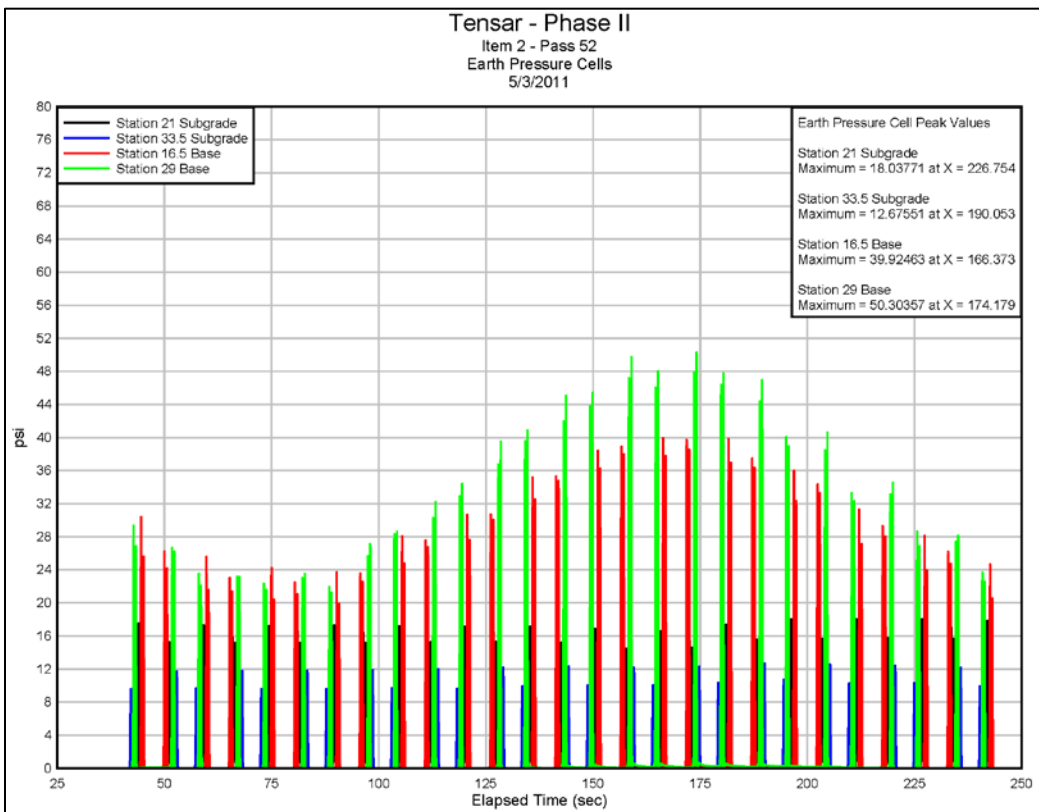
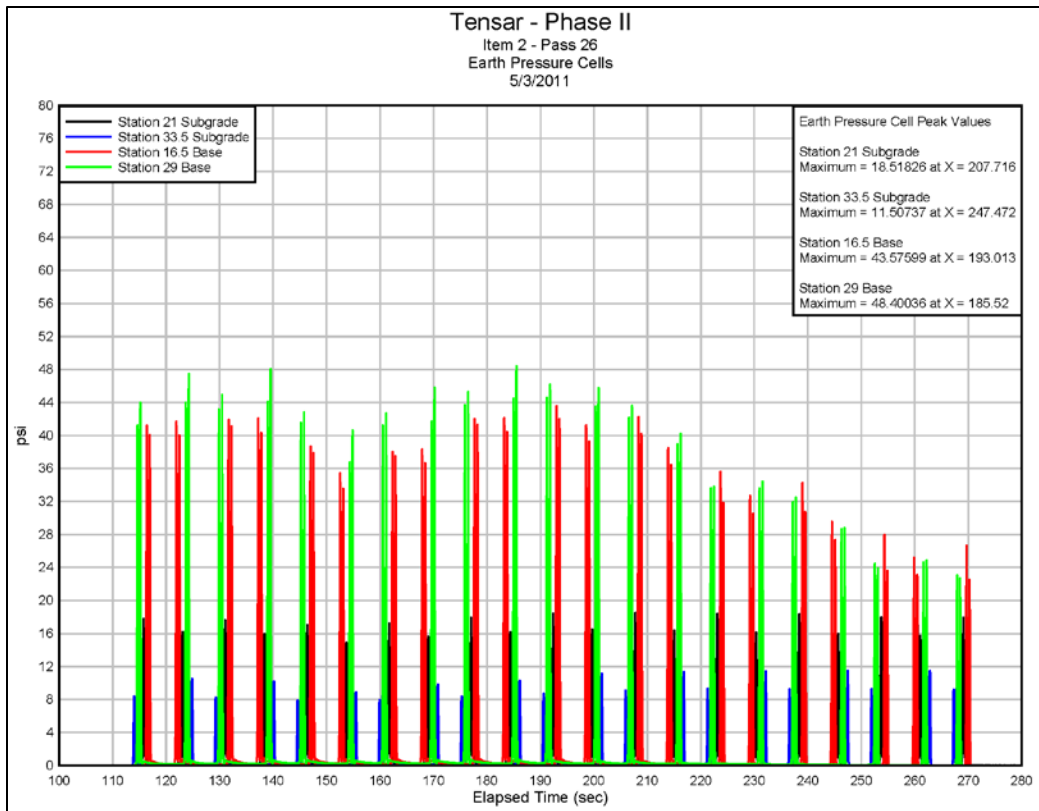


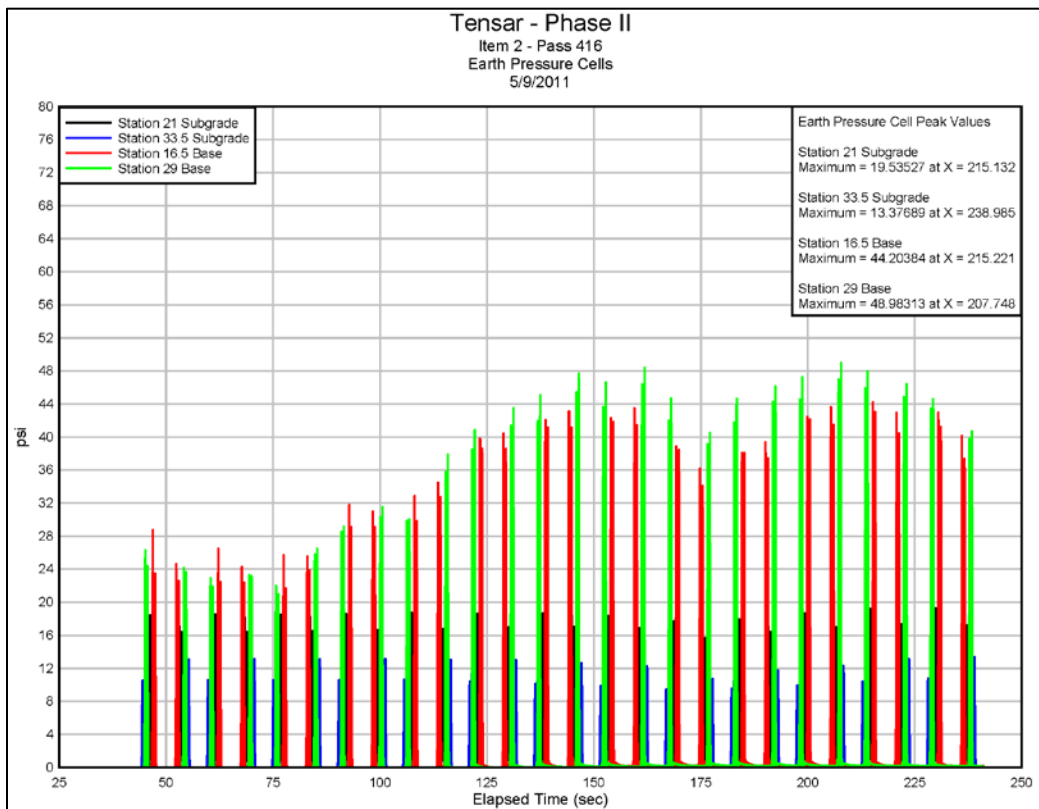
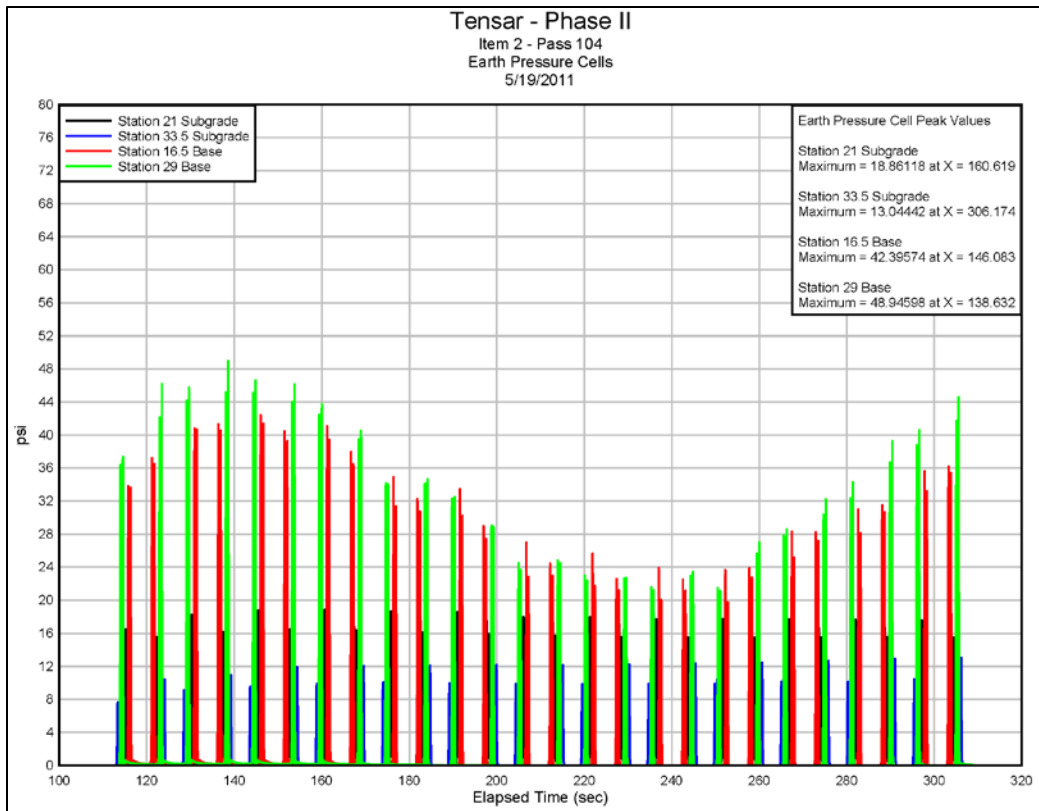


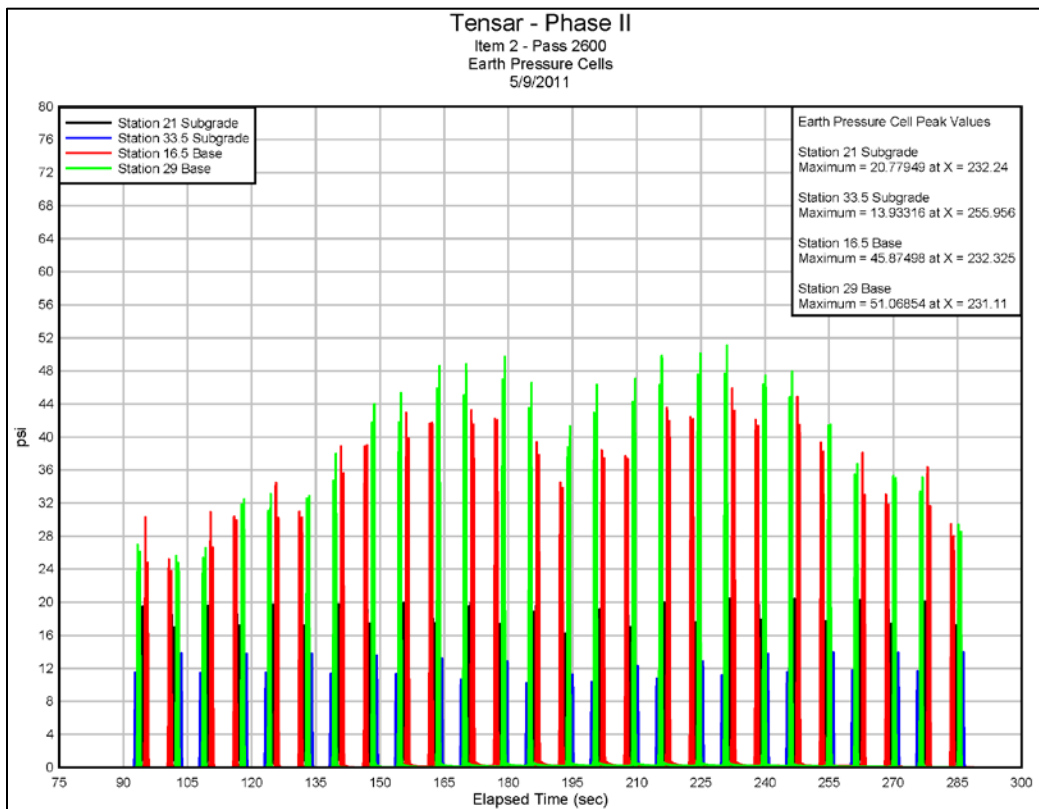
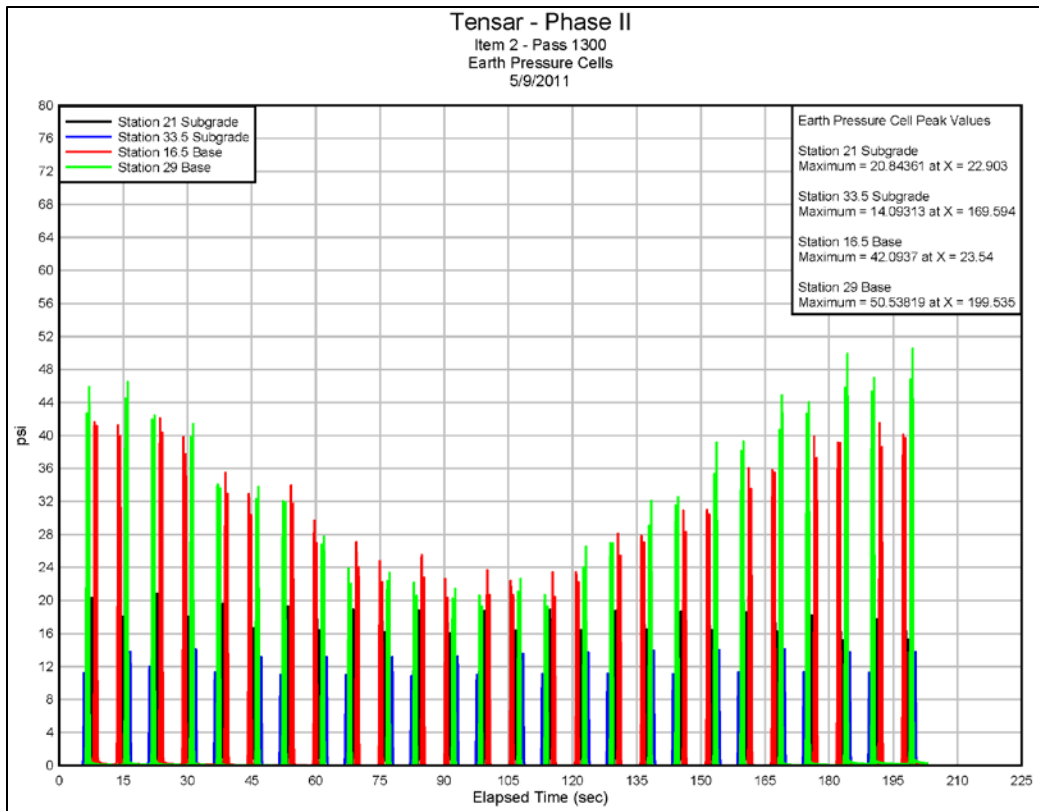


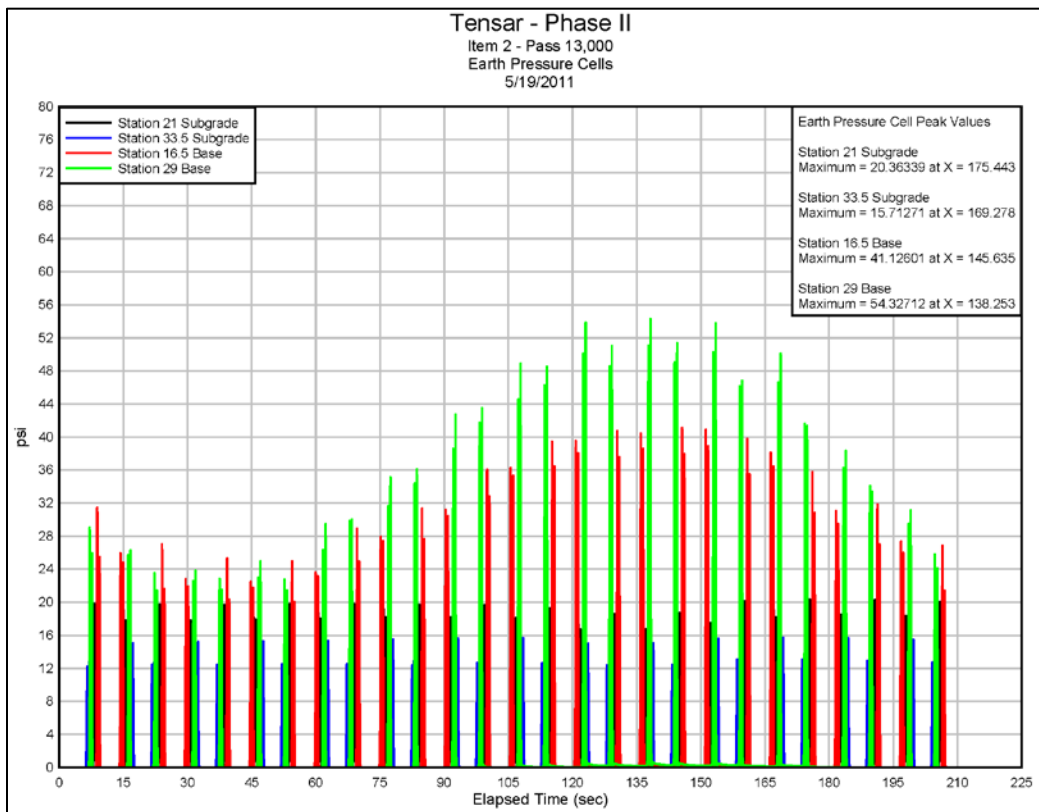
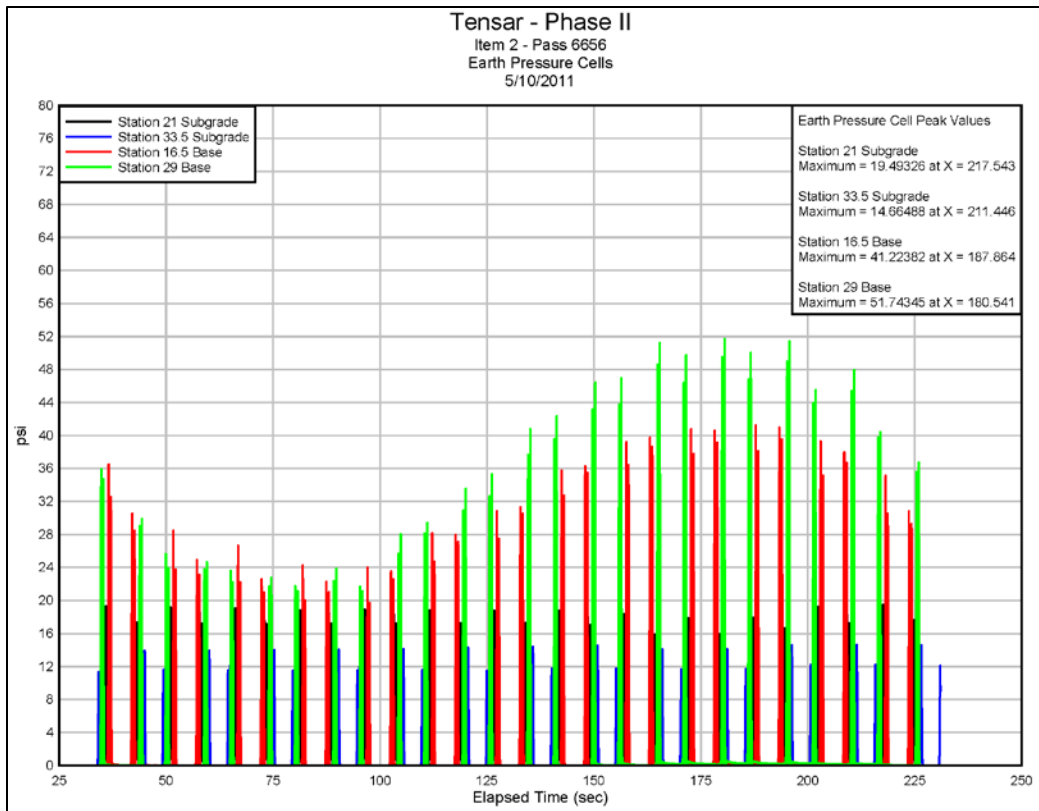


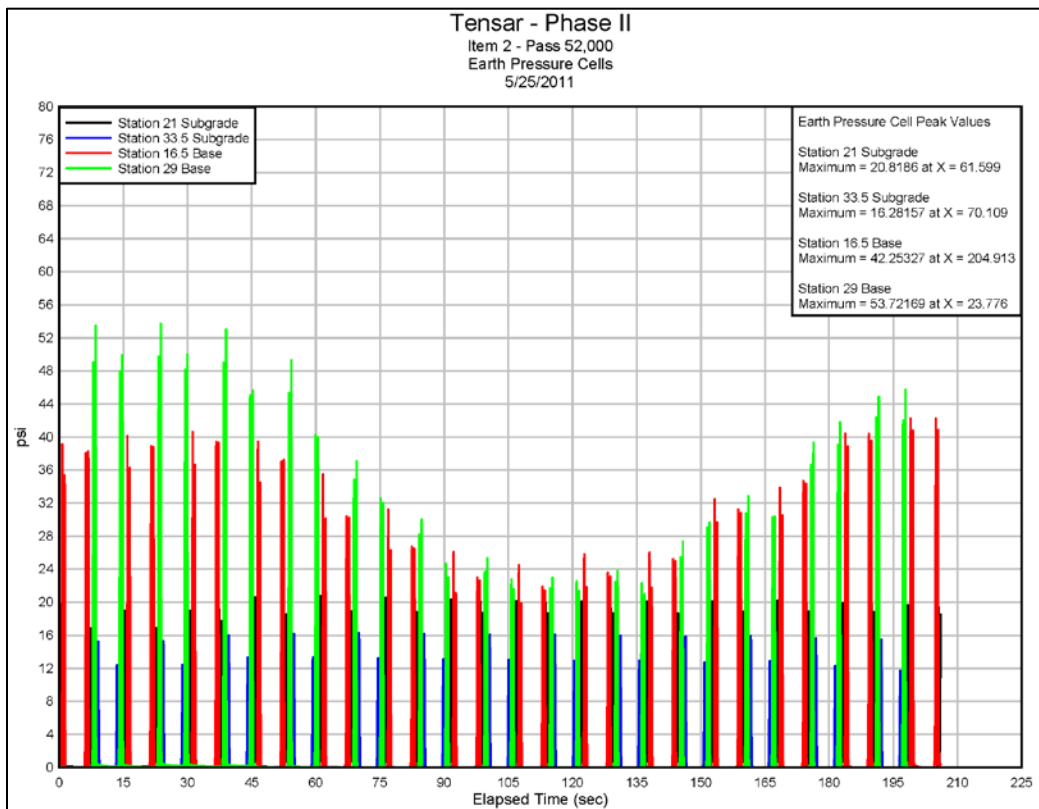
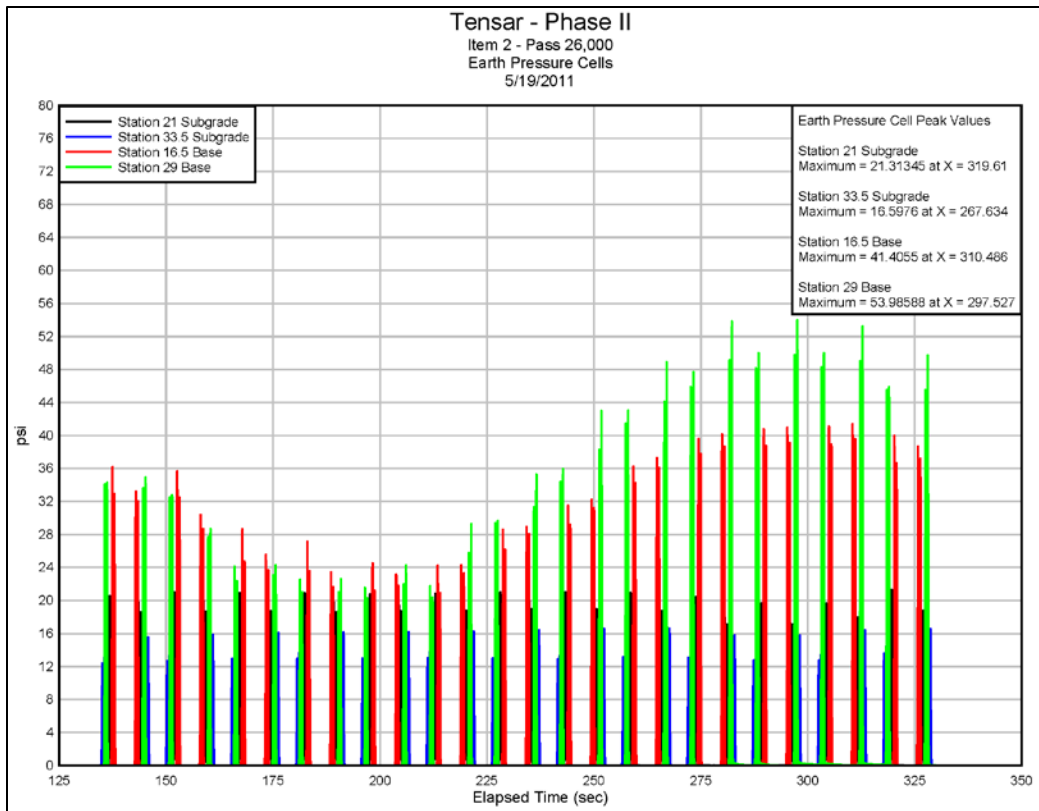


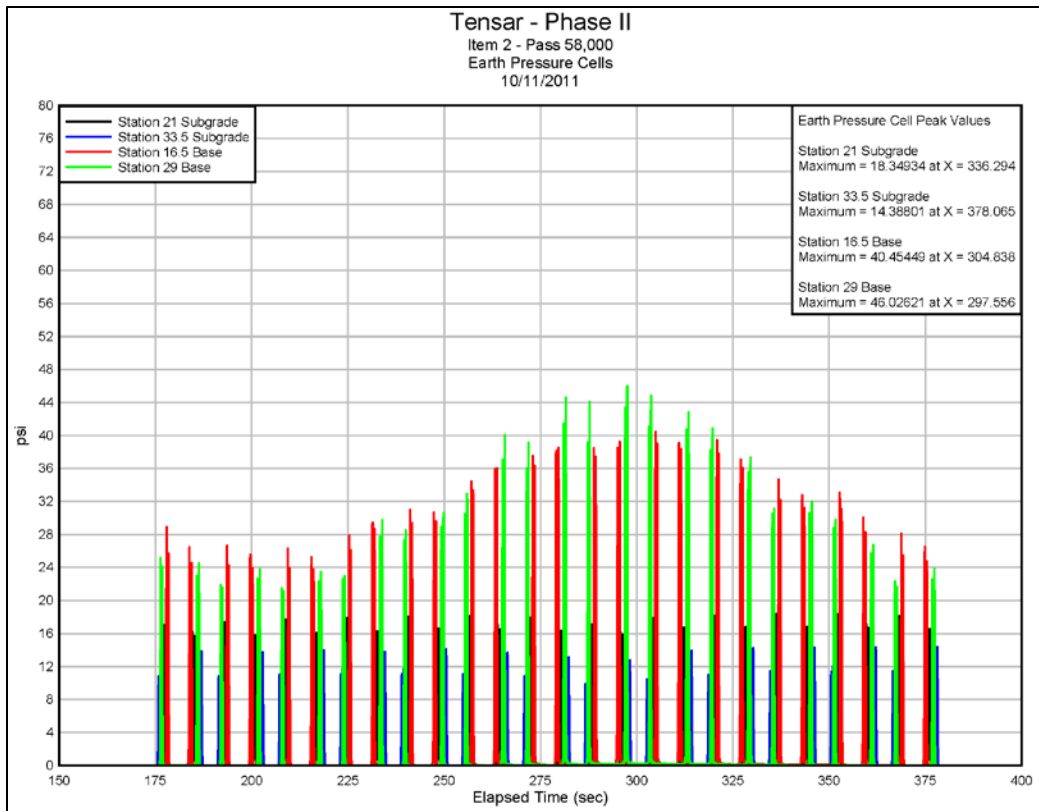




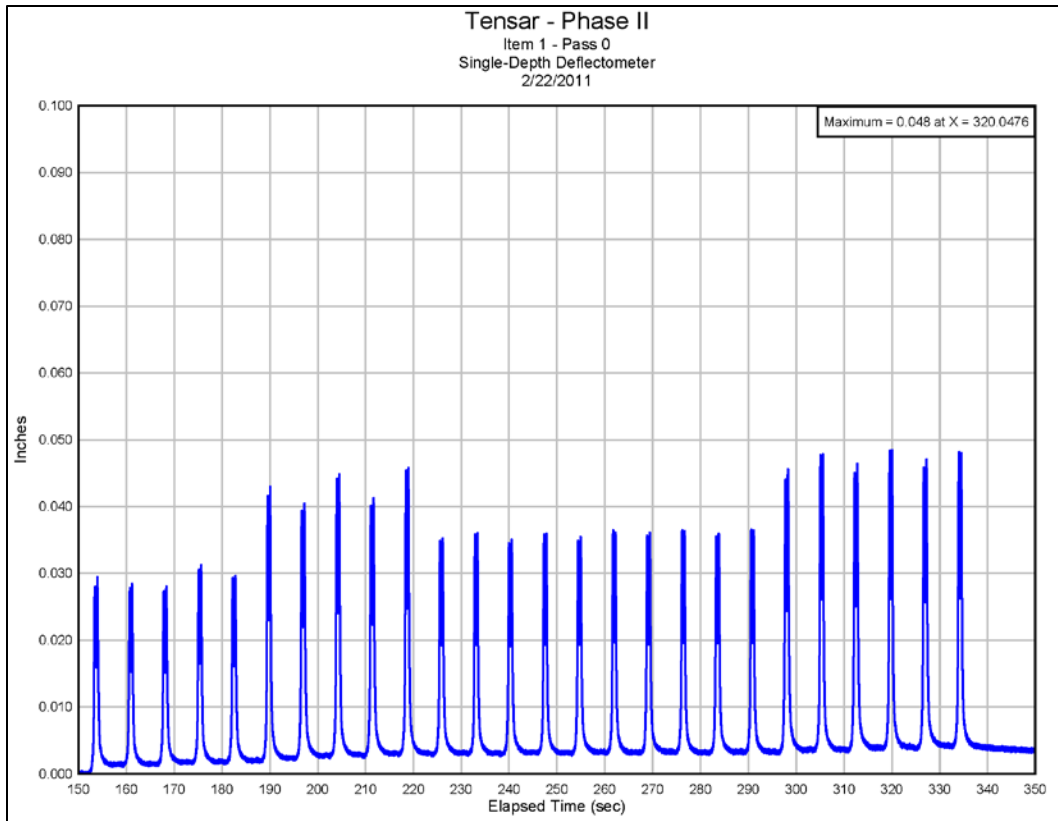


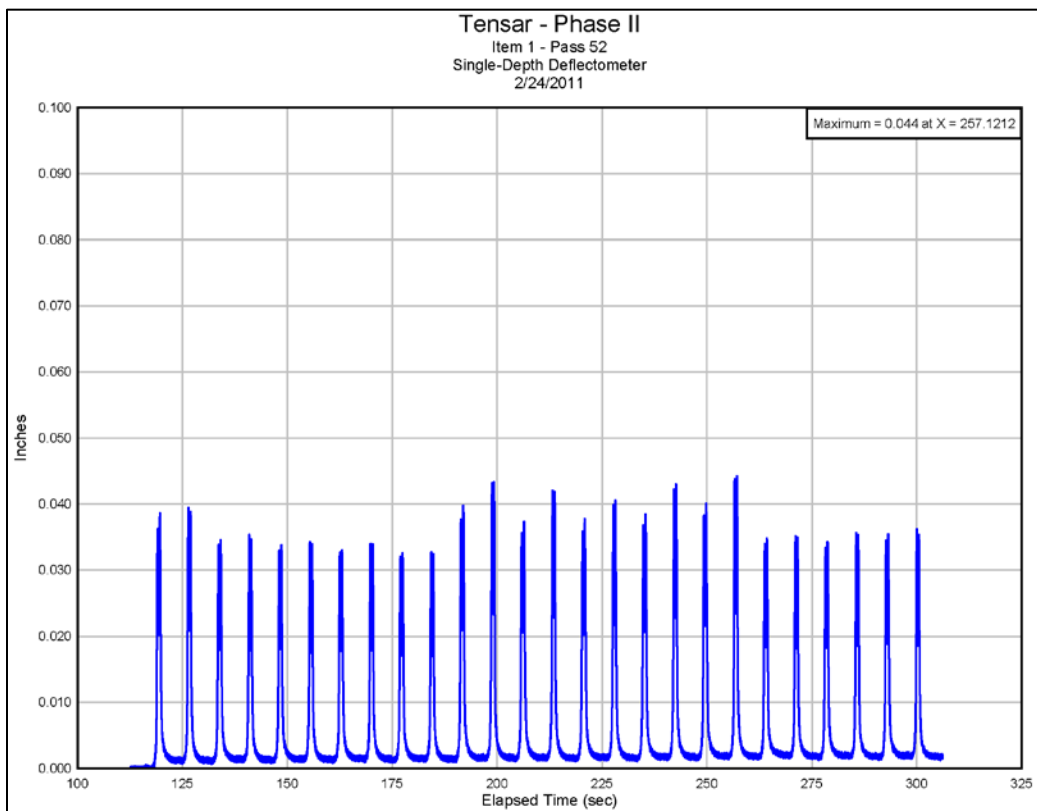
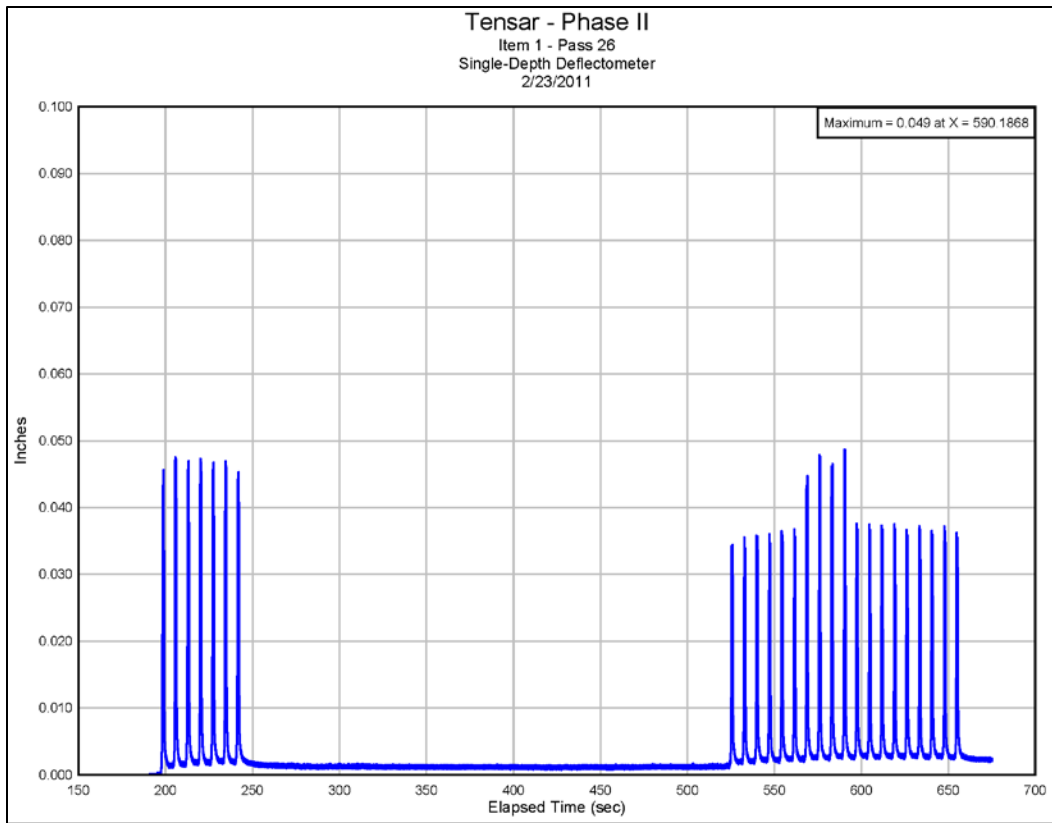


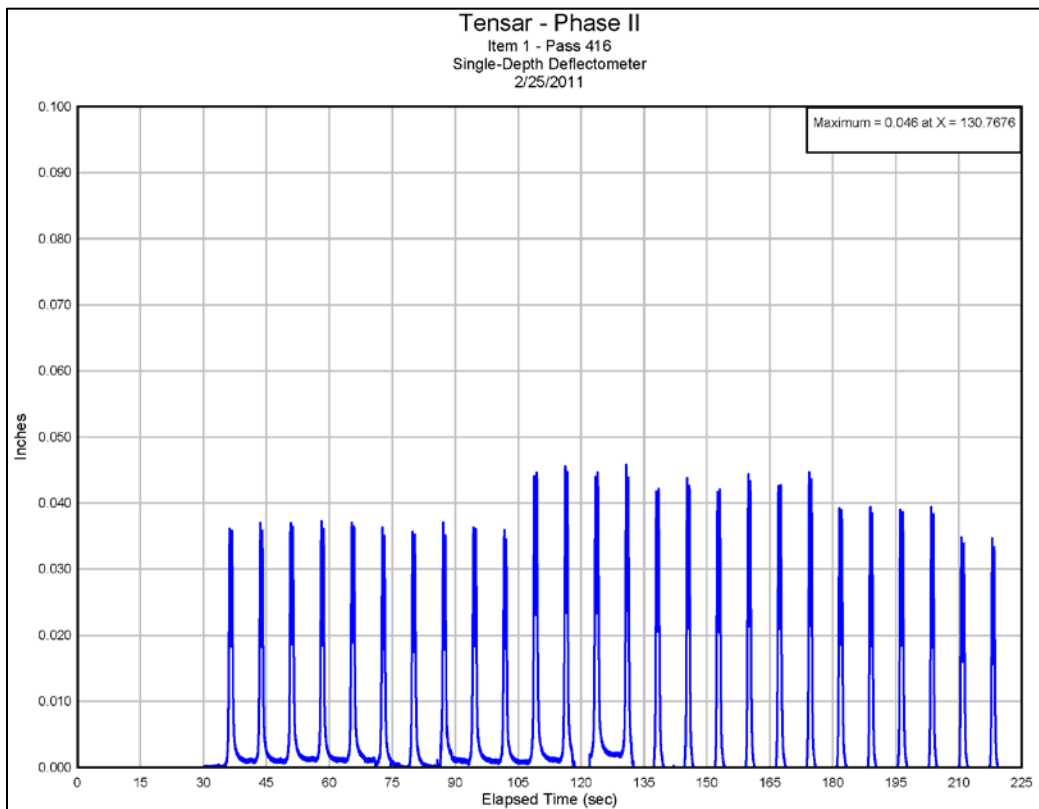
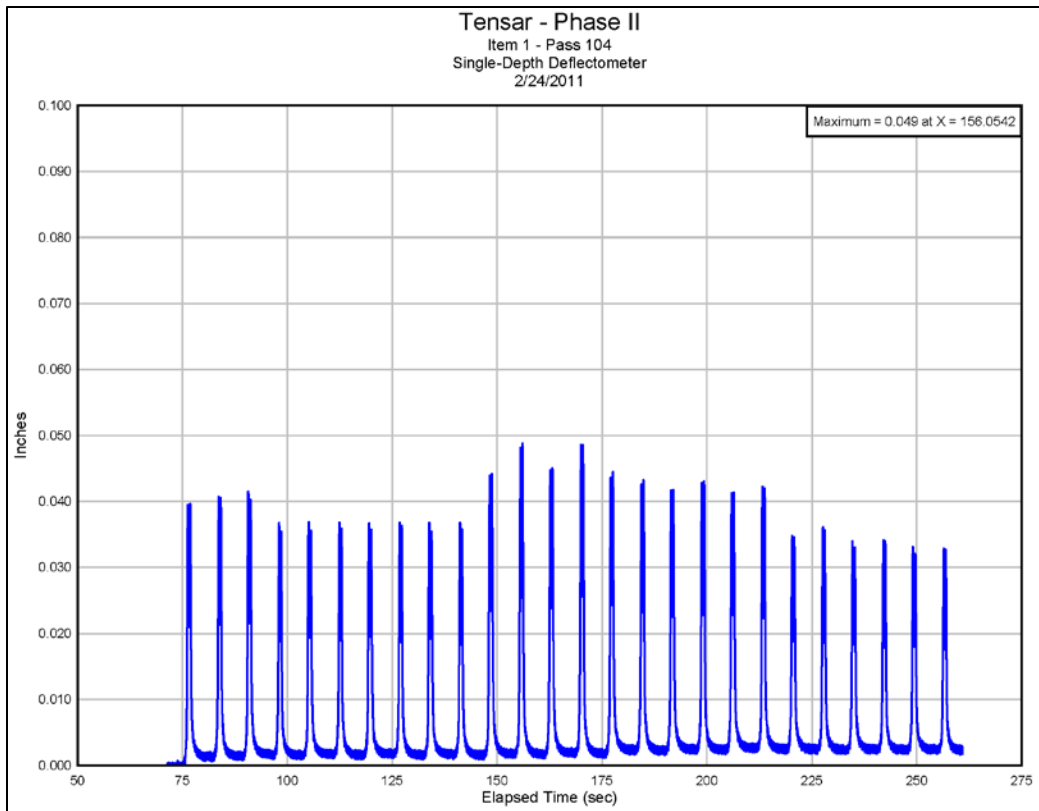


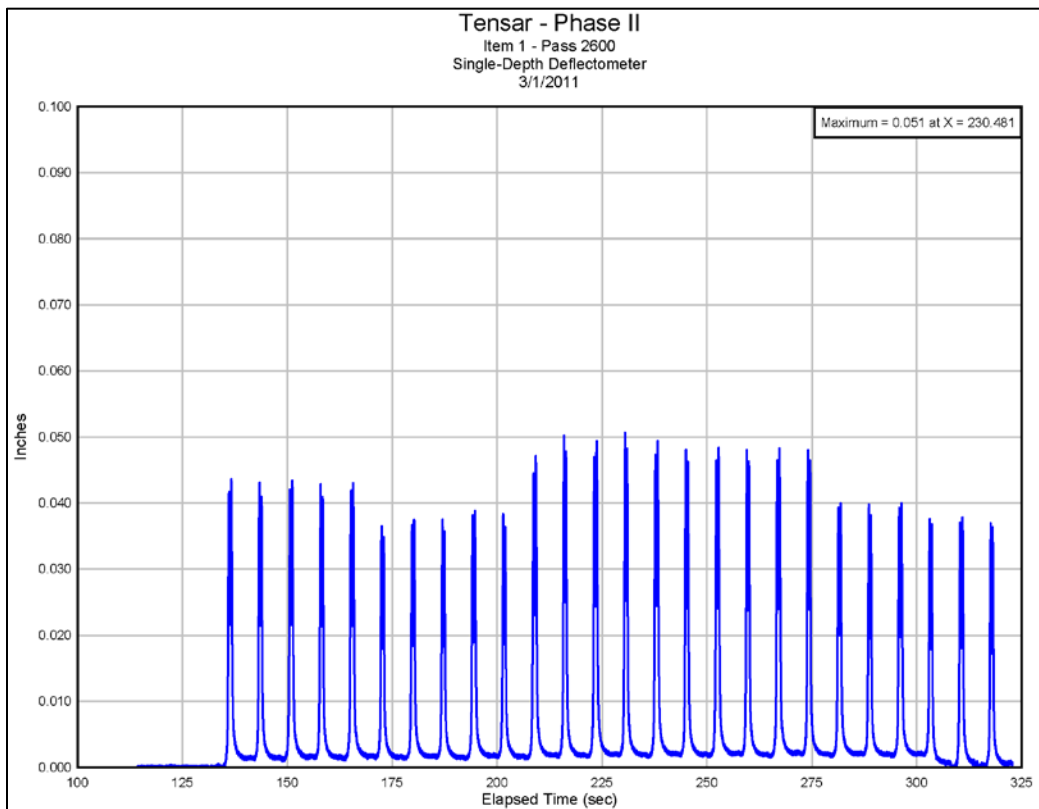
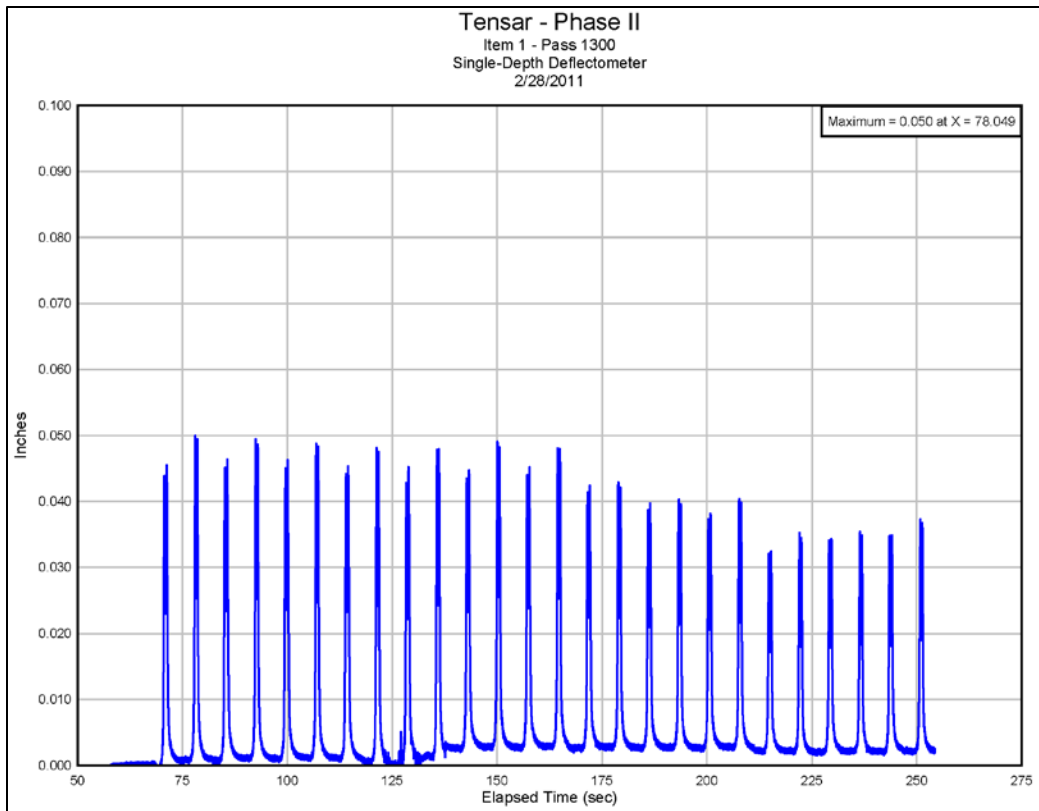


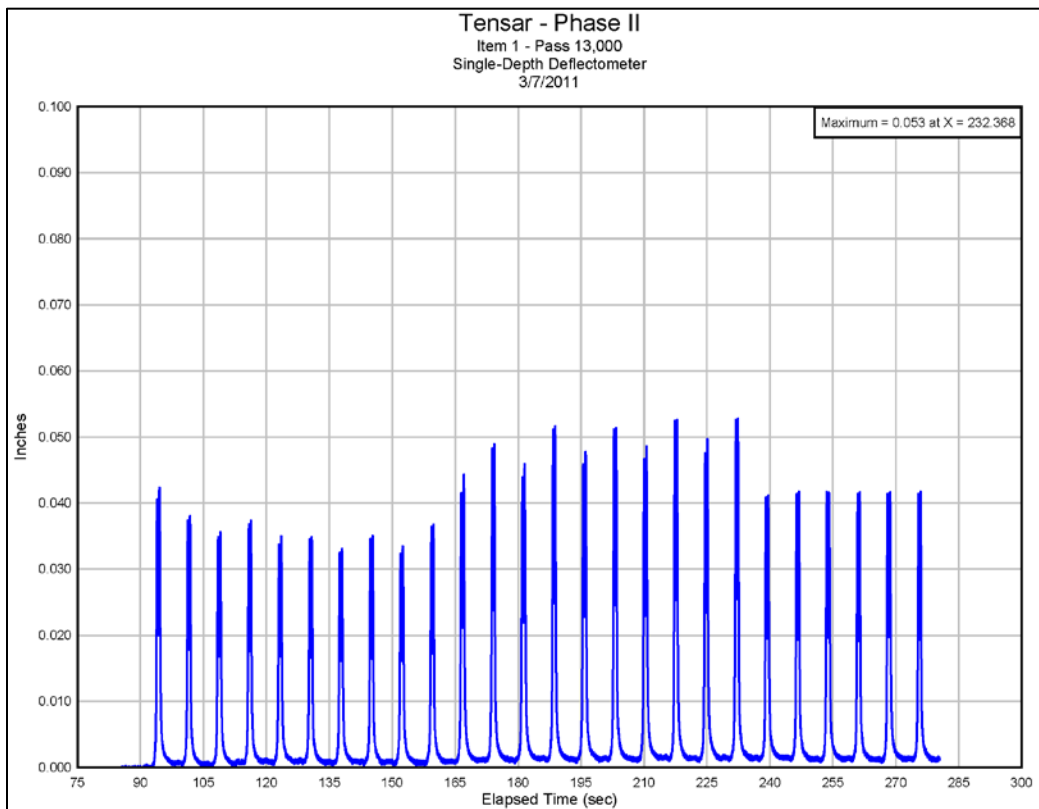
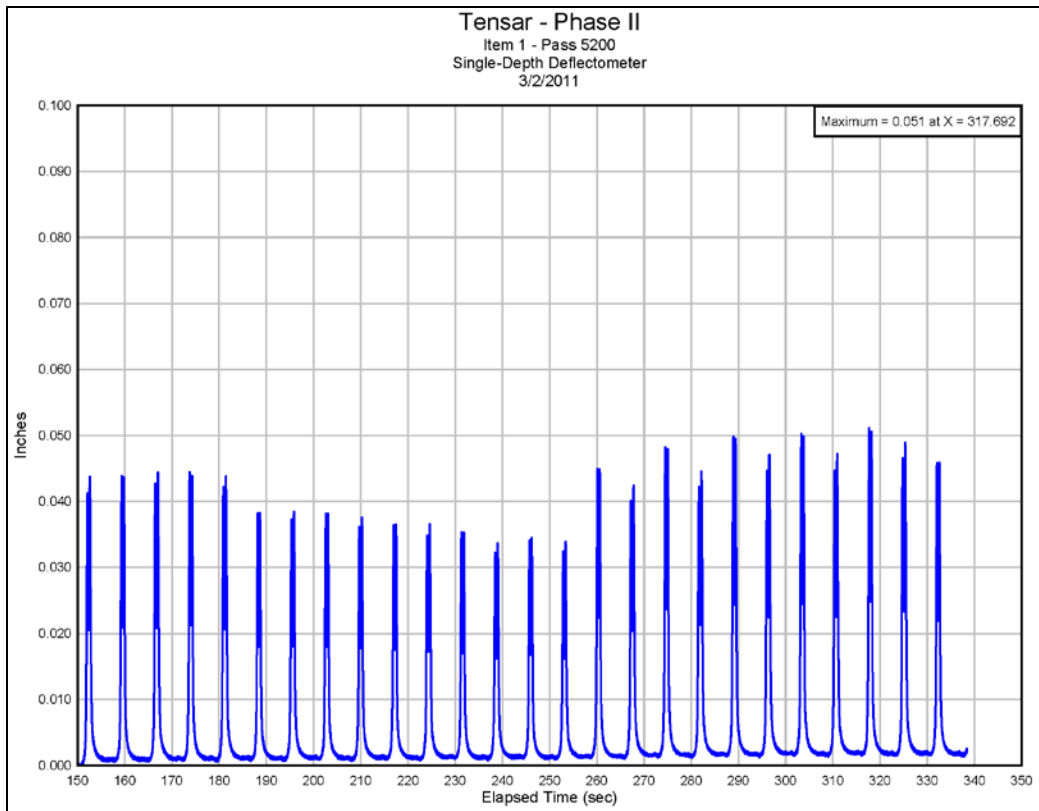
Appendix B: Single-Depth Deflectometer Responses

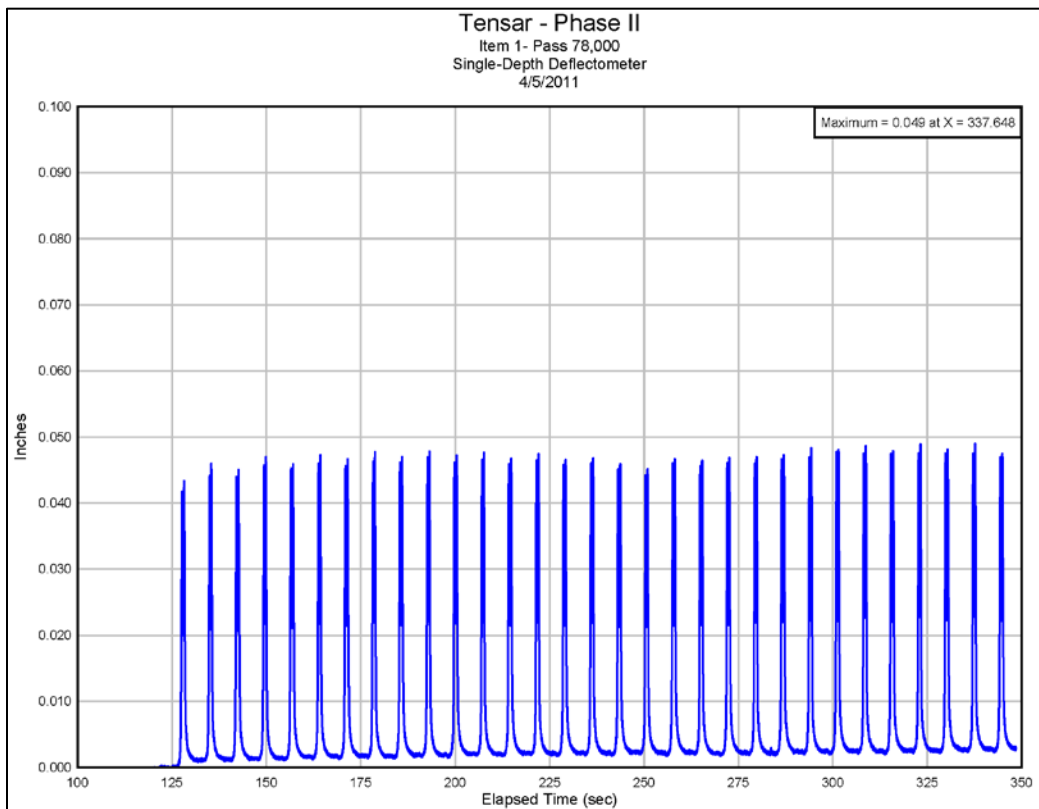
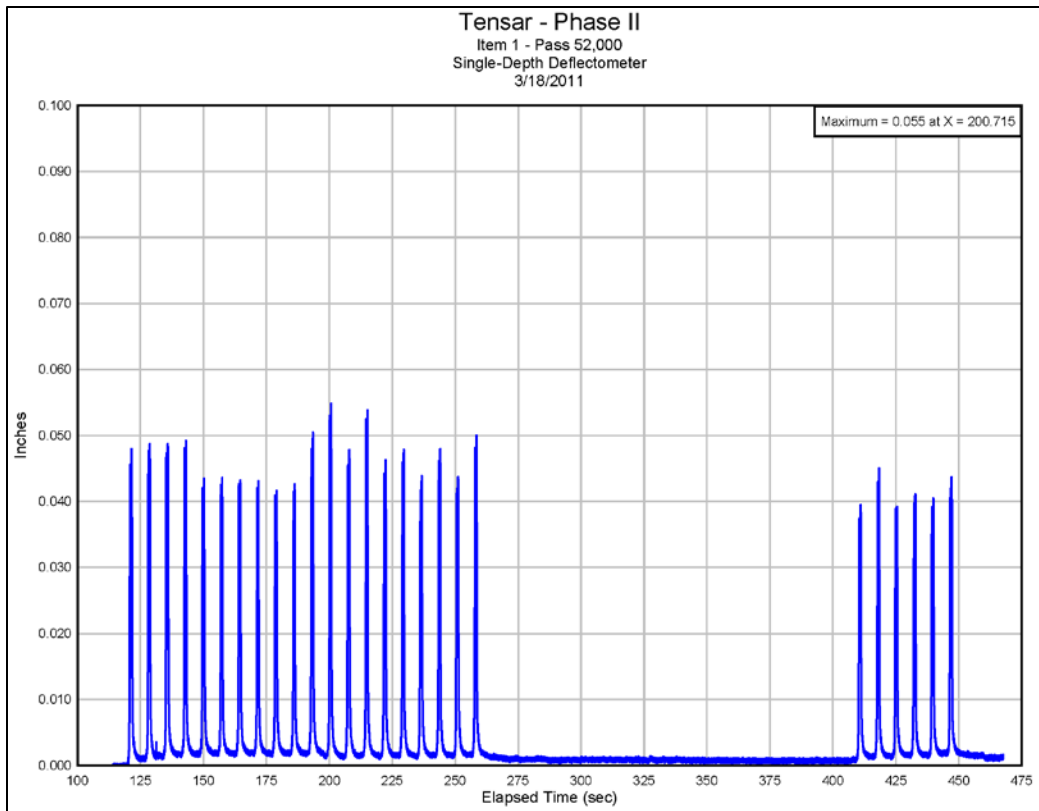


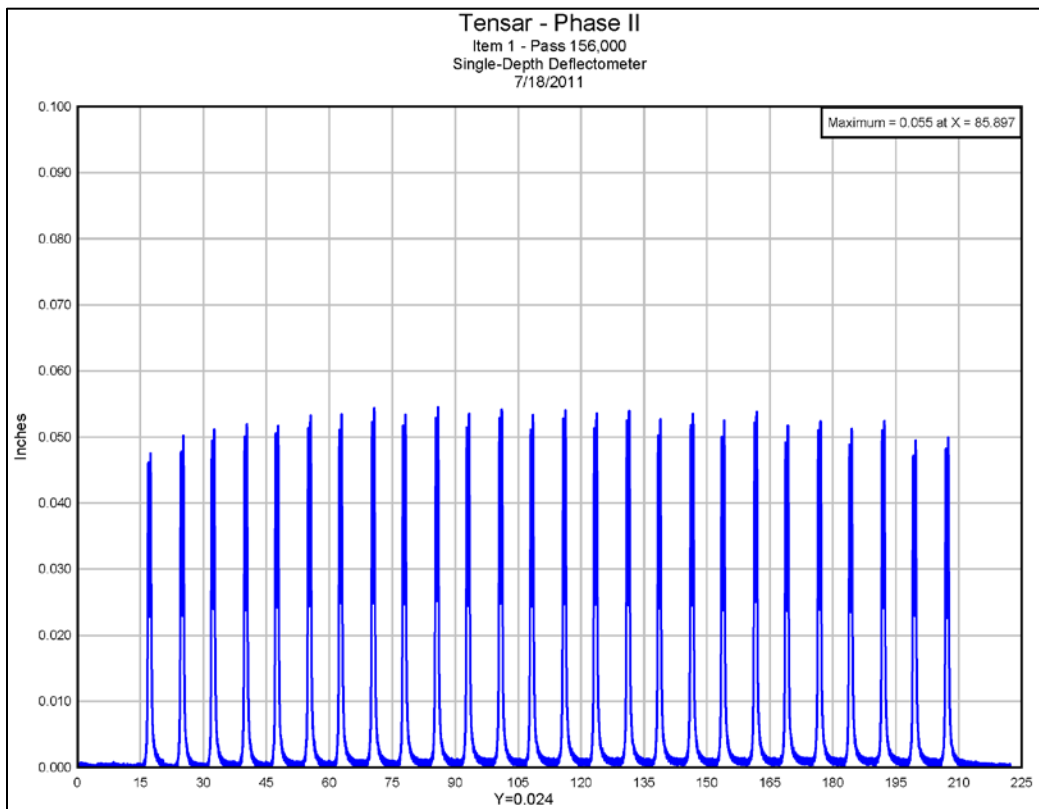
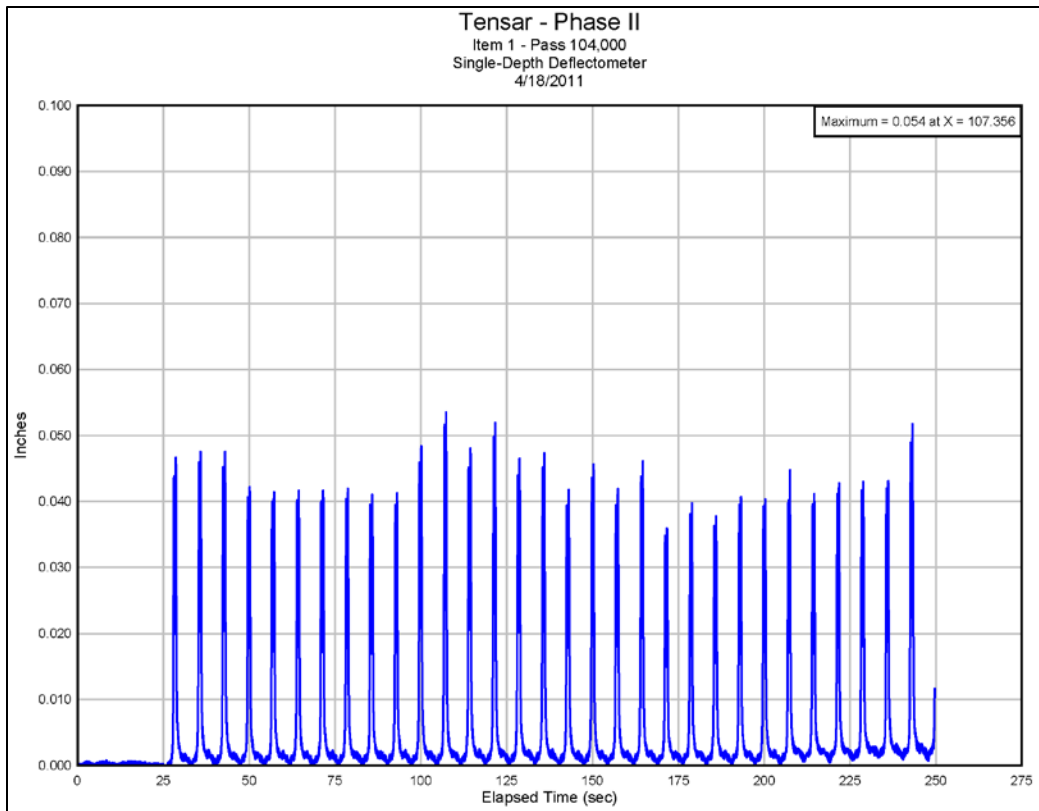


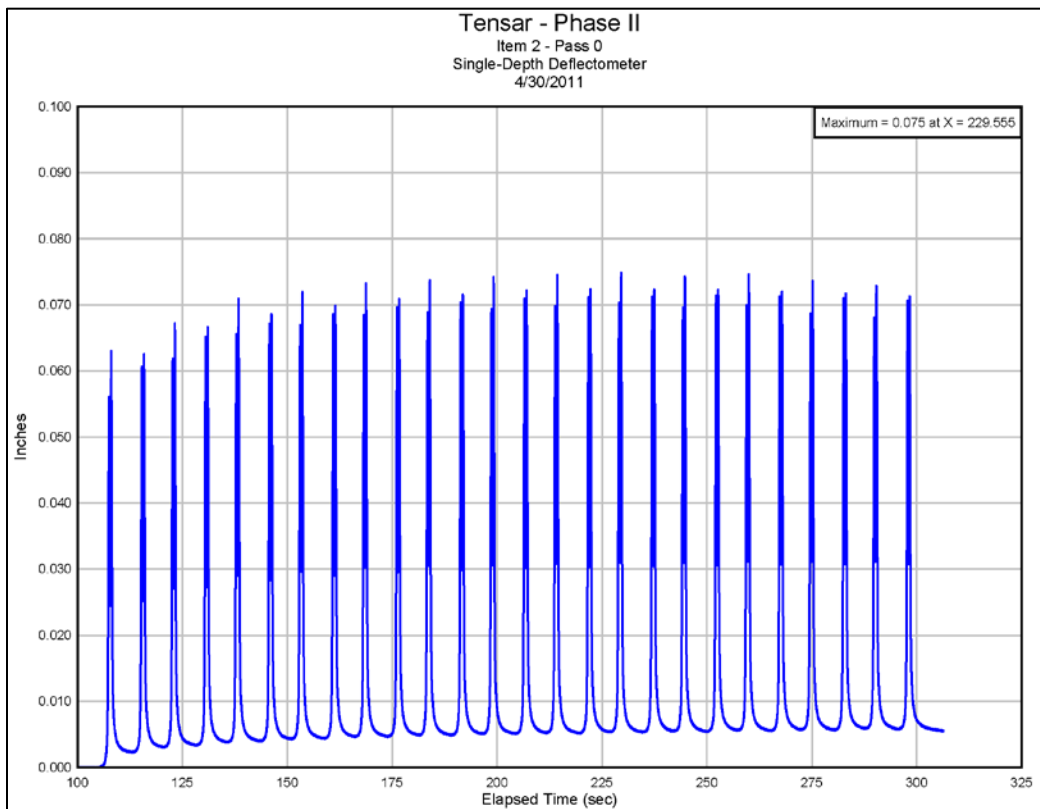
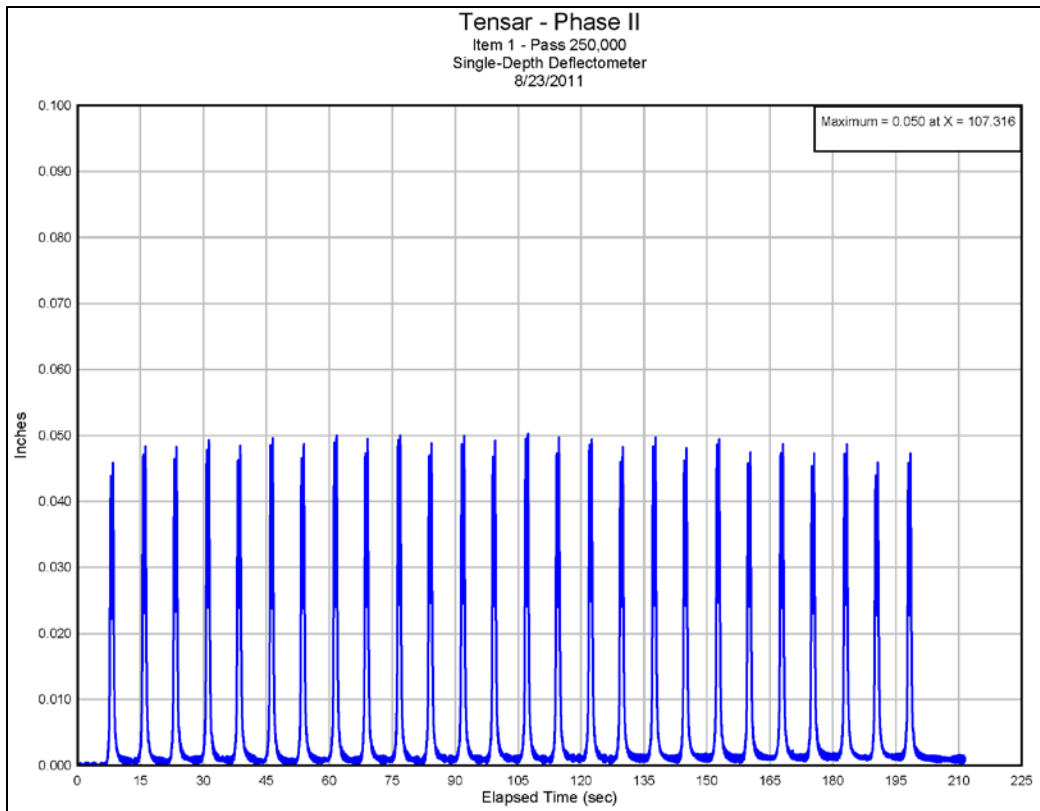


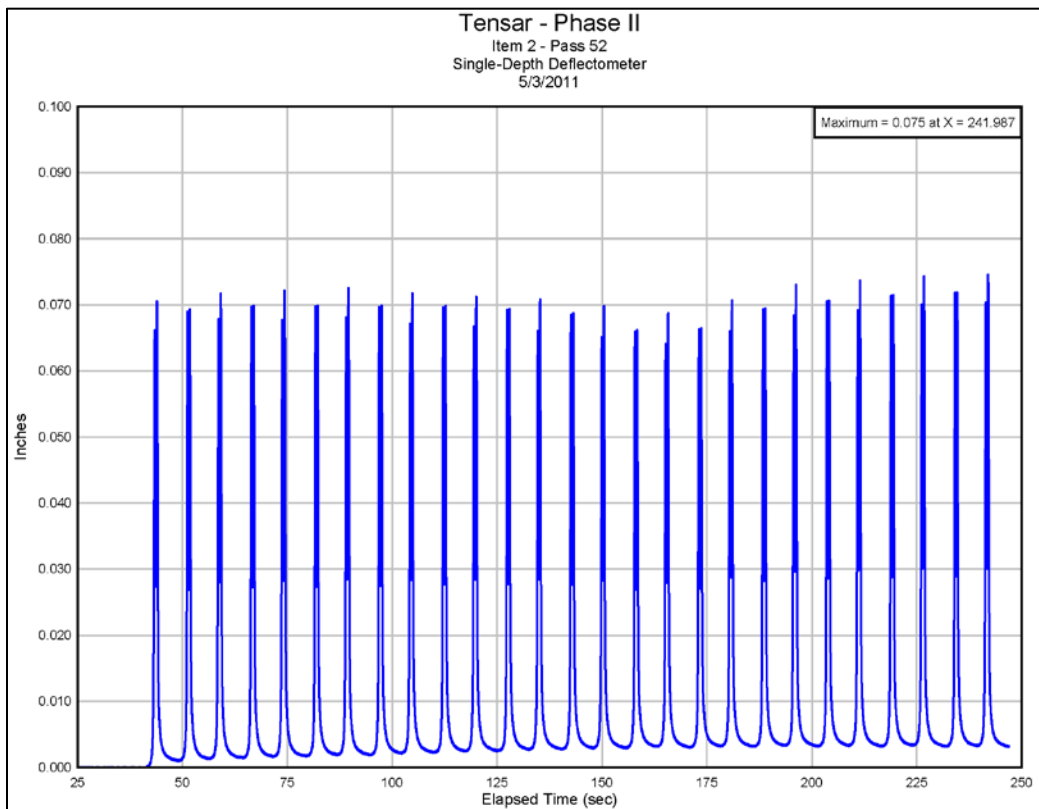
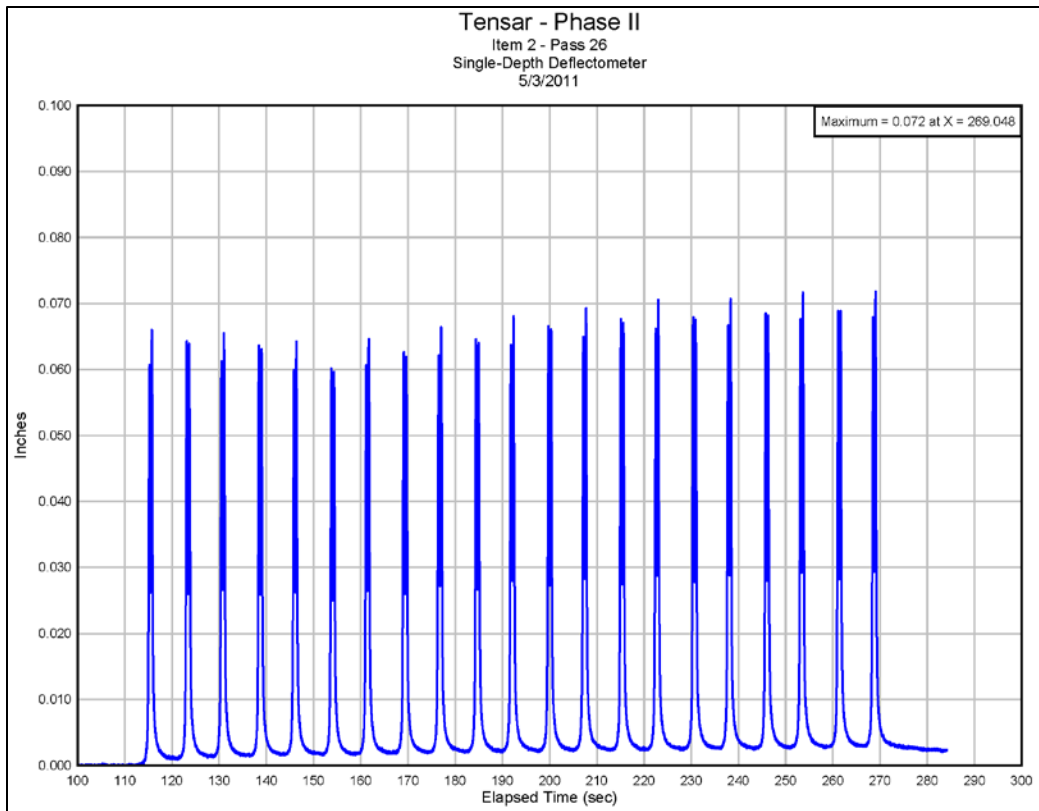


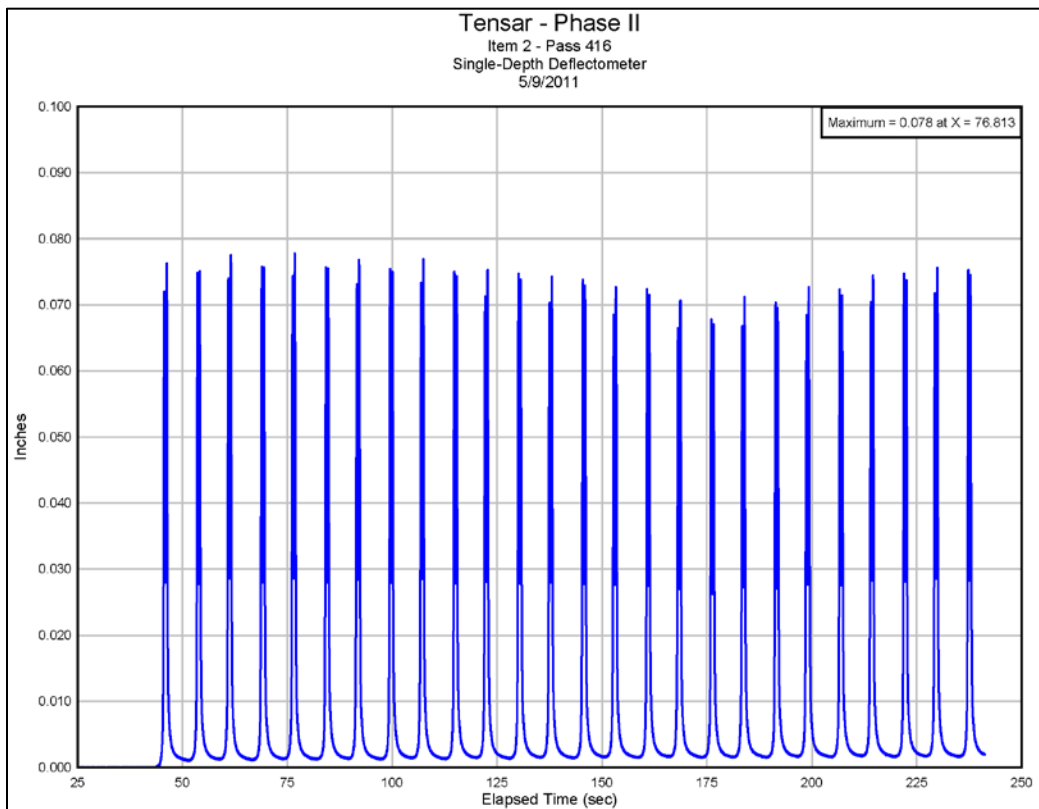
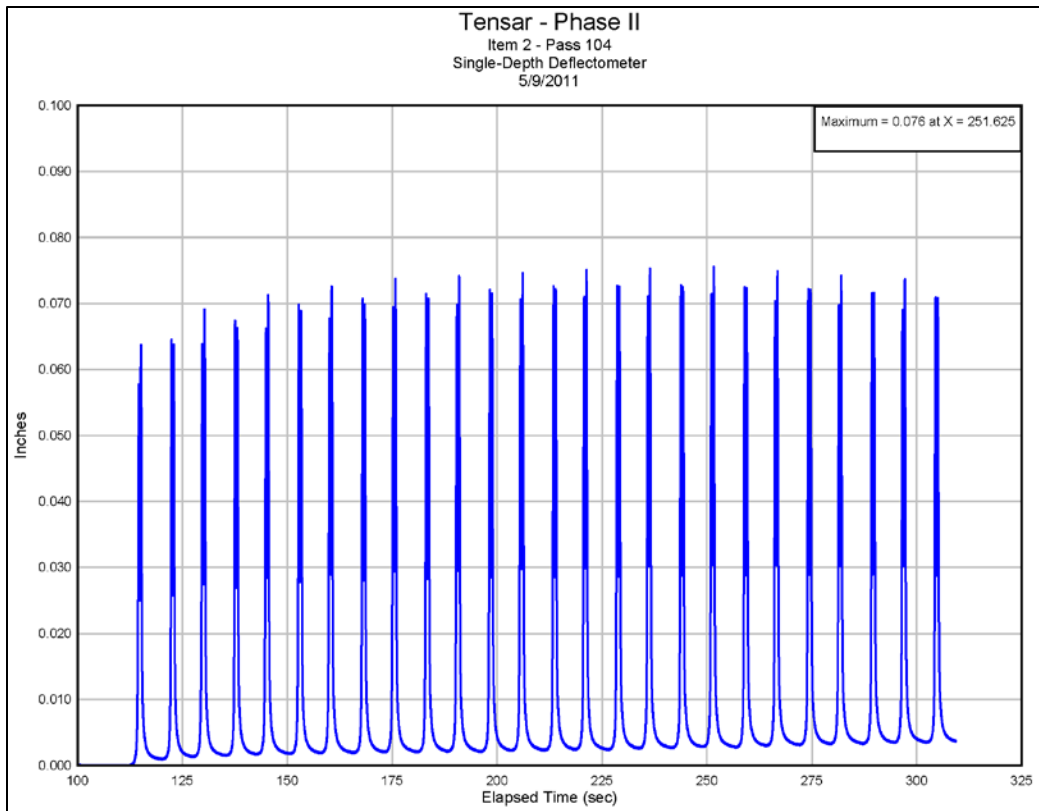


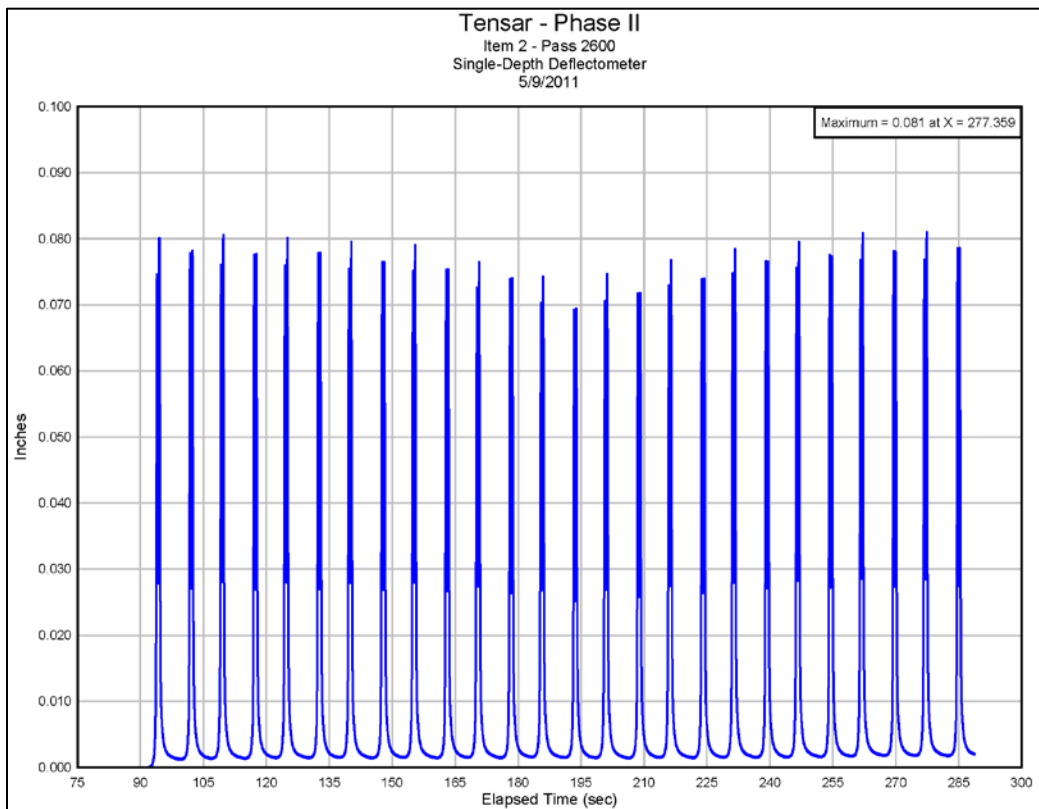
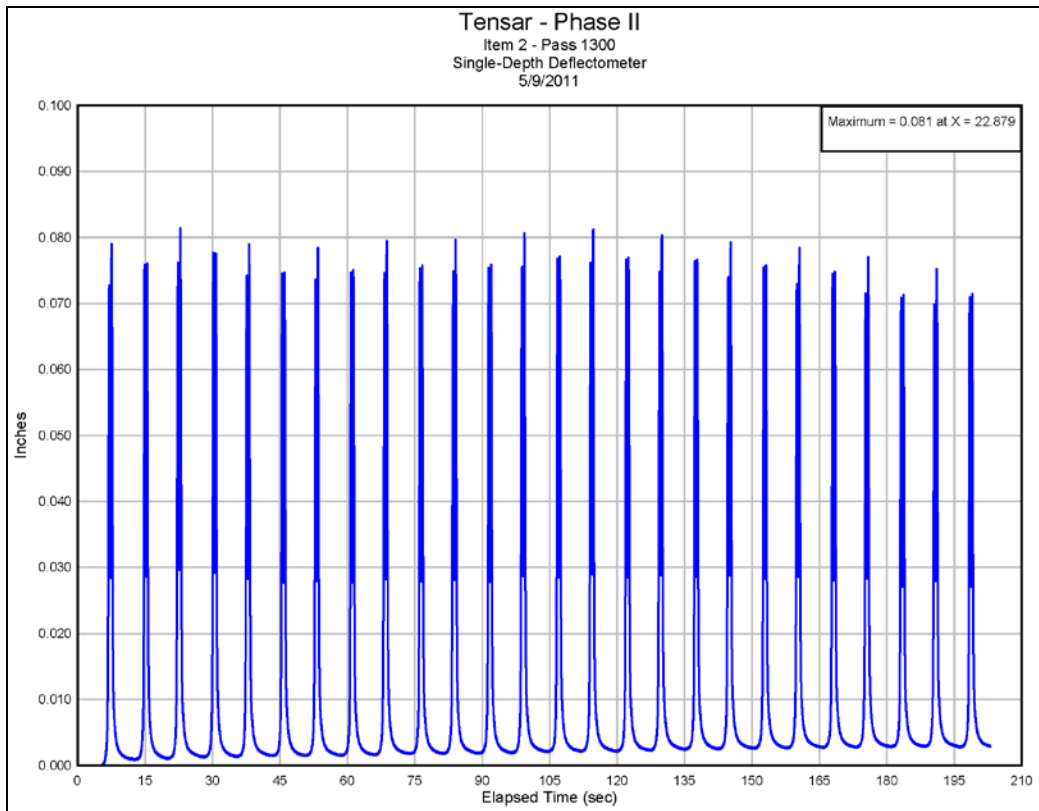


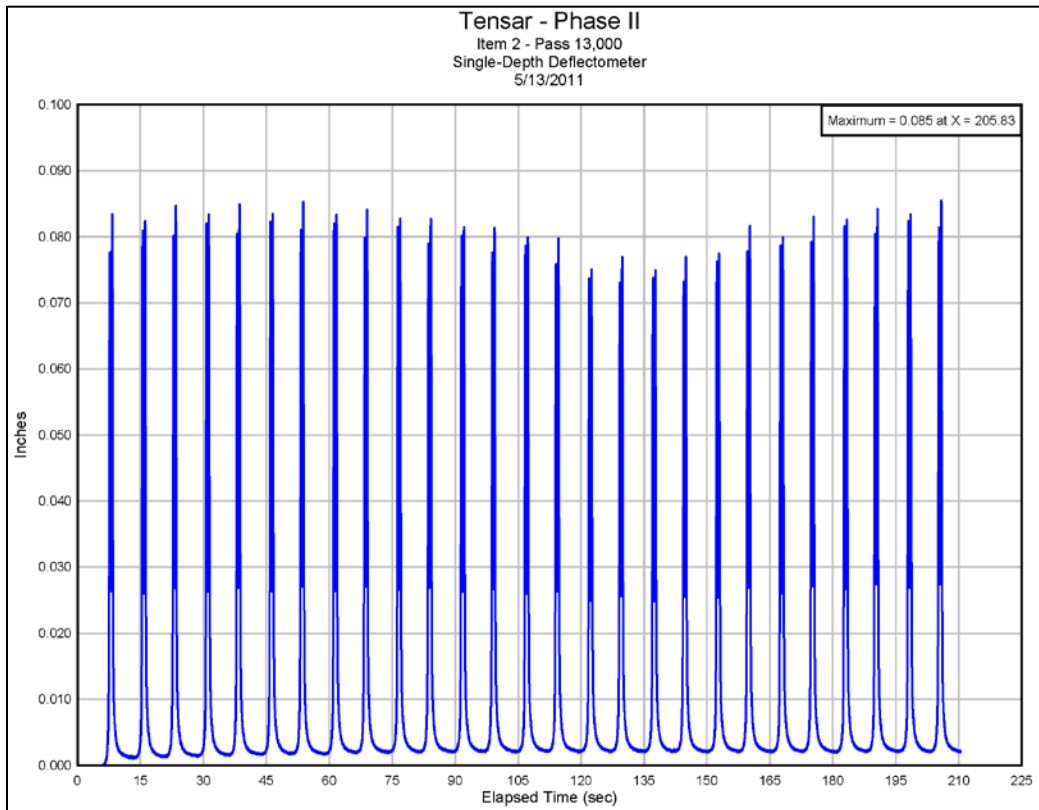
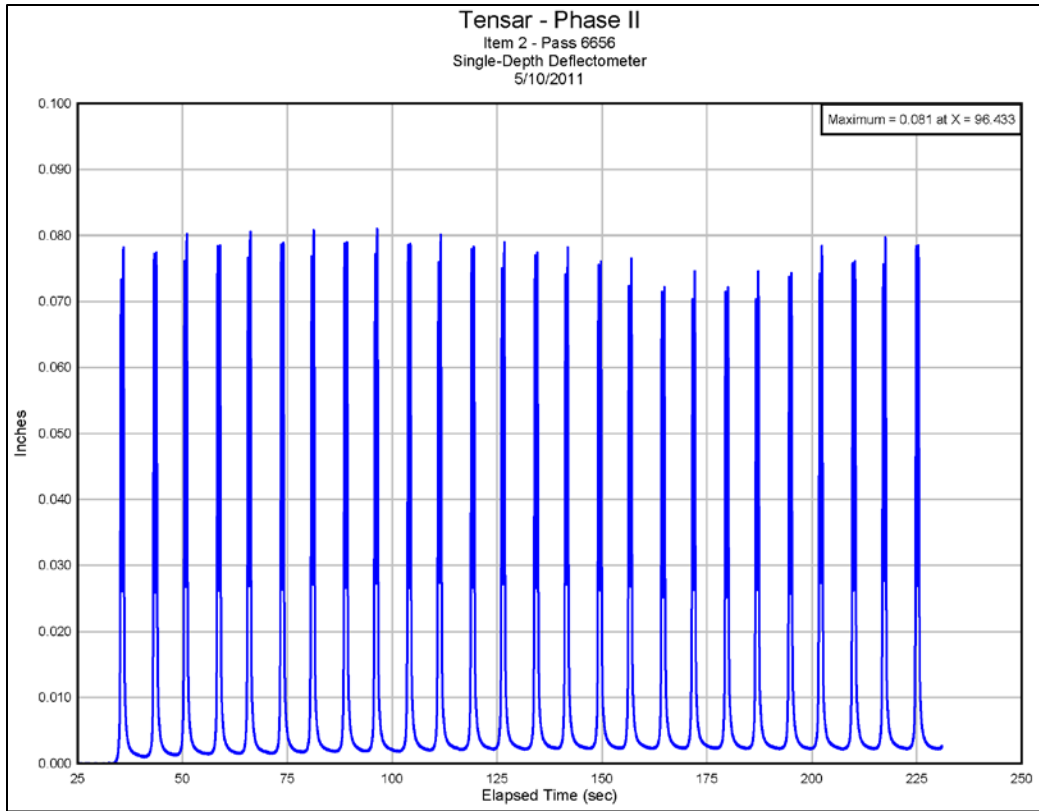


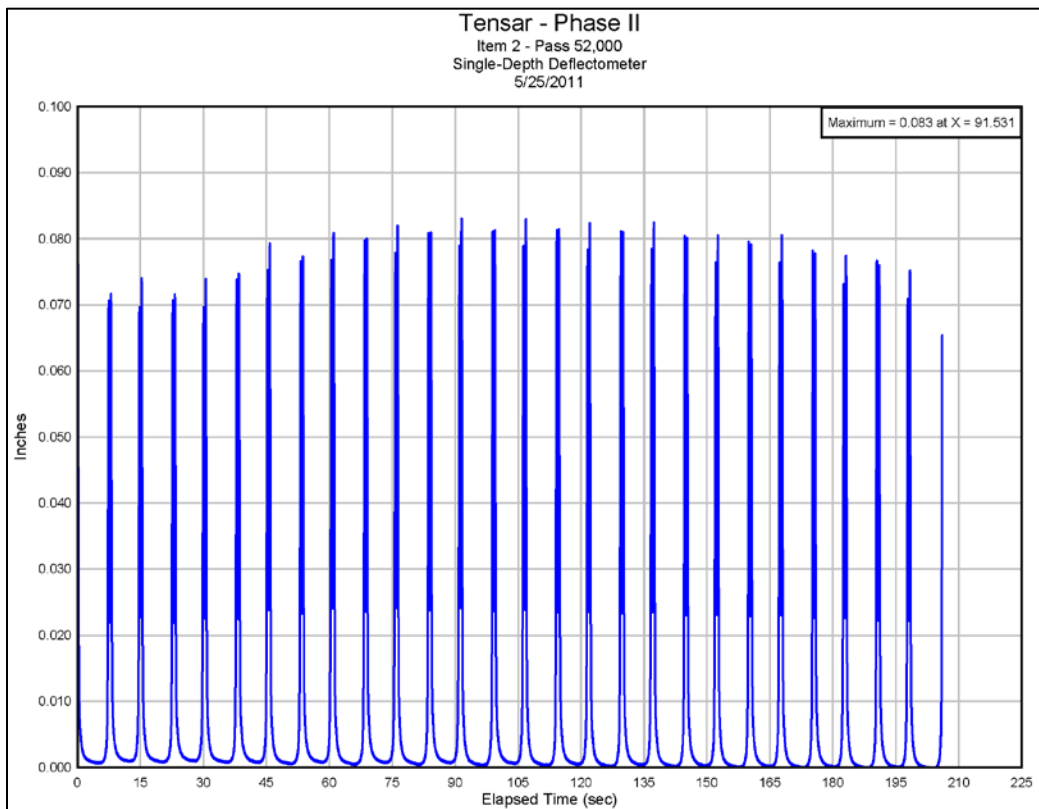
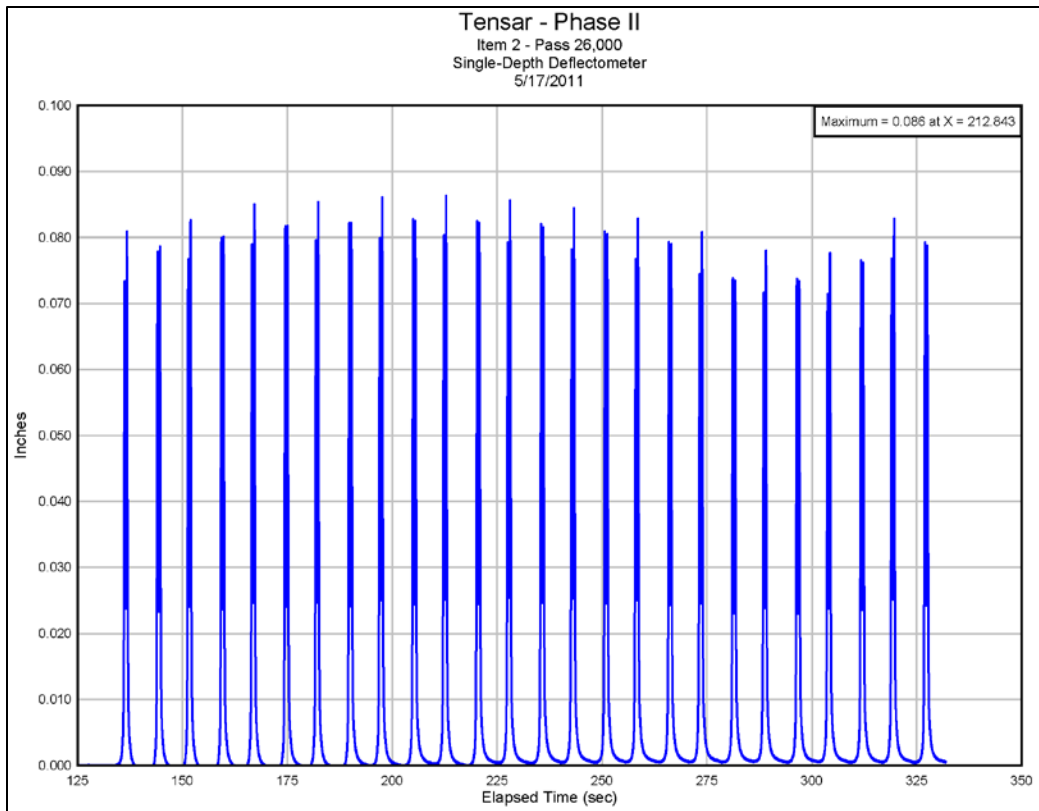


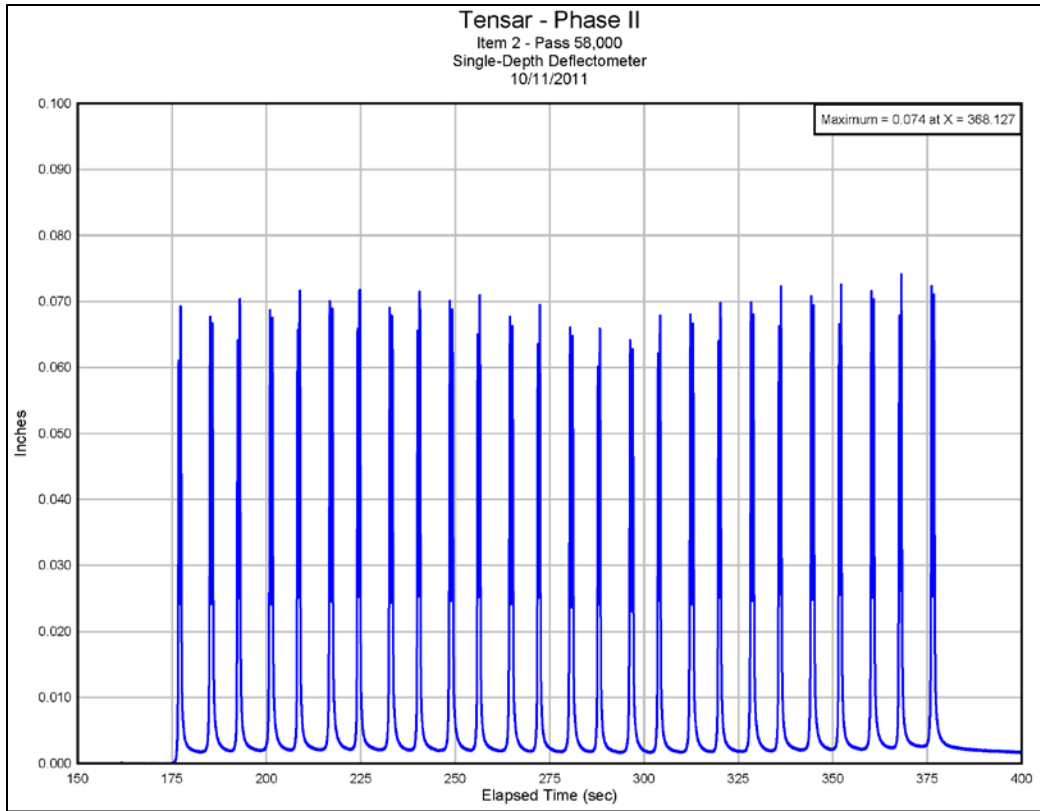




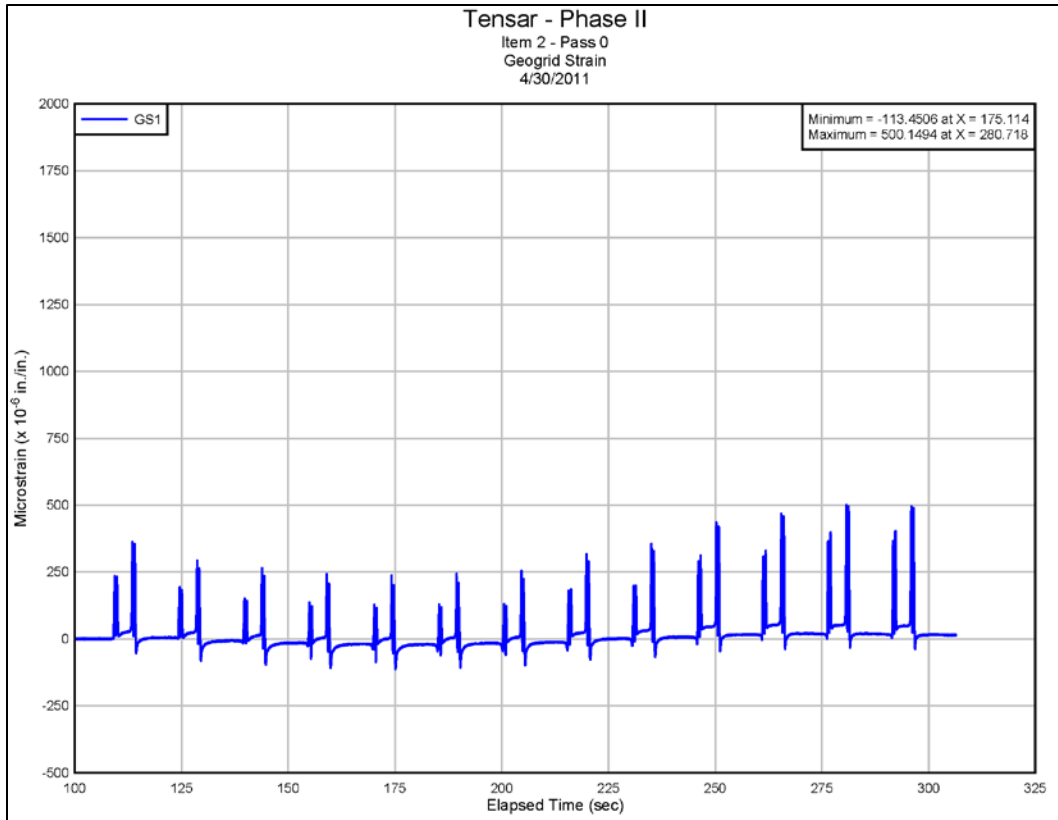


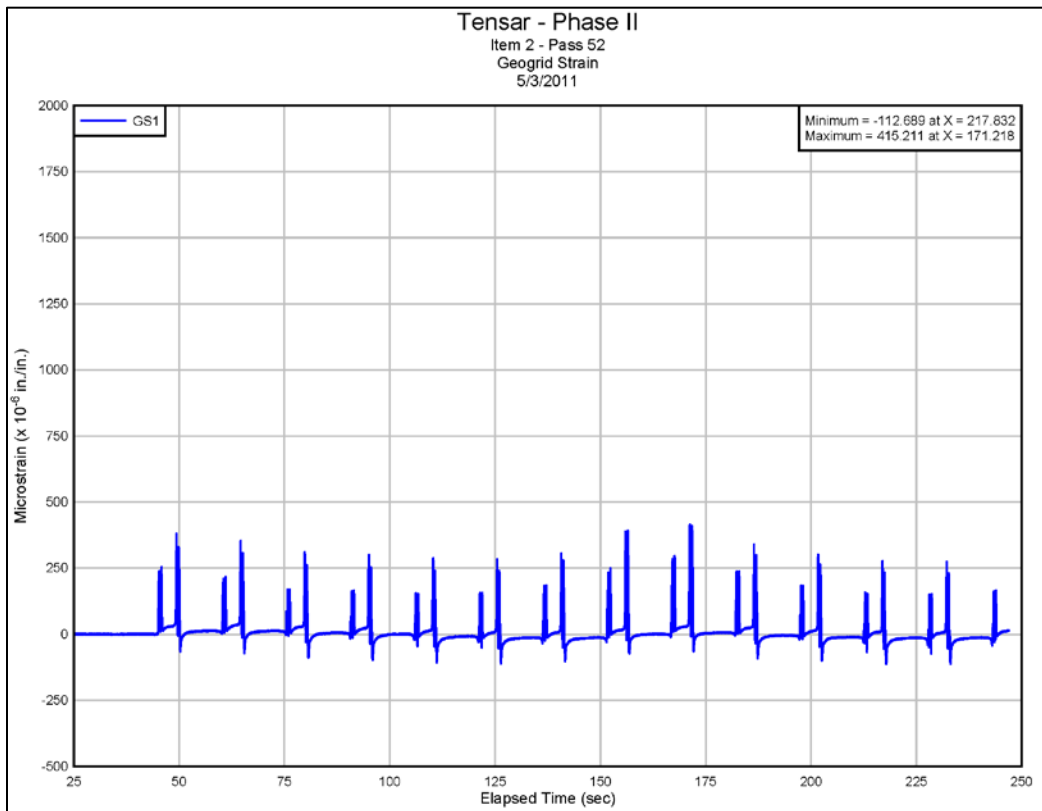
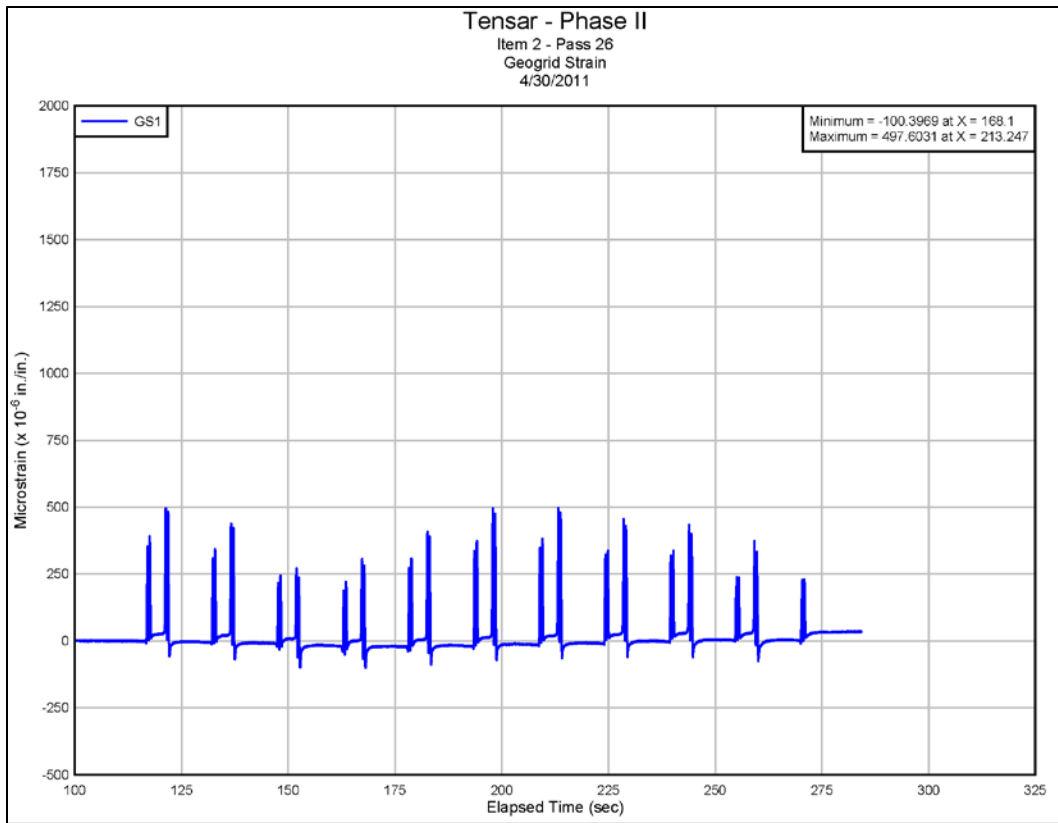


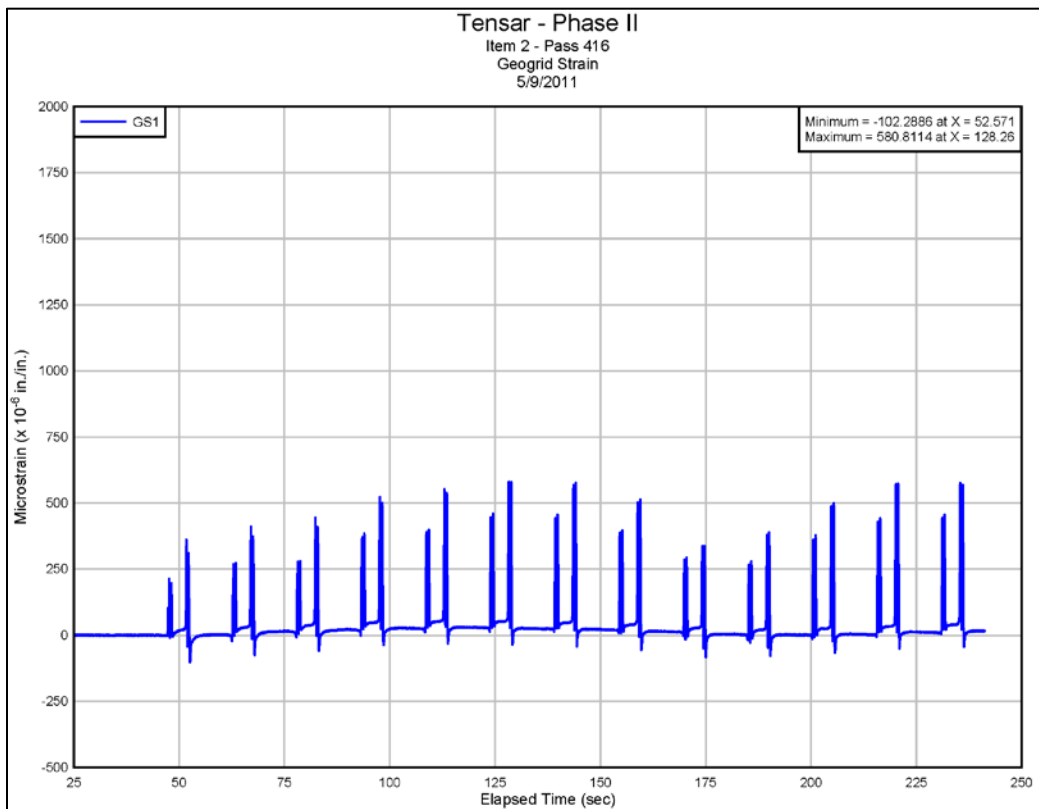
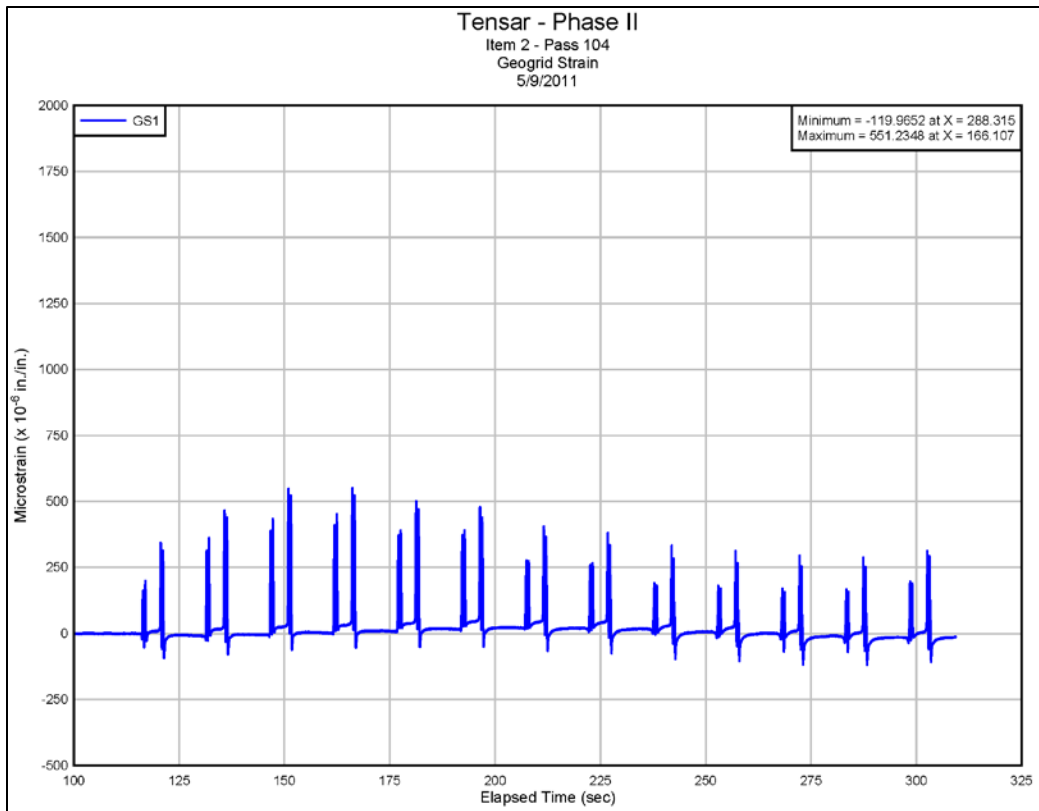


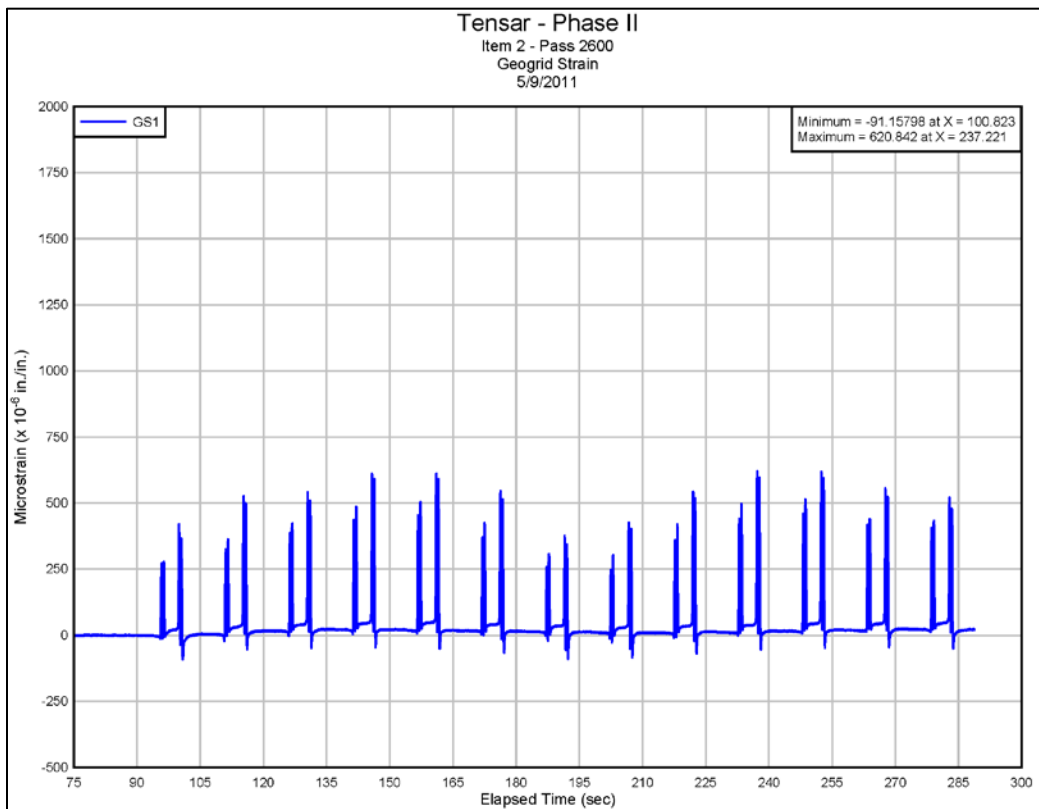
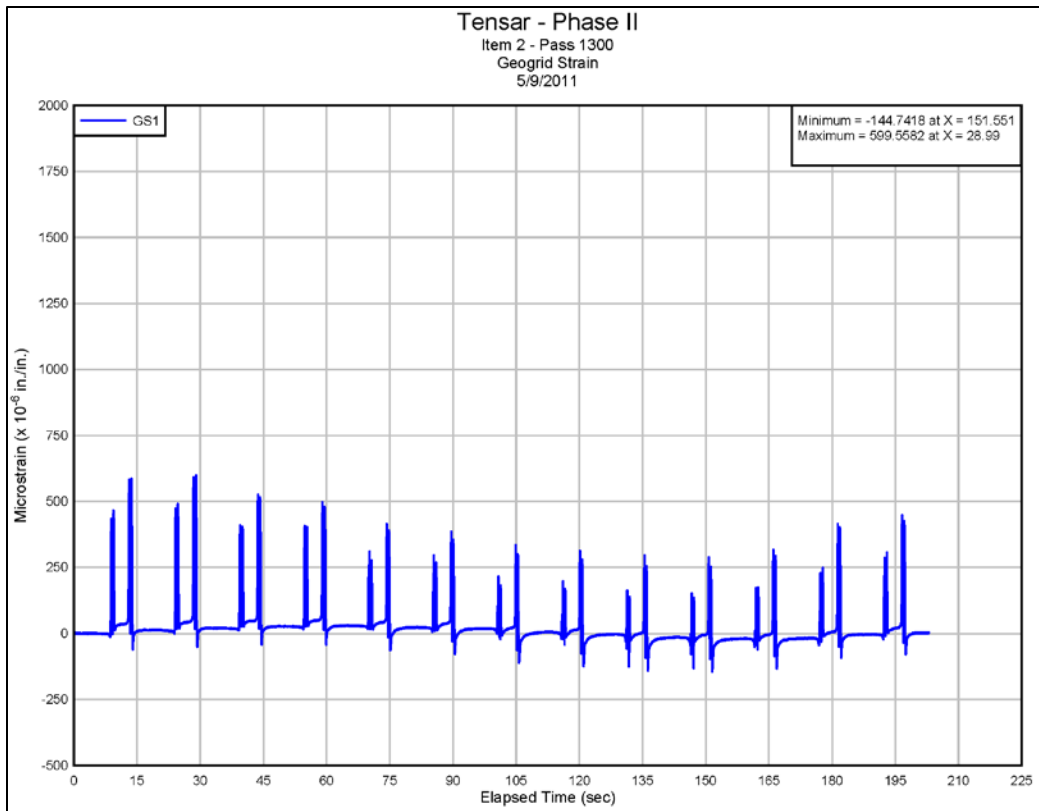


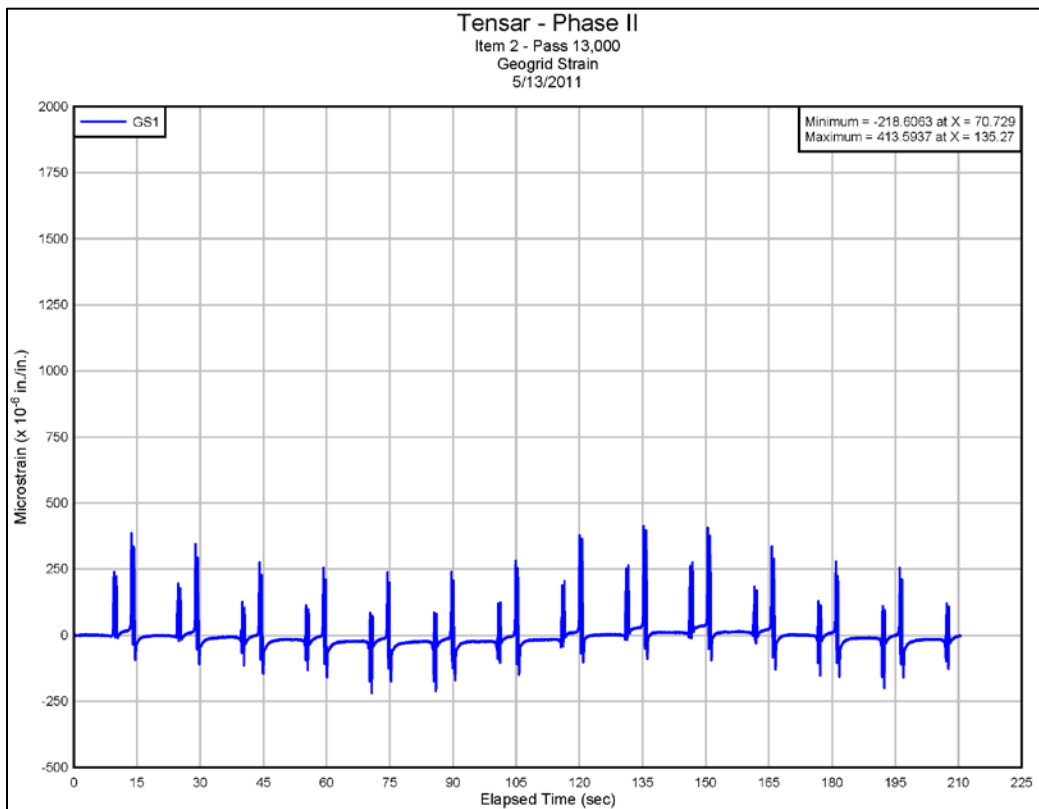
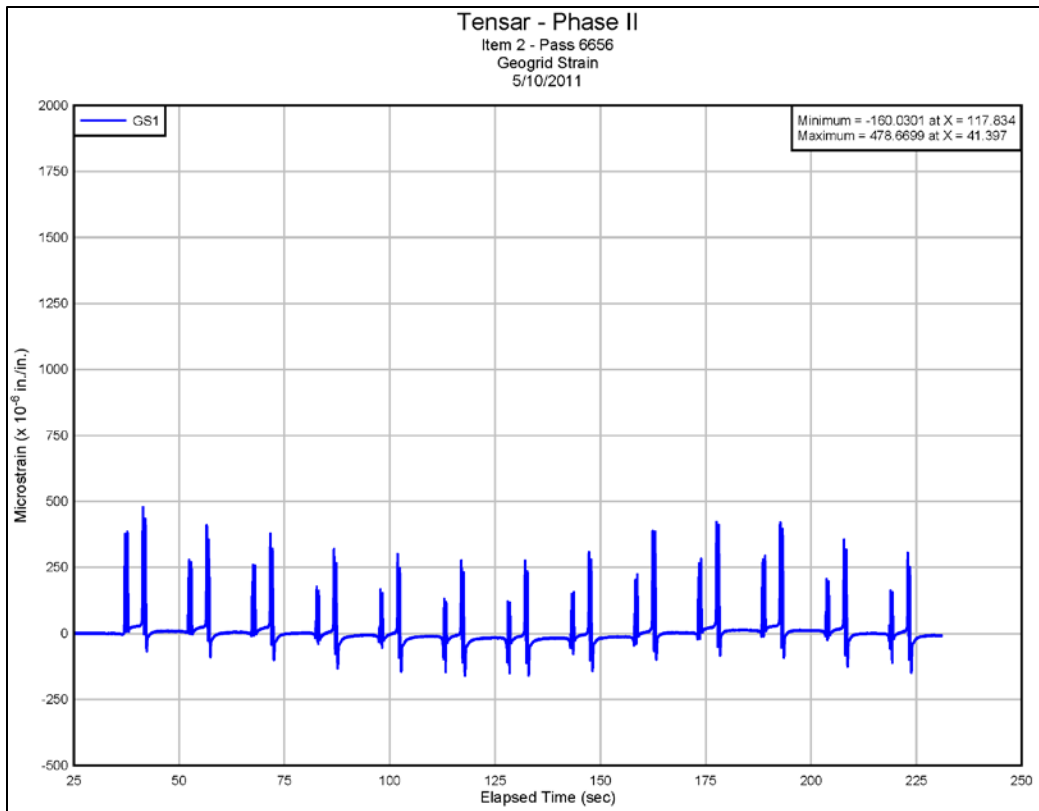
Appendix C: Geogrid Strain Response

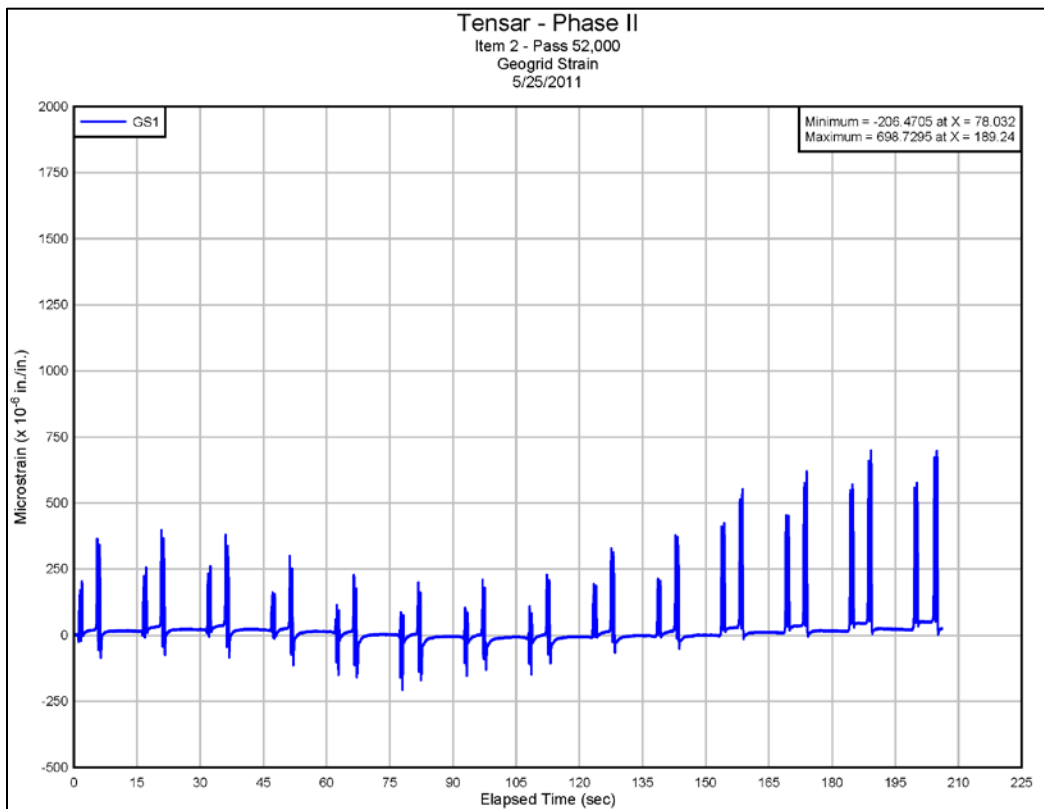
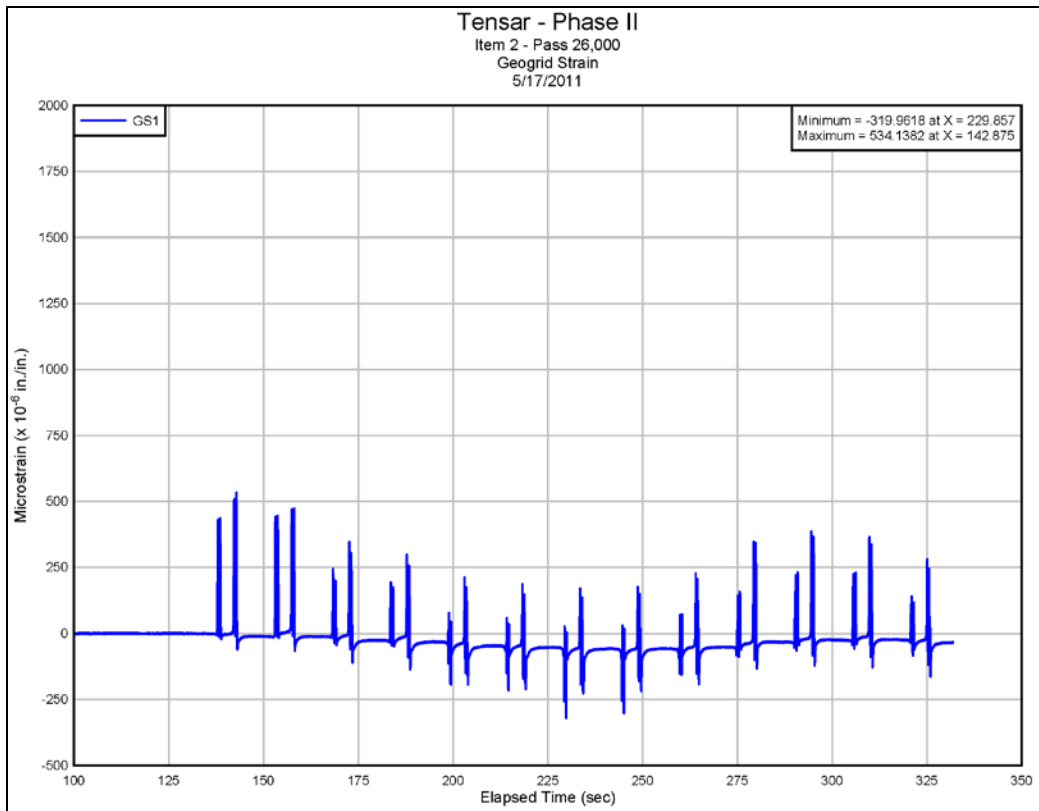


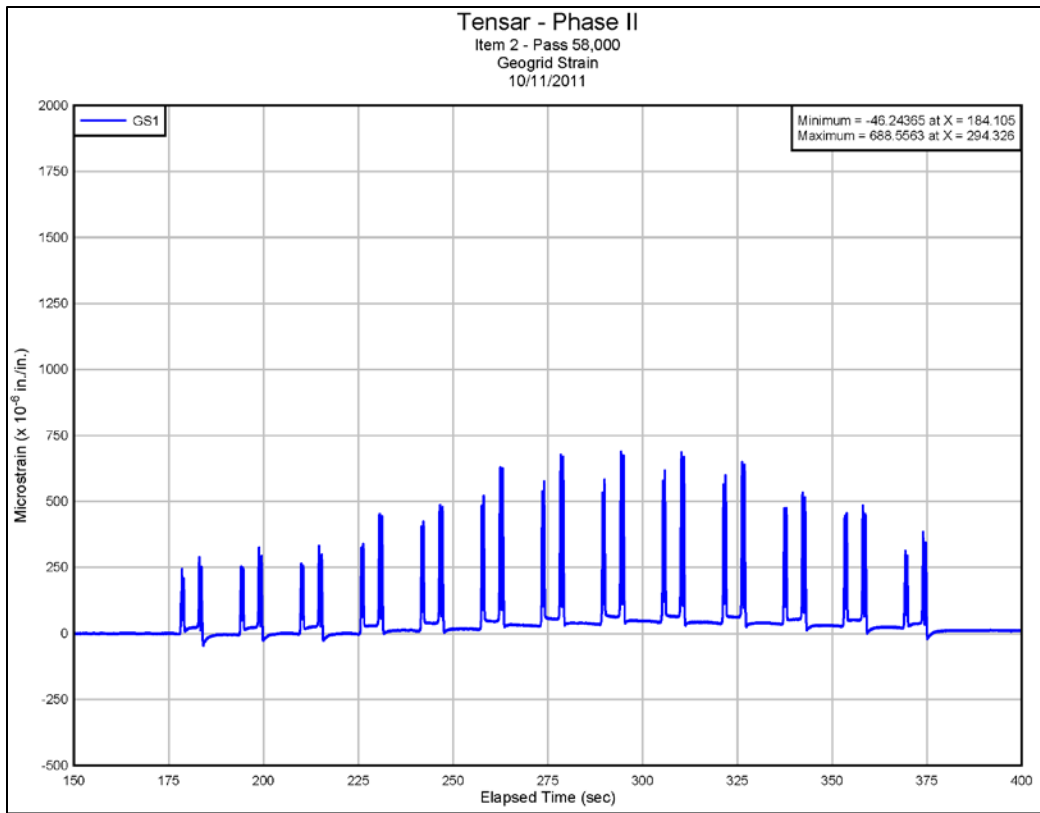




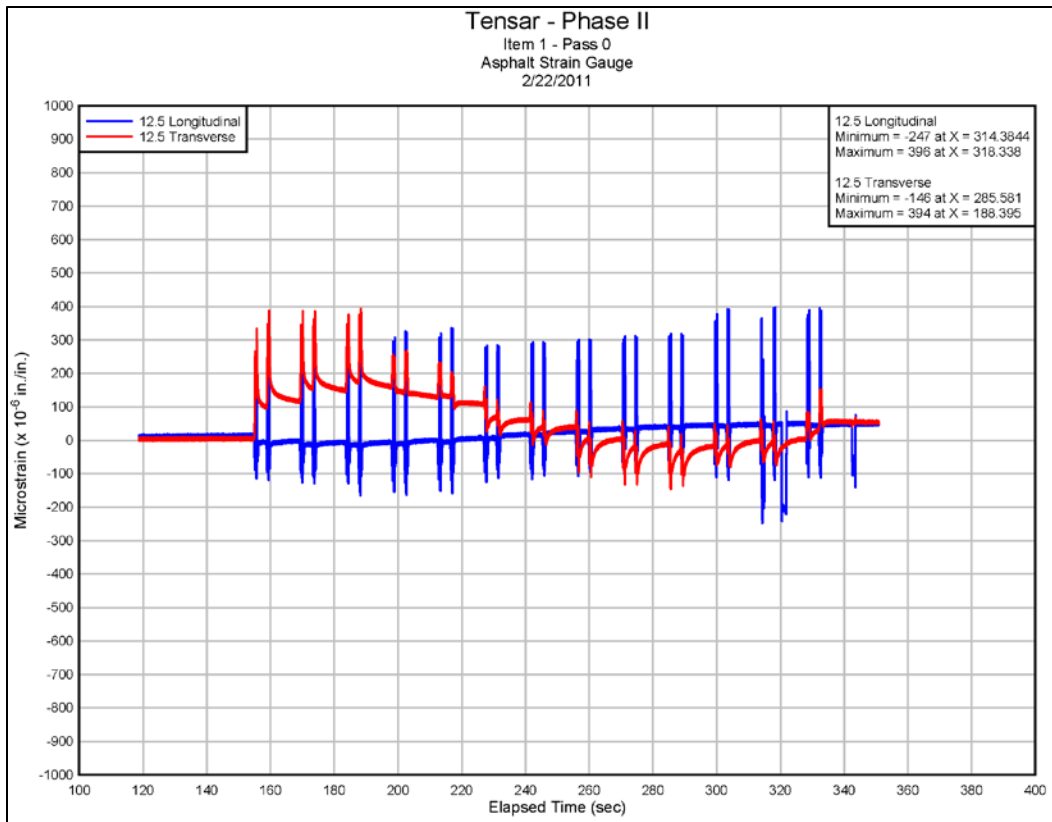


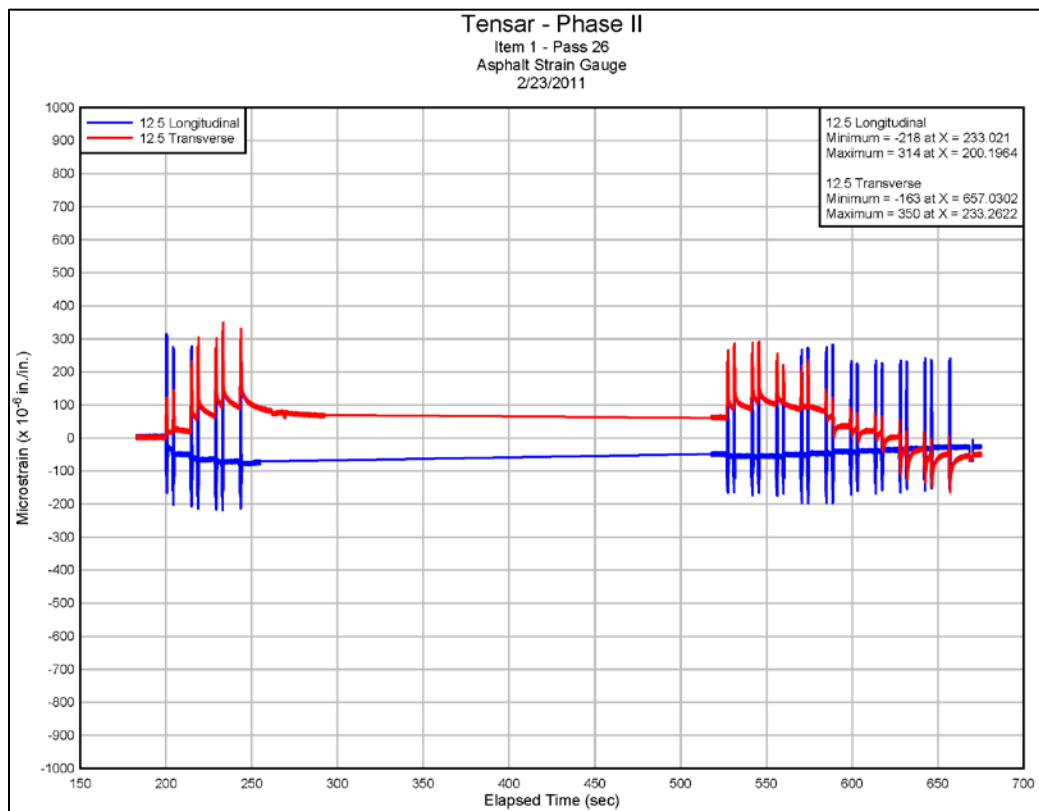
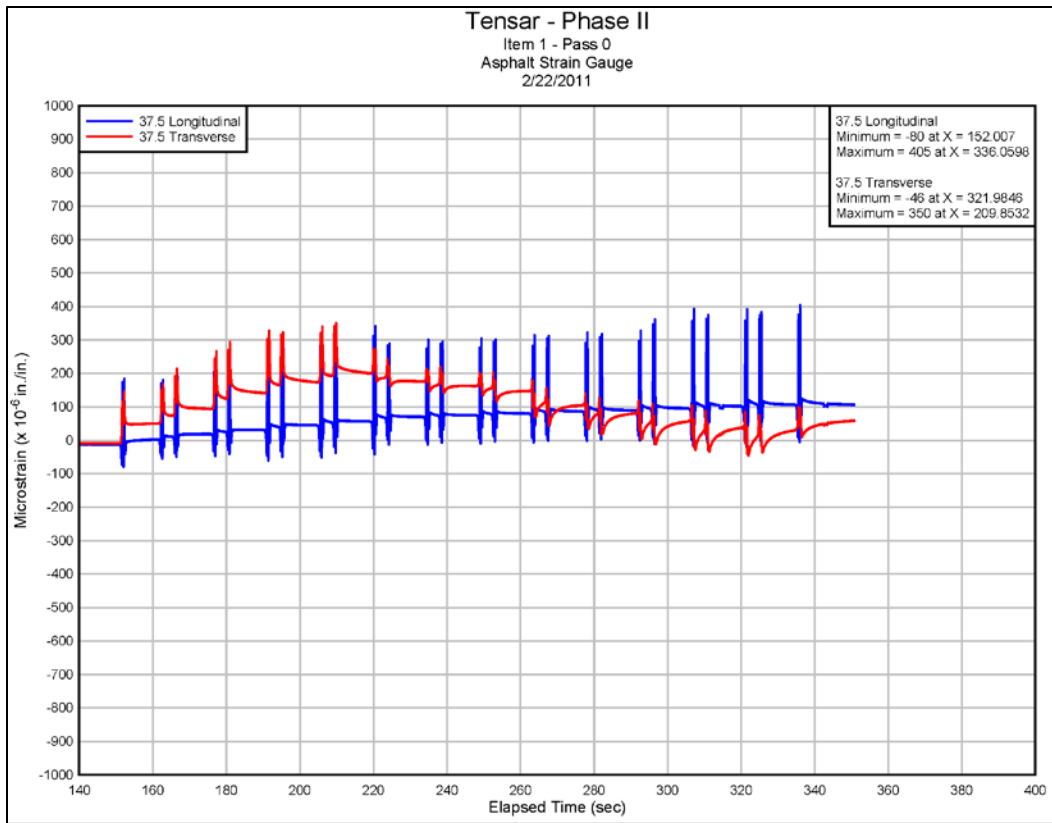


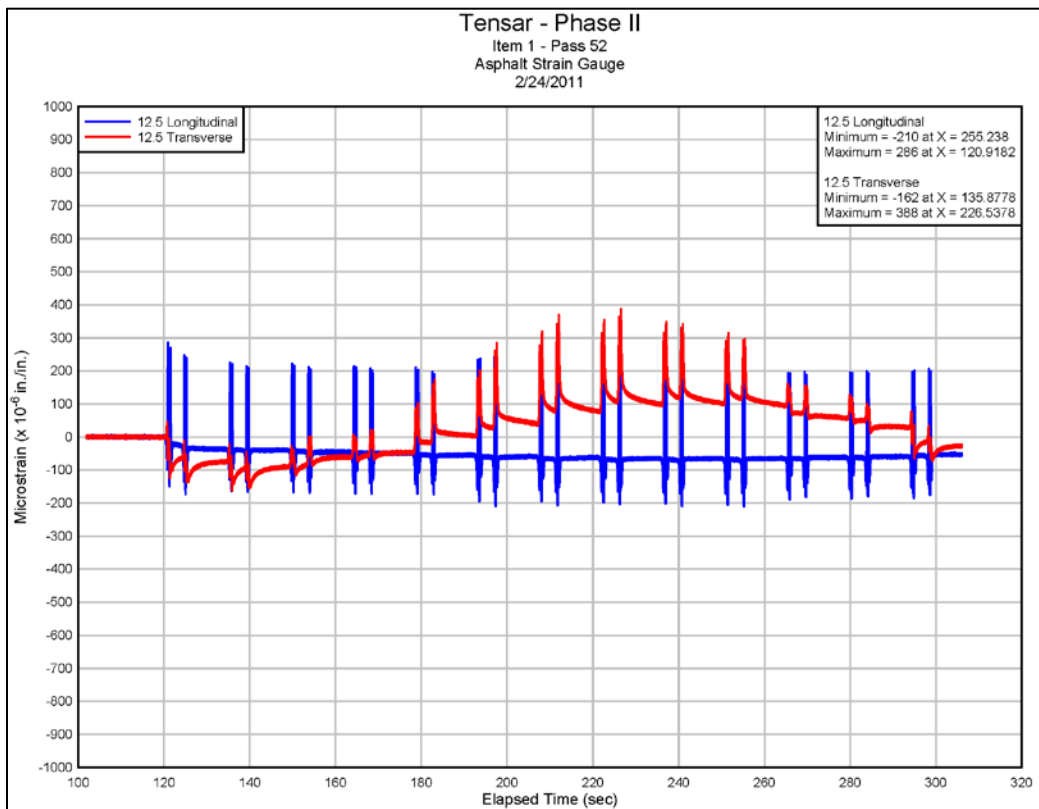
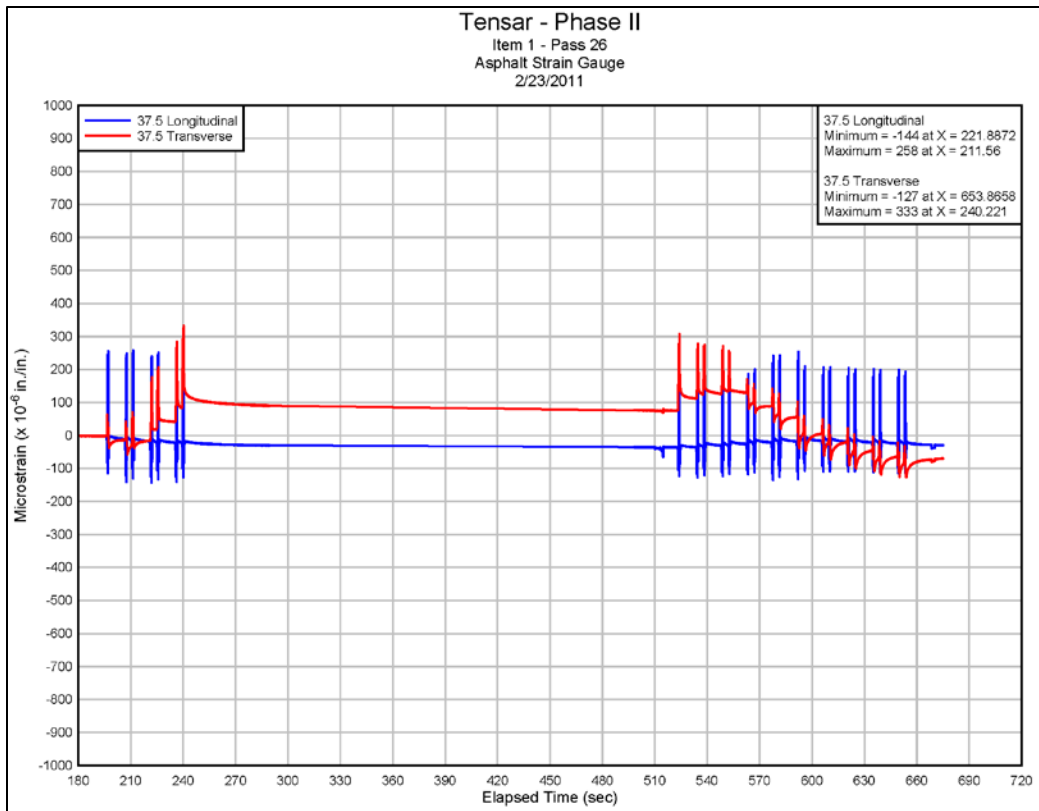


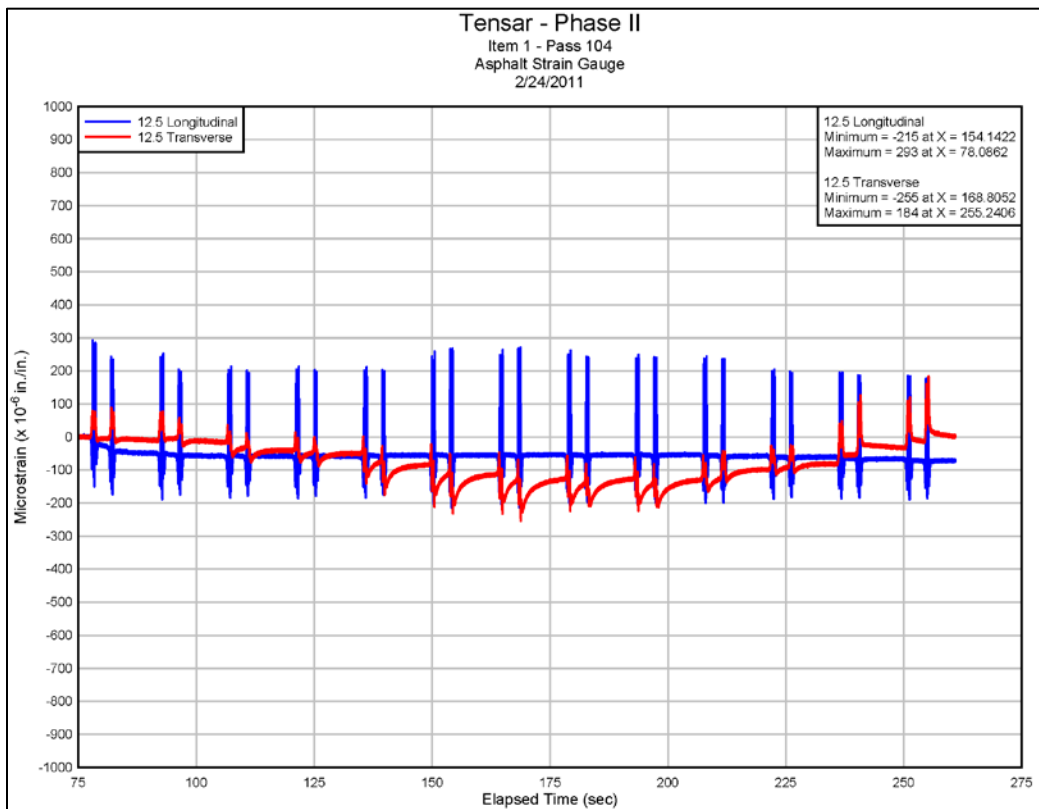
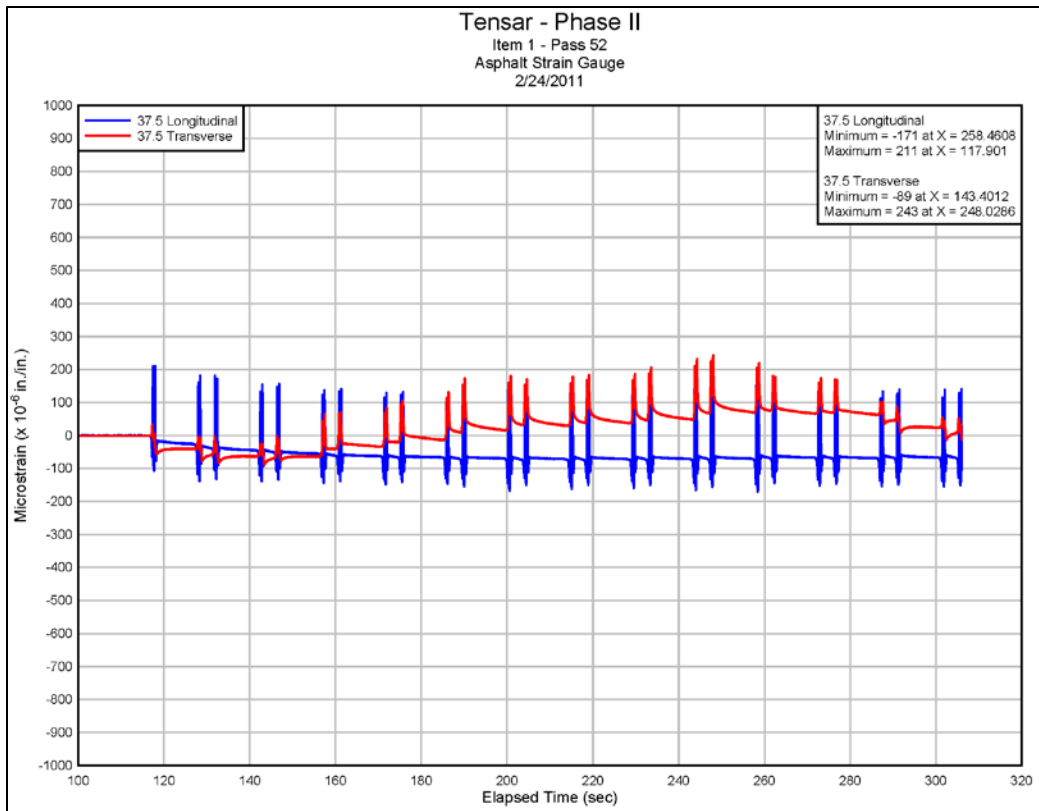


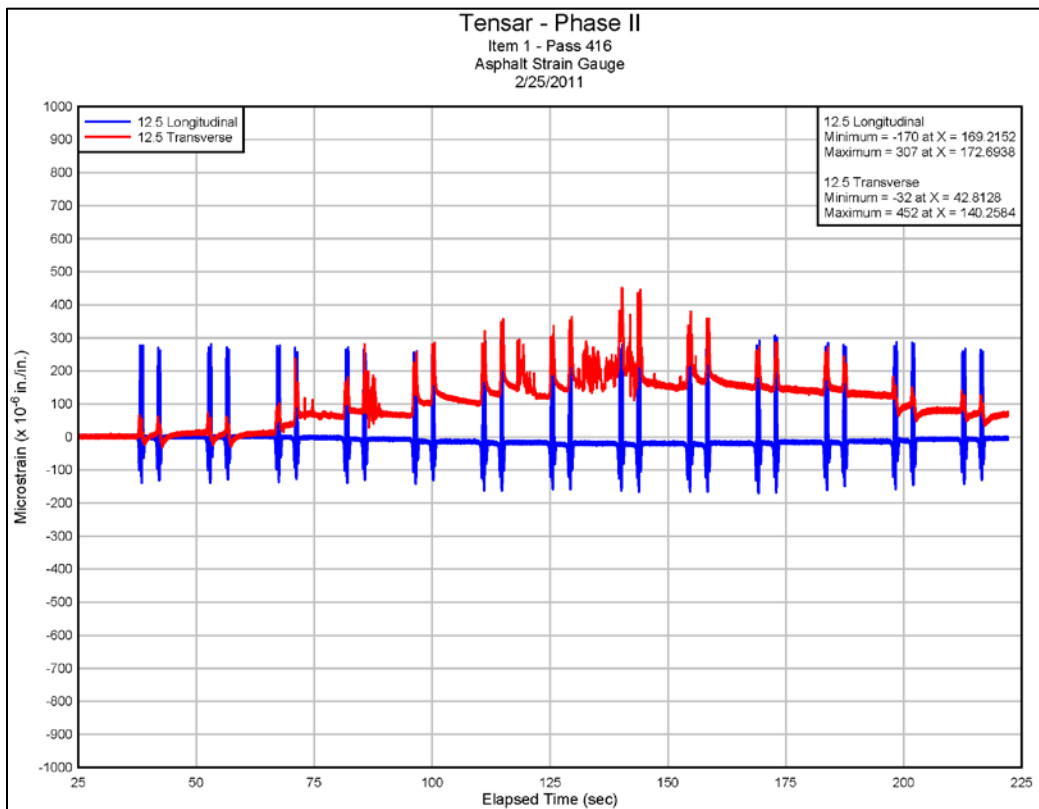
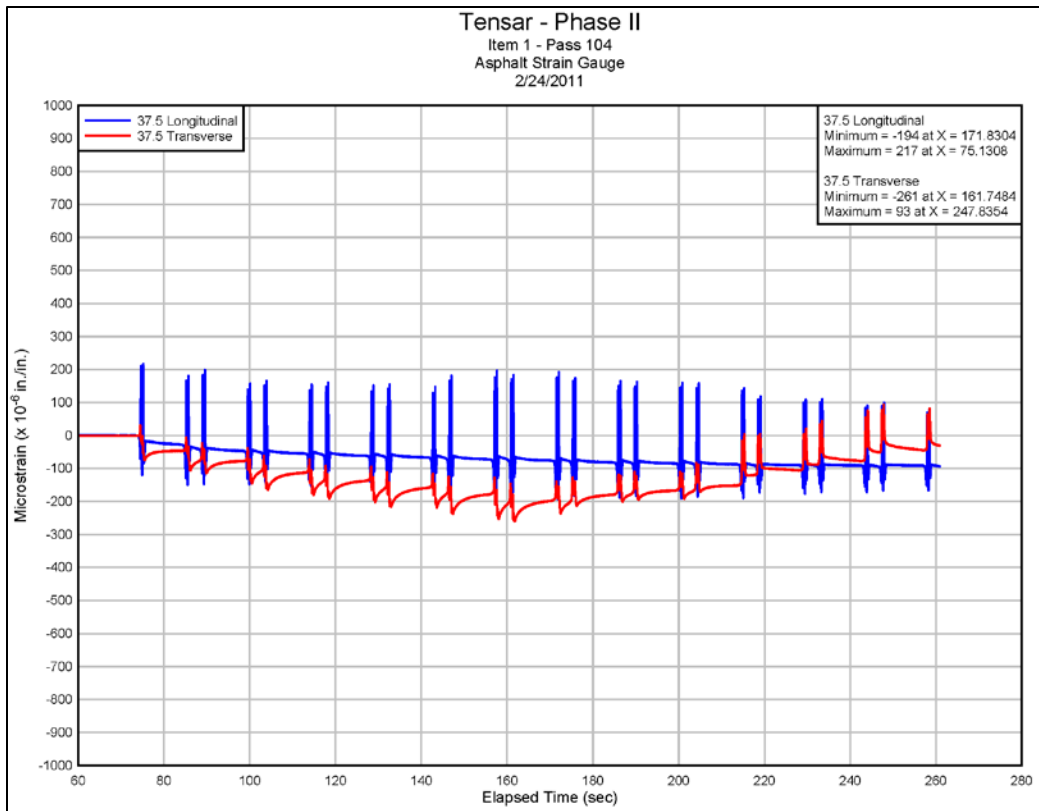
Appendix D: Asphalt Strain Response

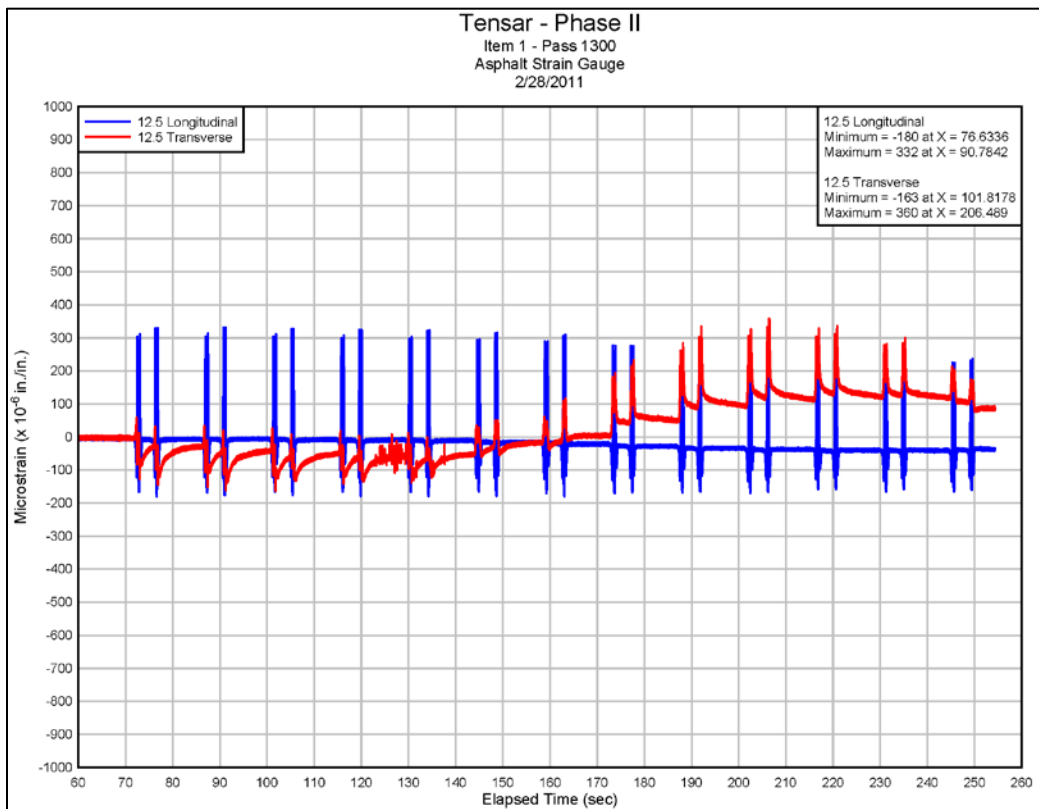
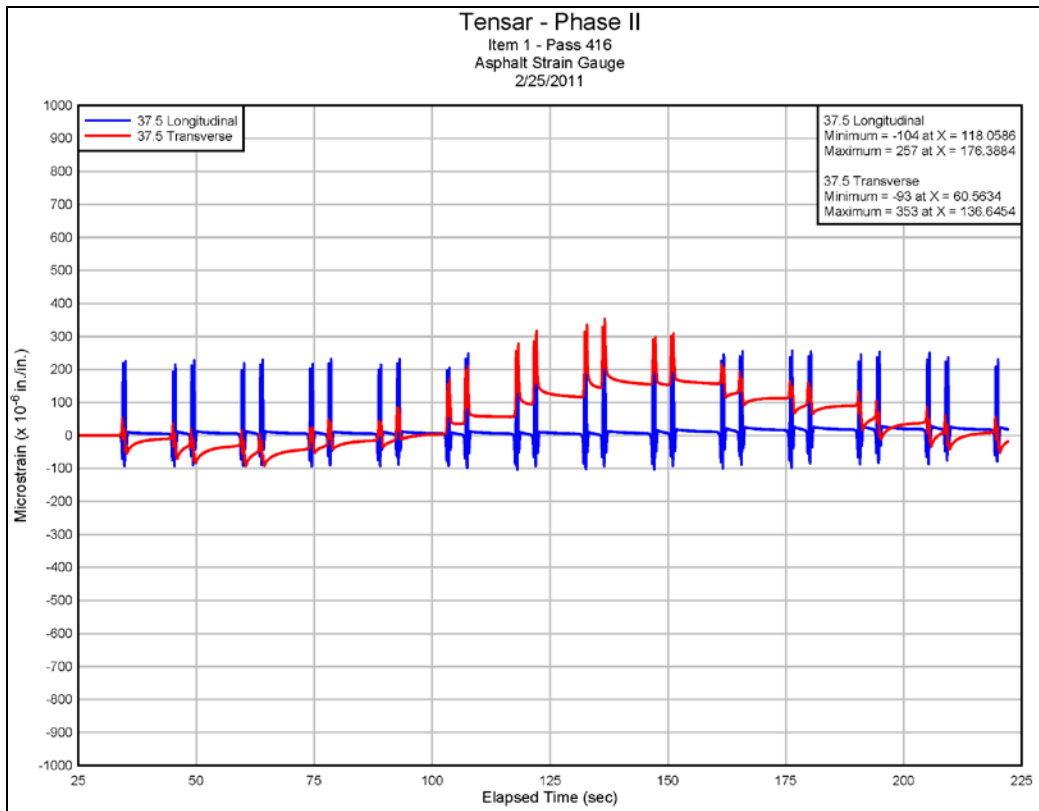


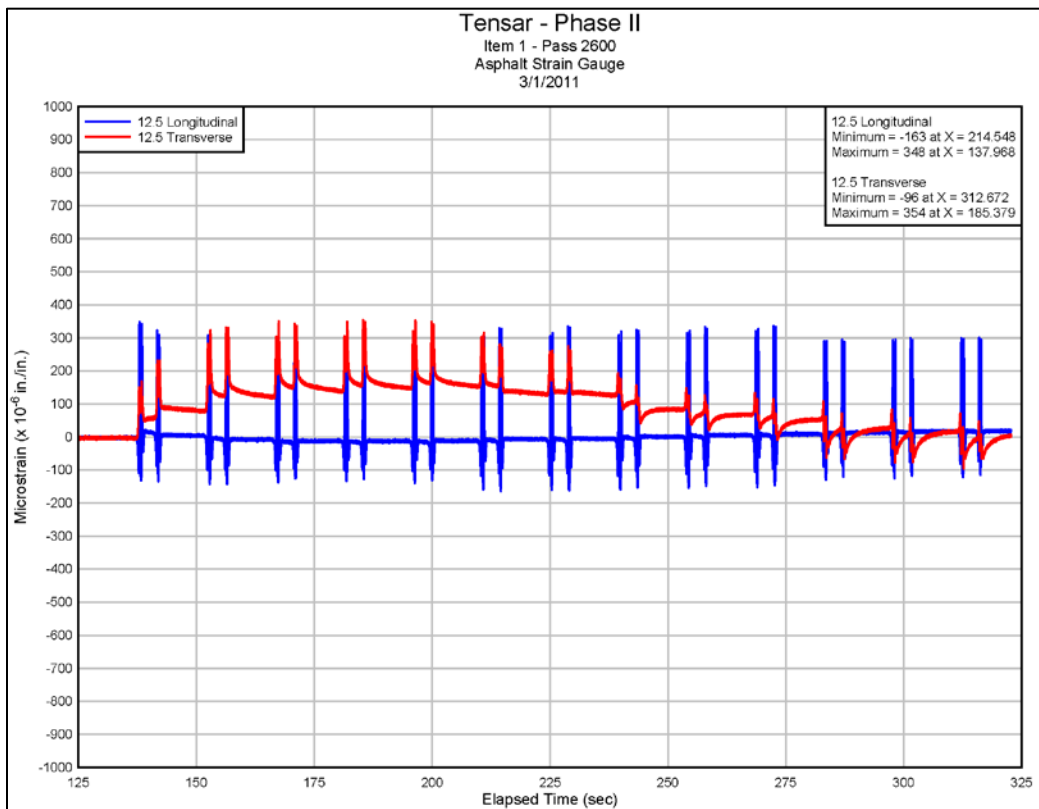
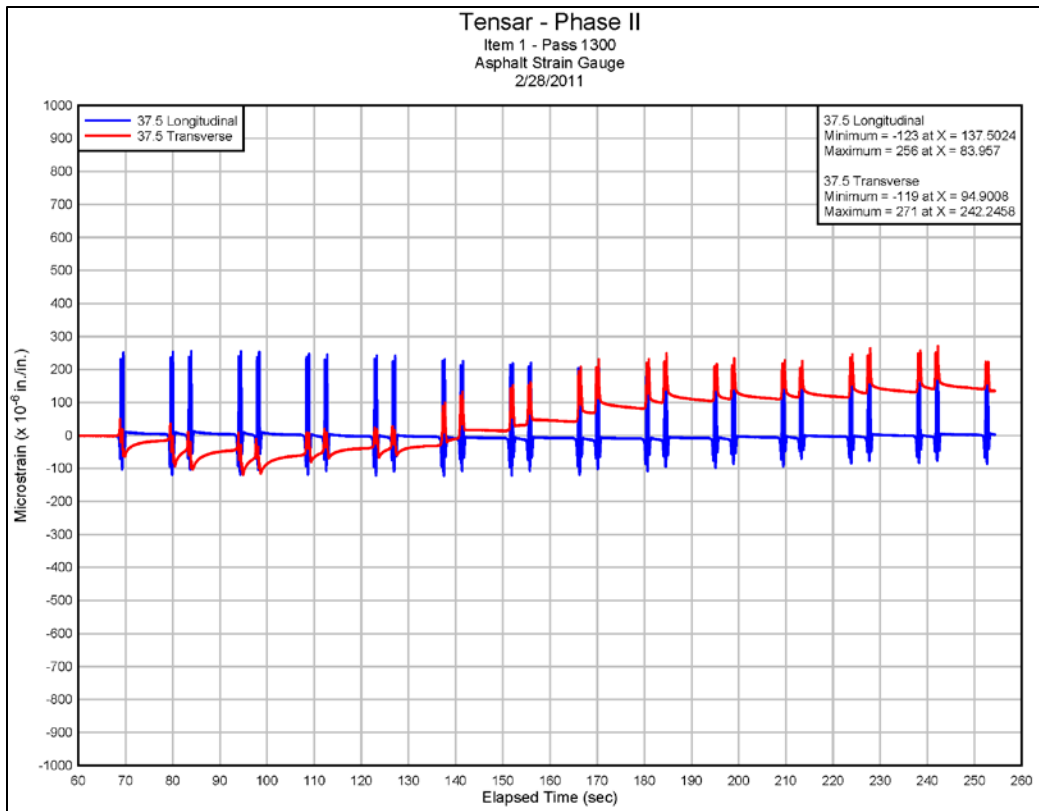


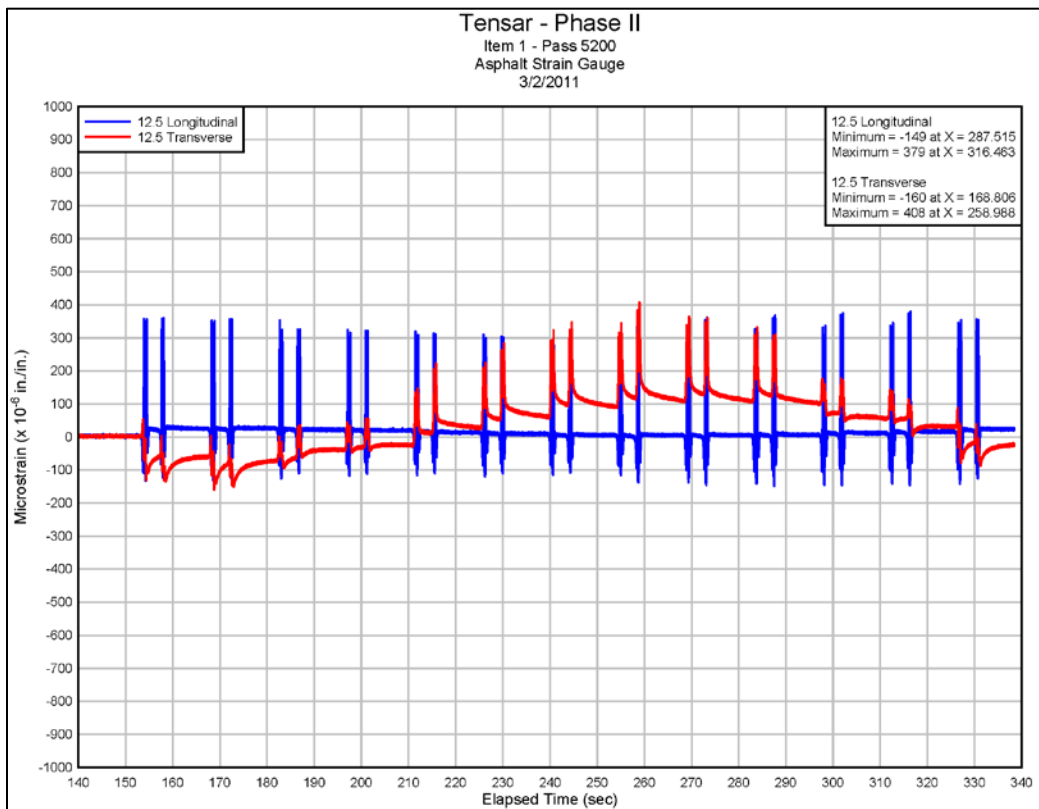
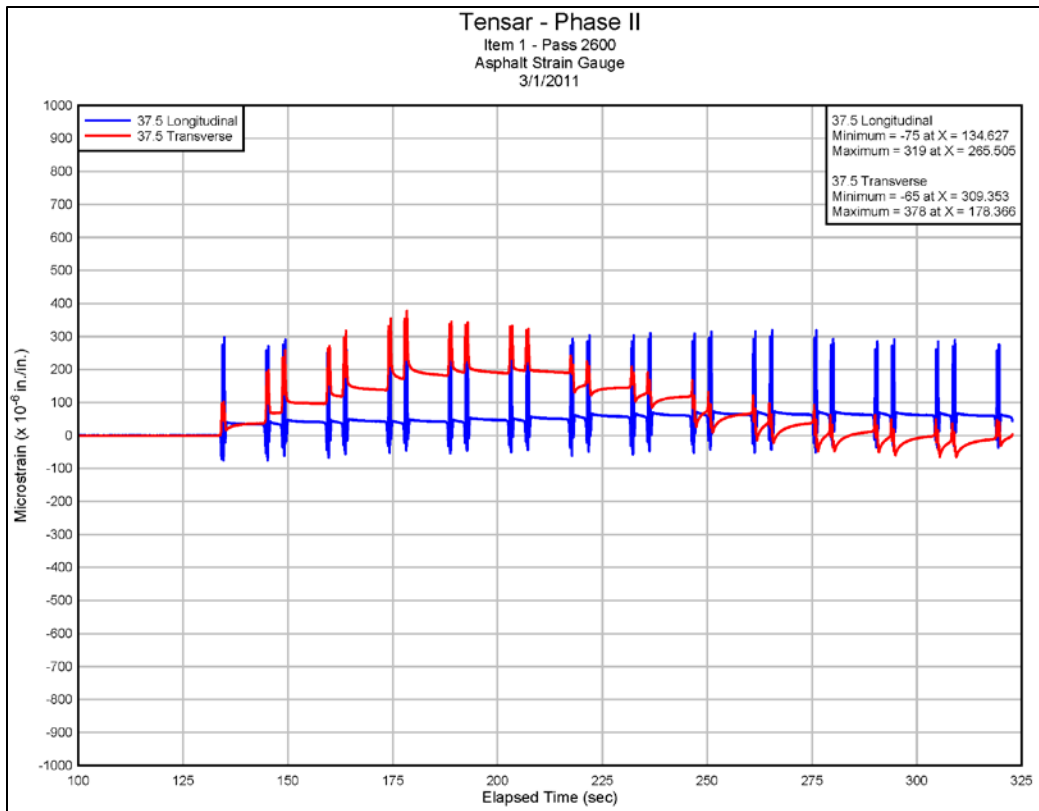


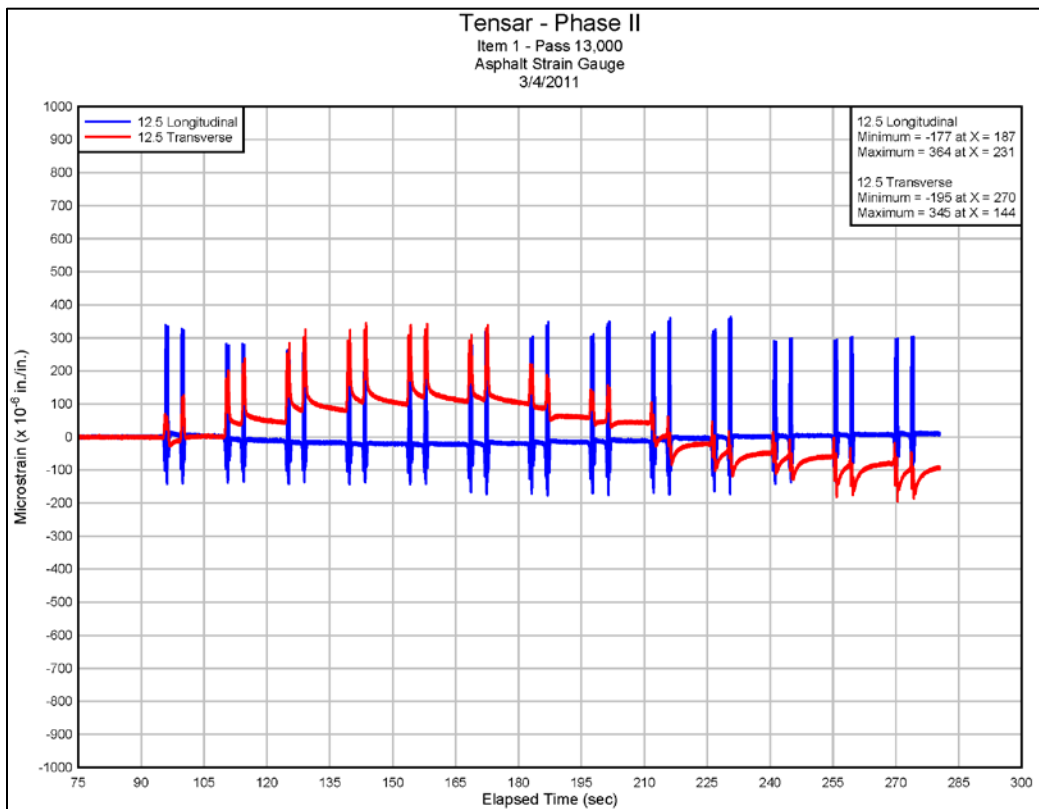
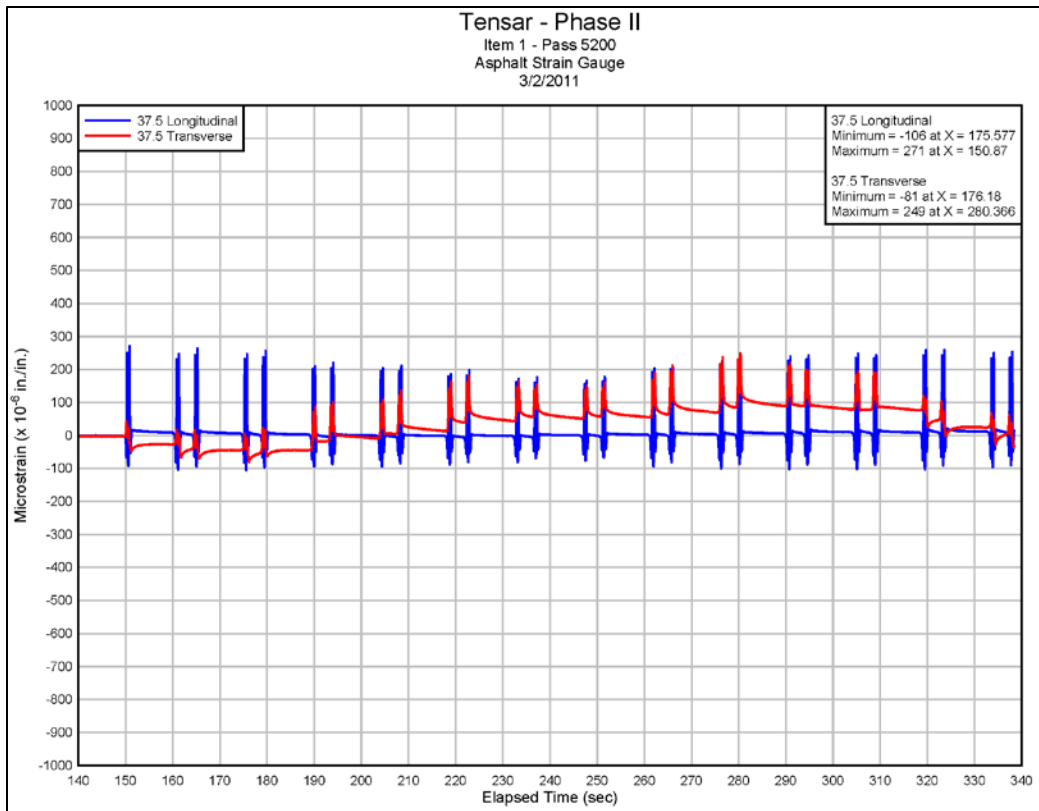


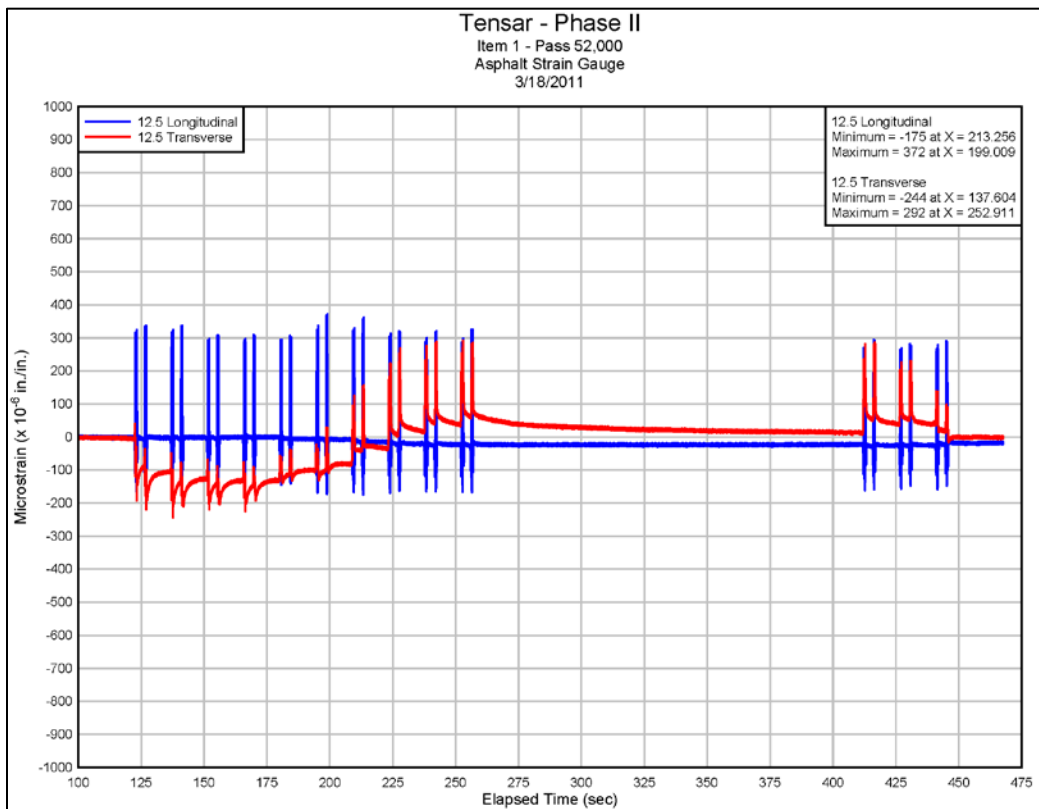
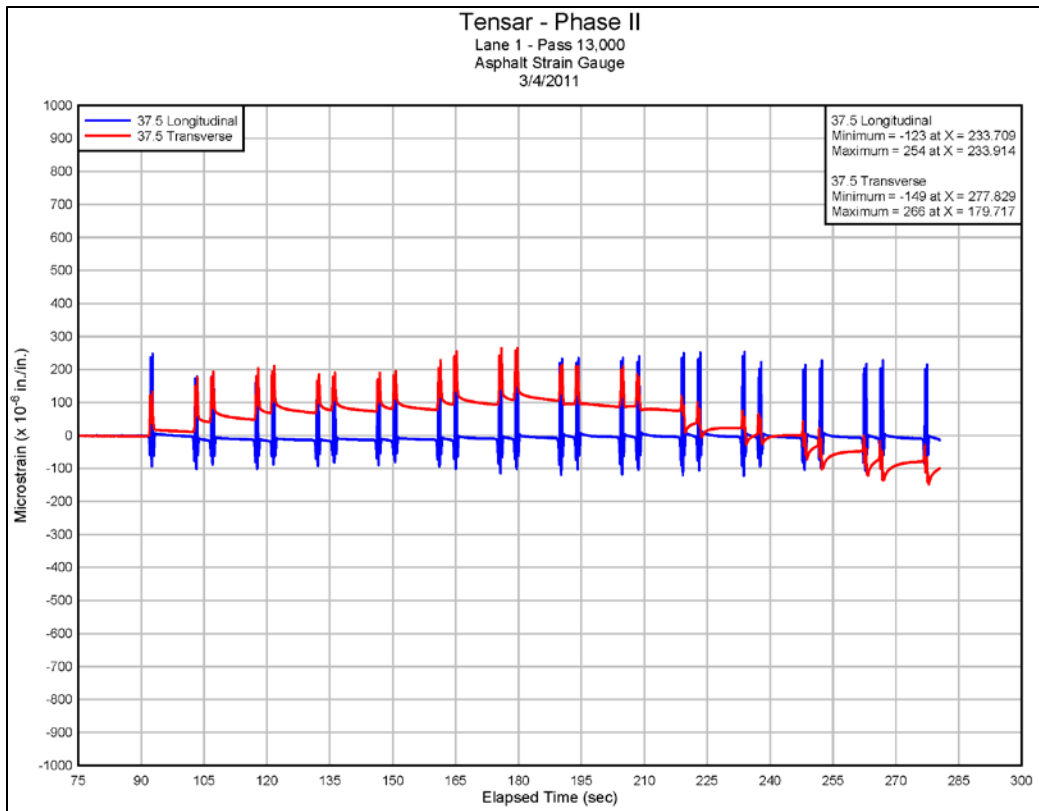


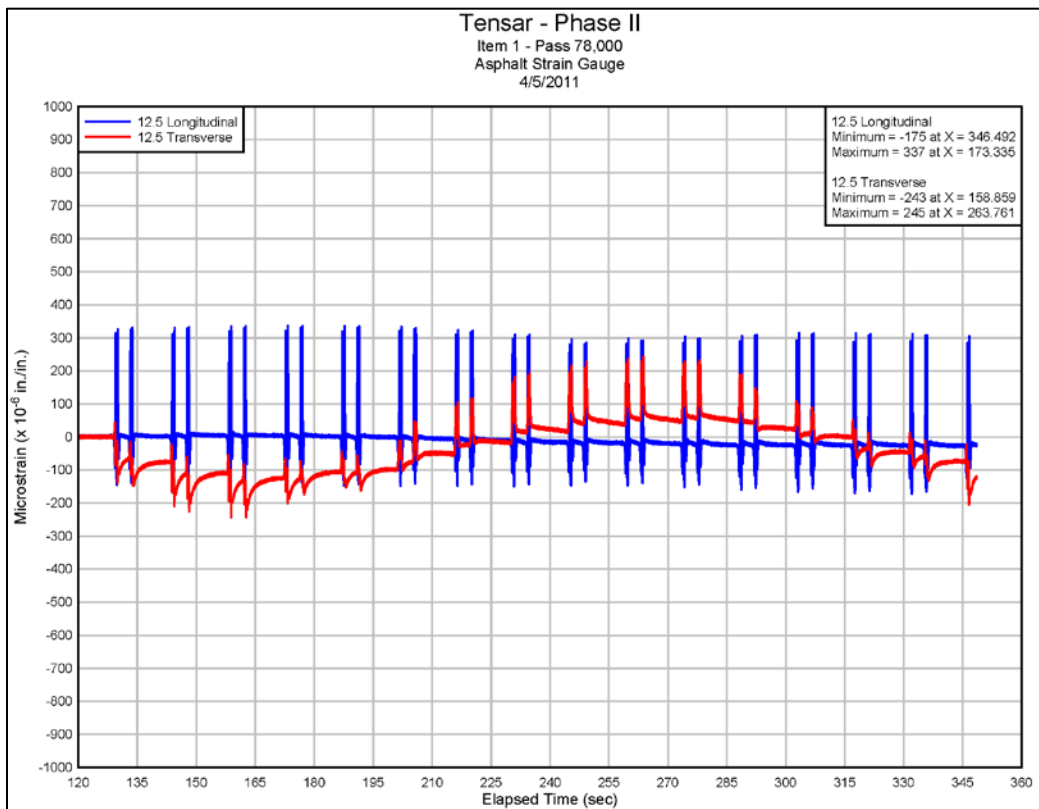
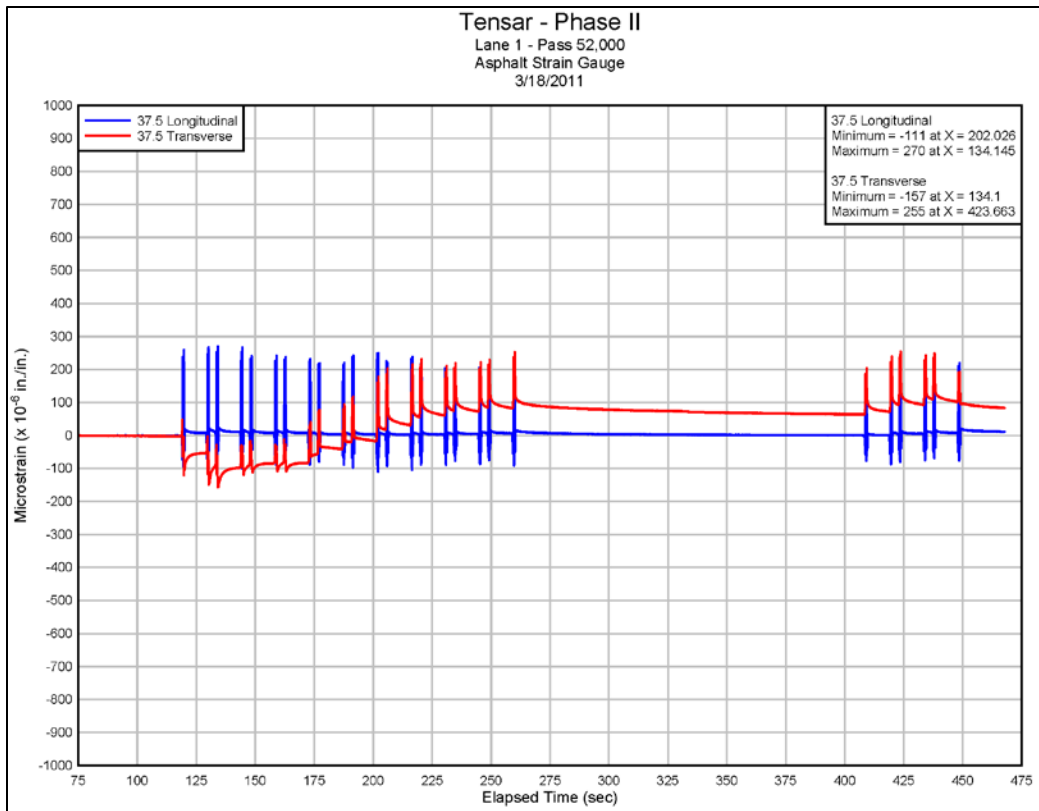


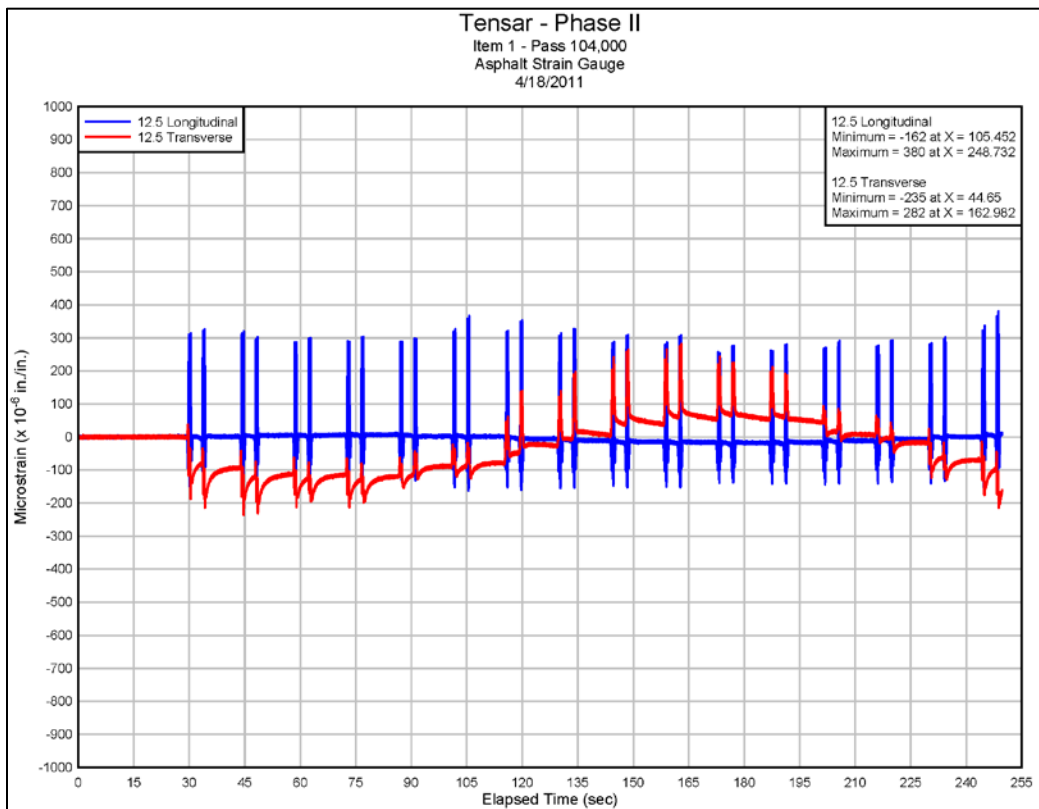
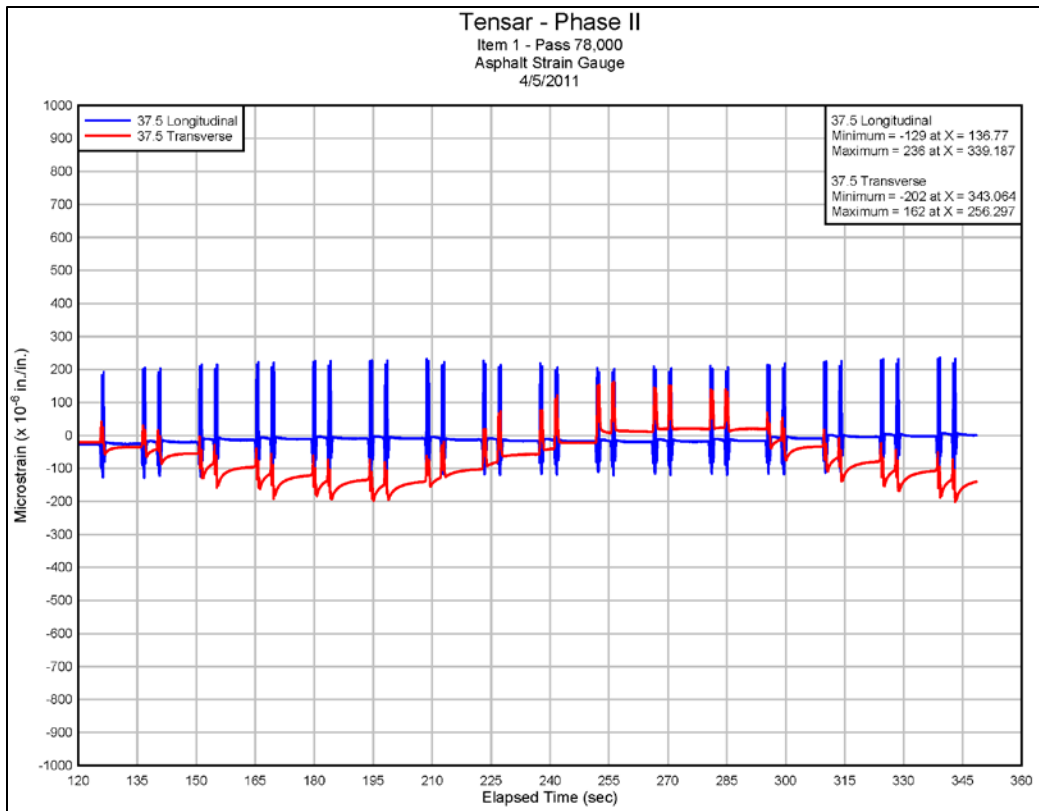


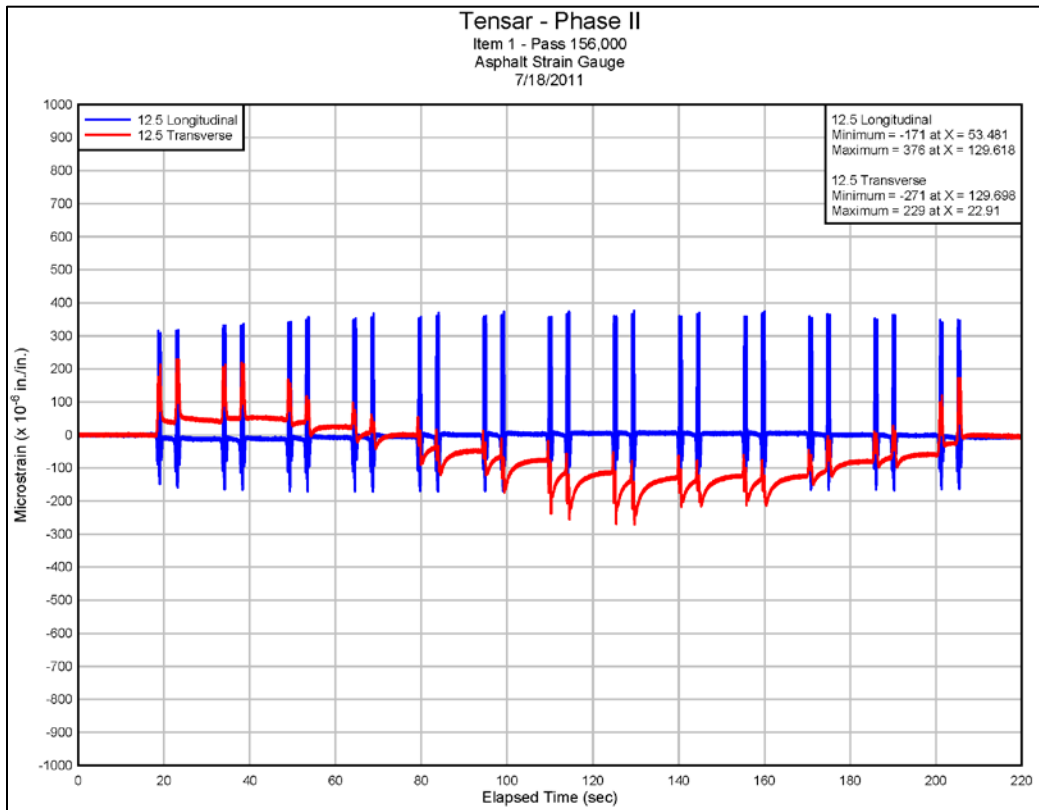
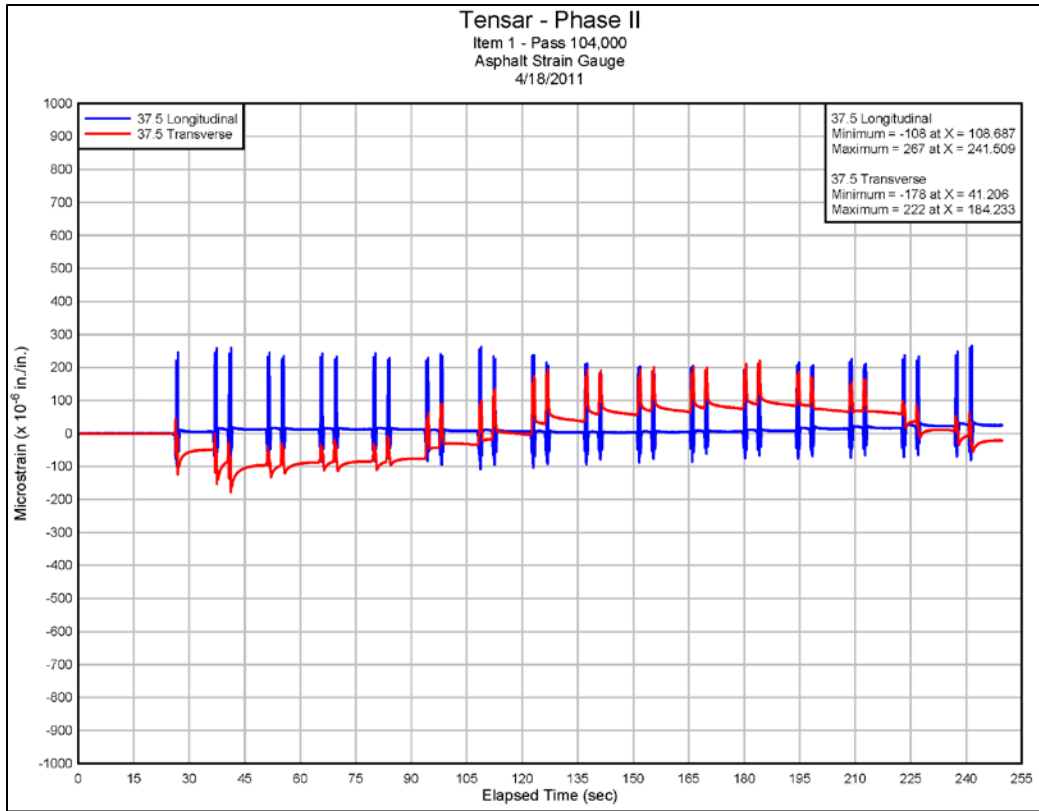


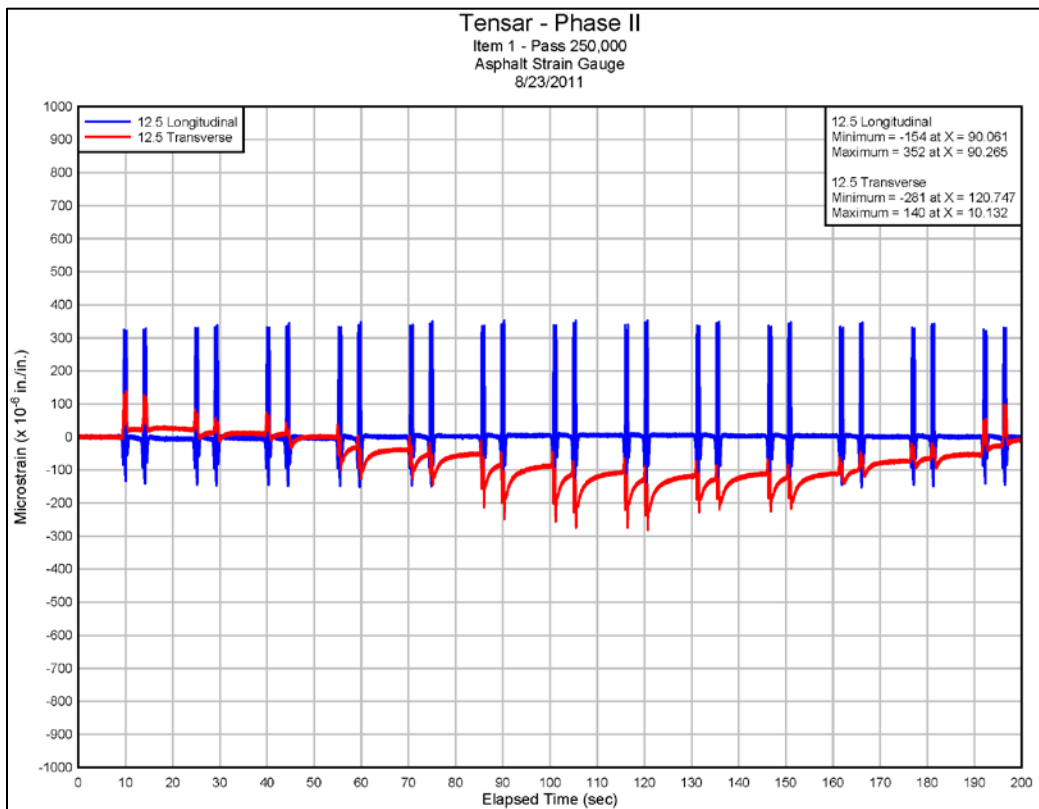
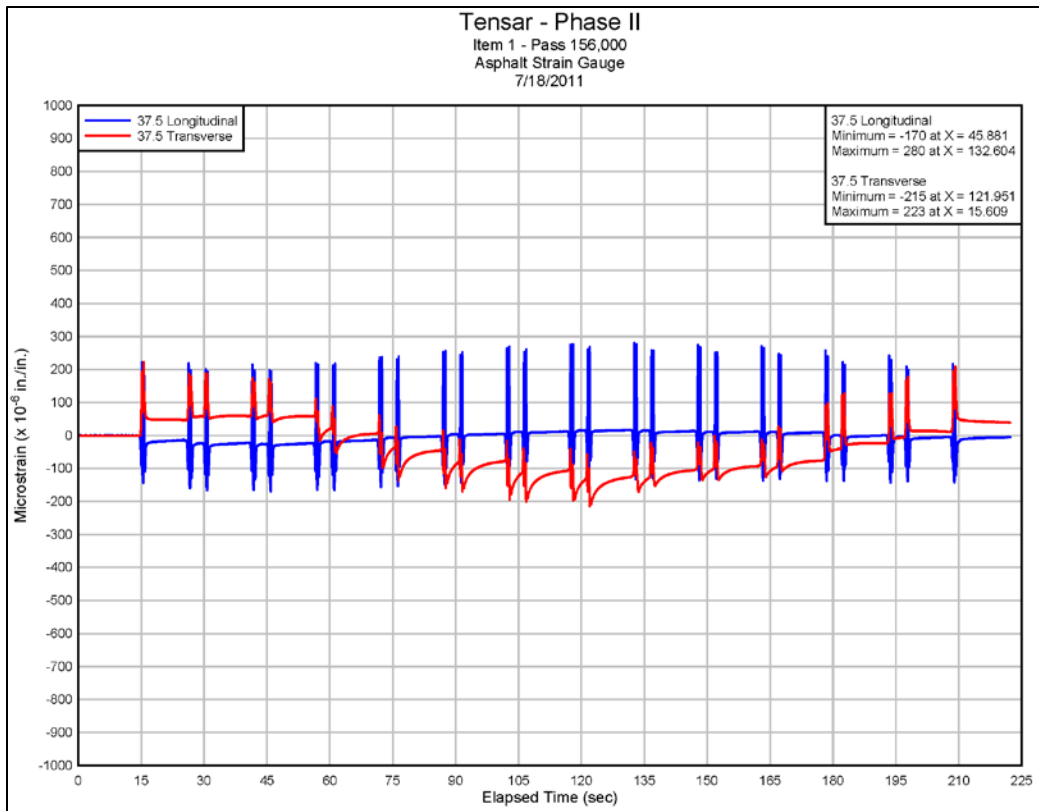


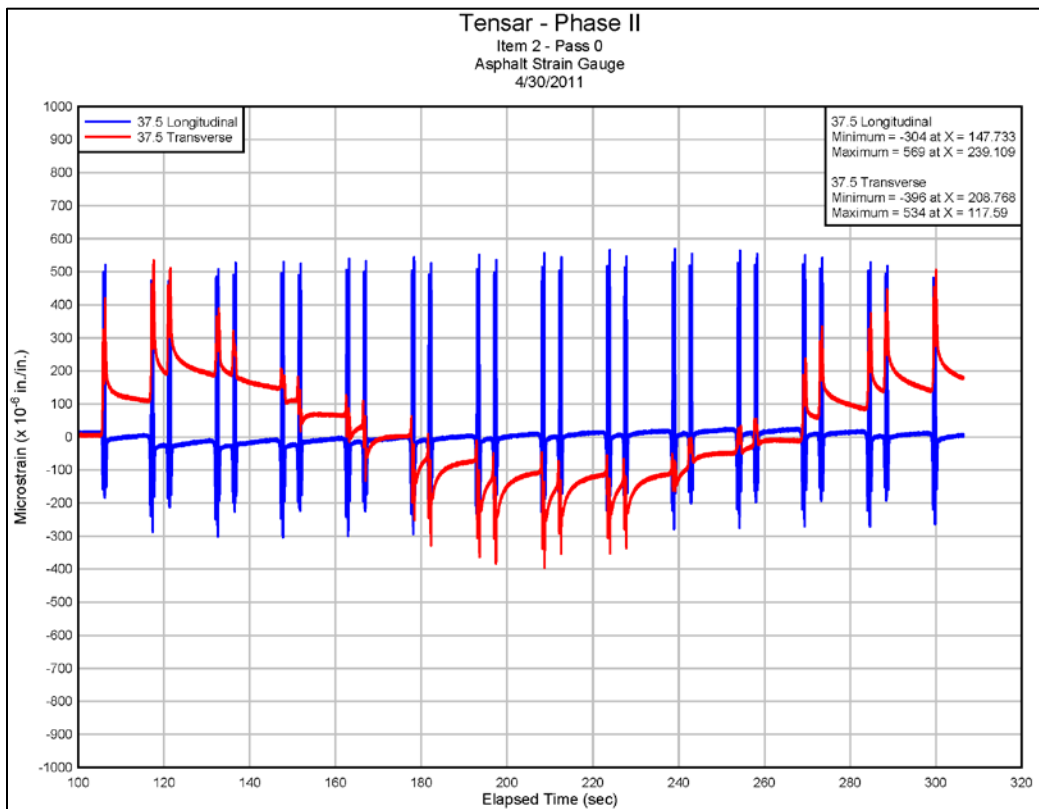
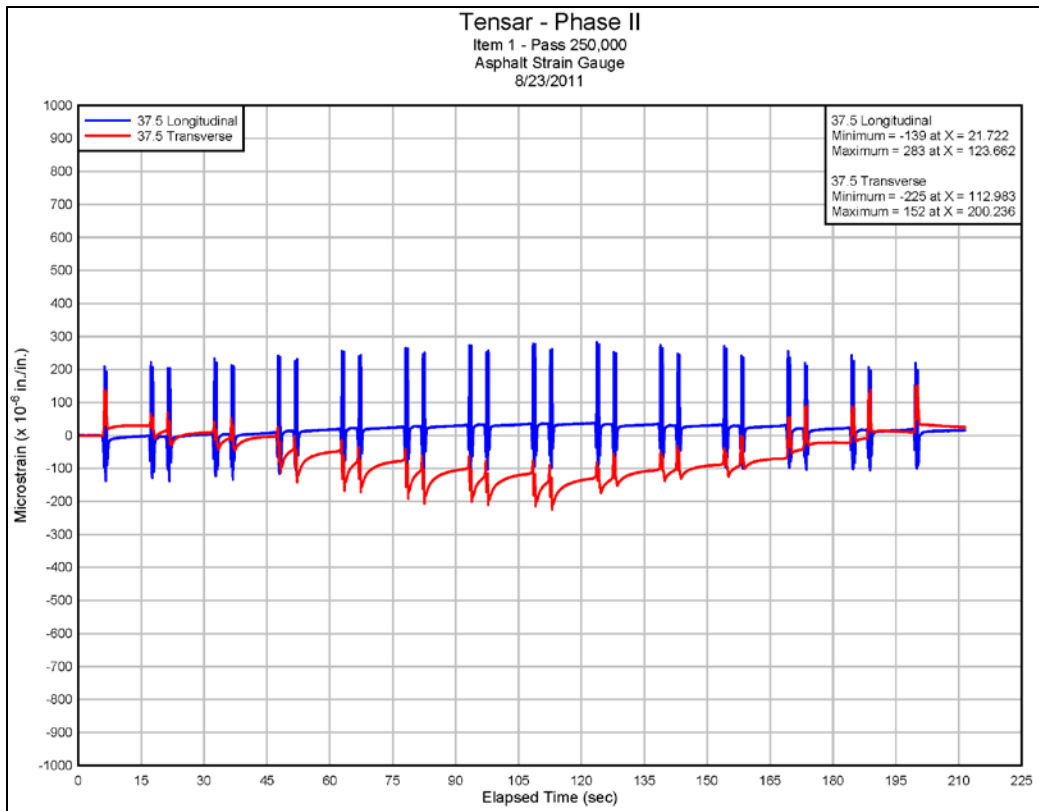


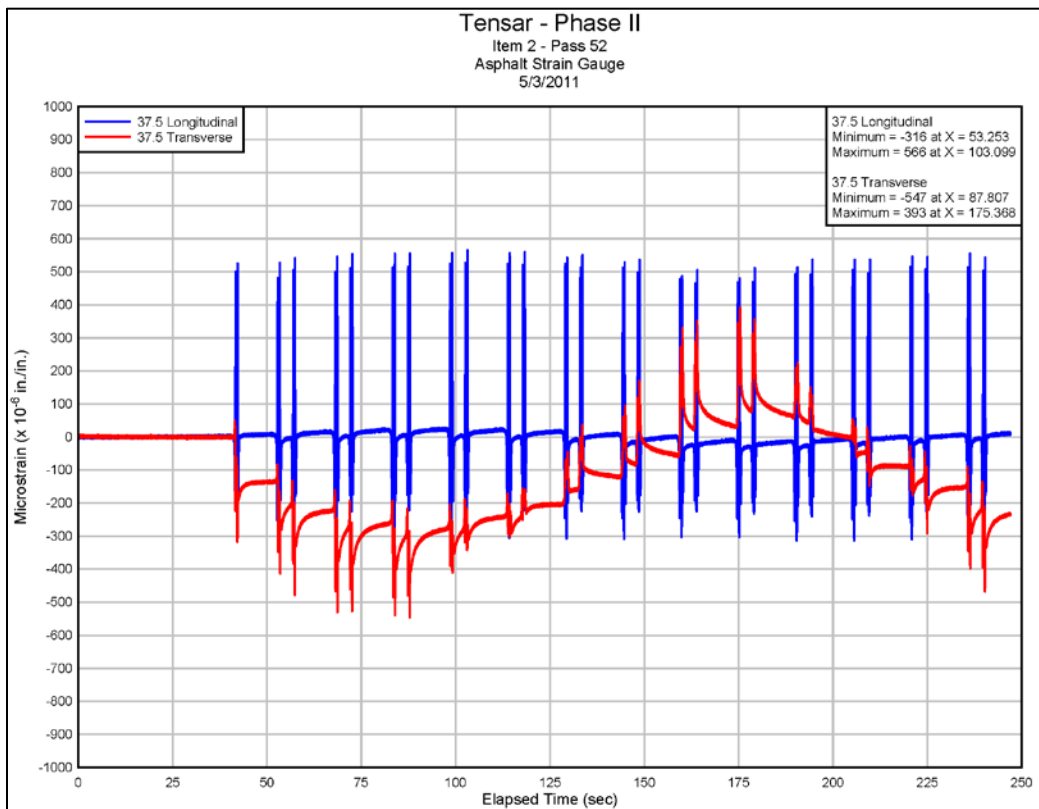
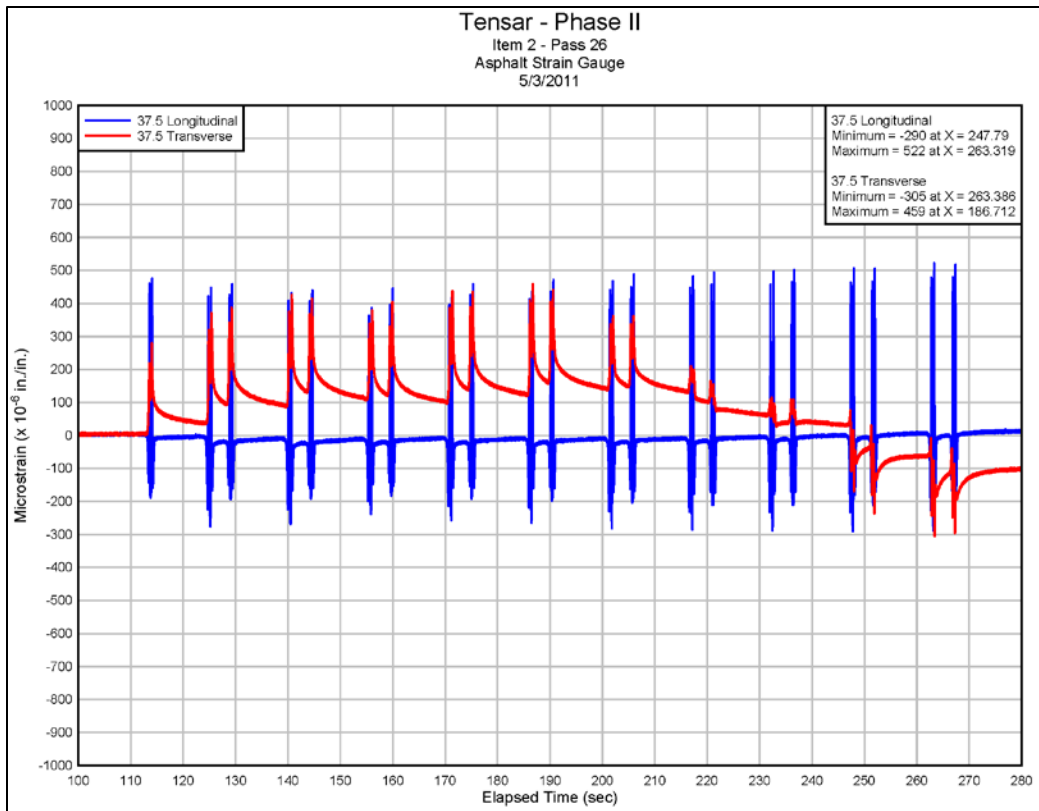


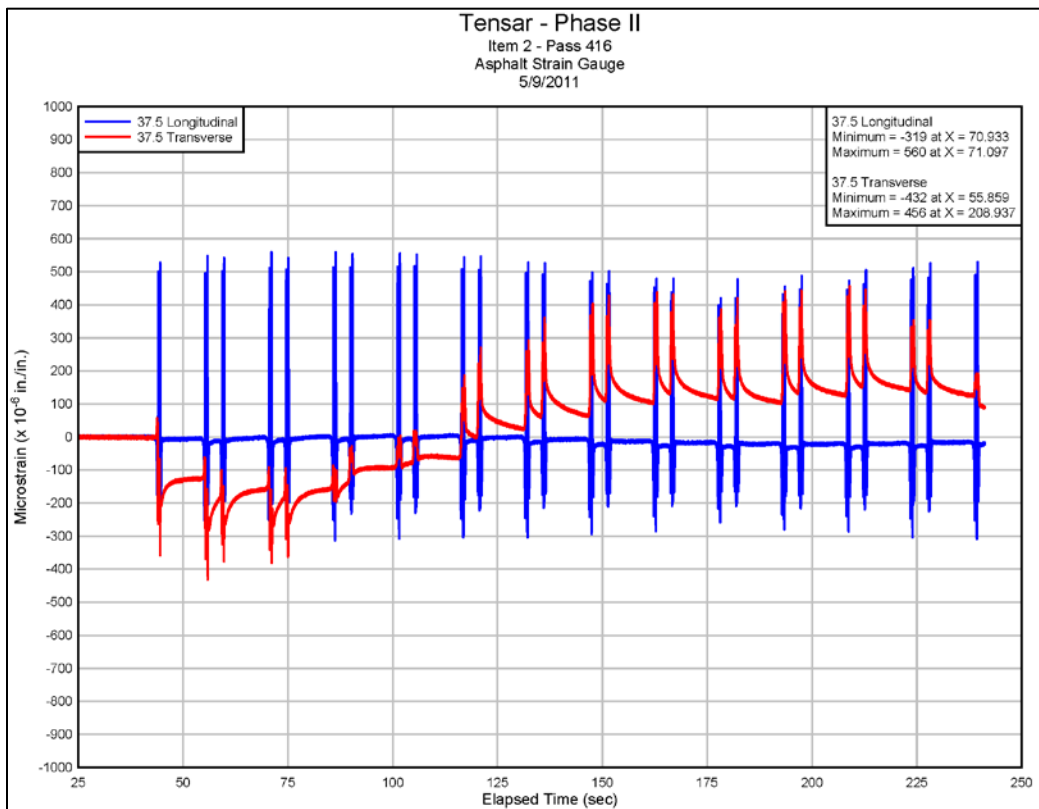
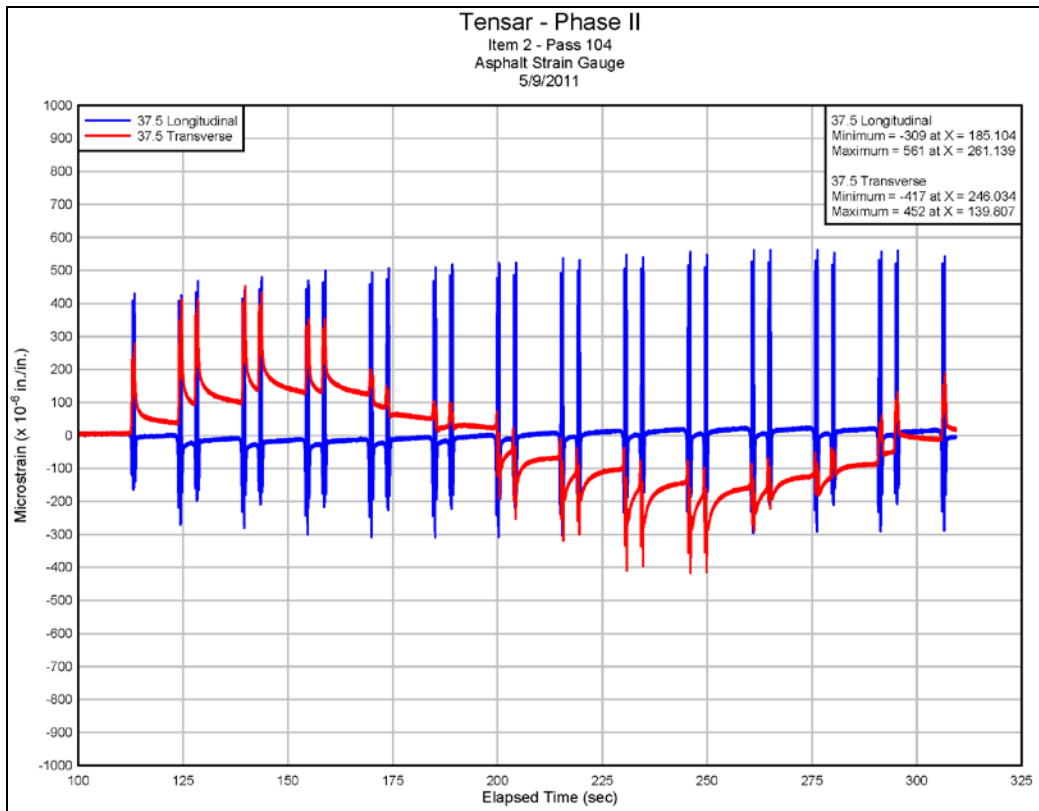


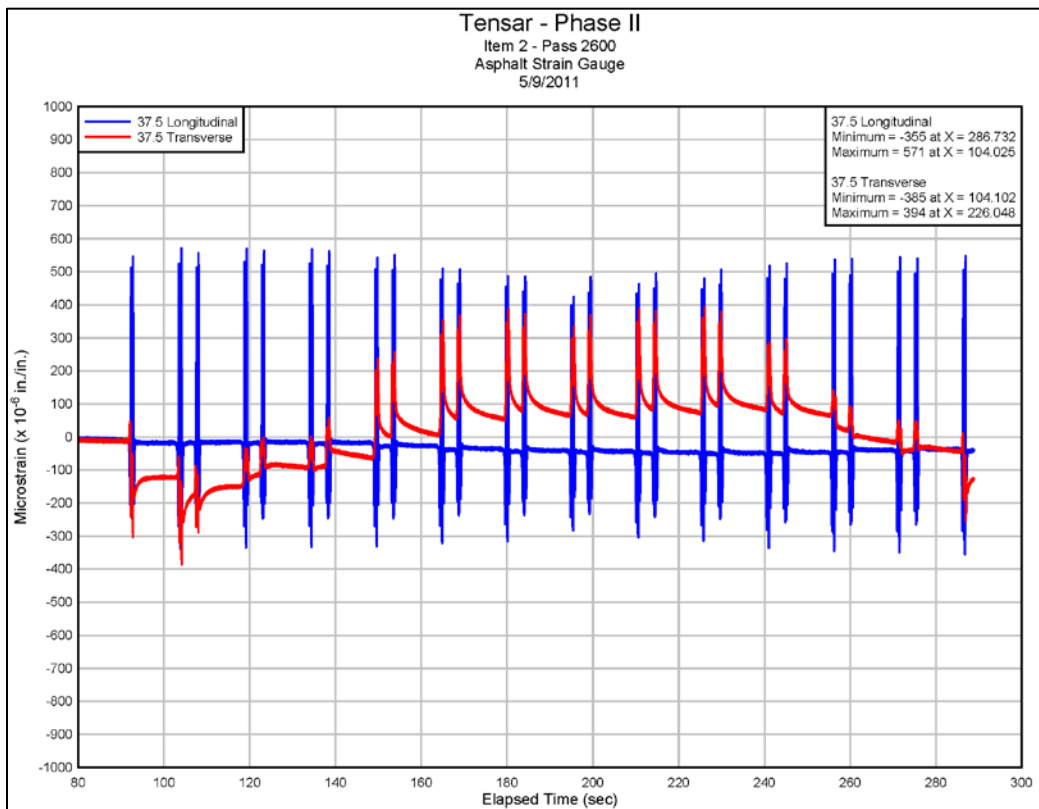
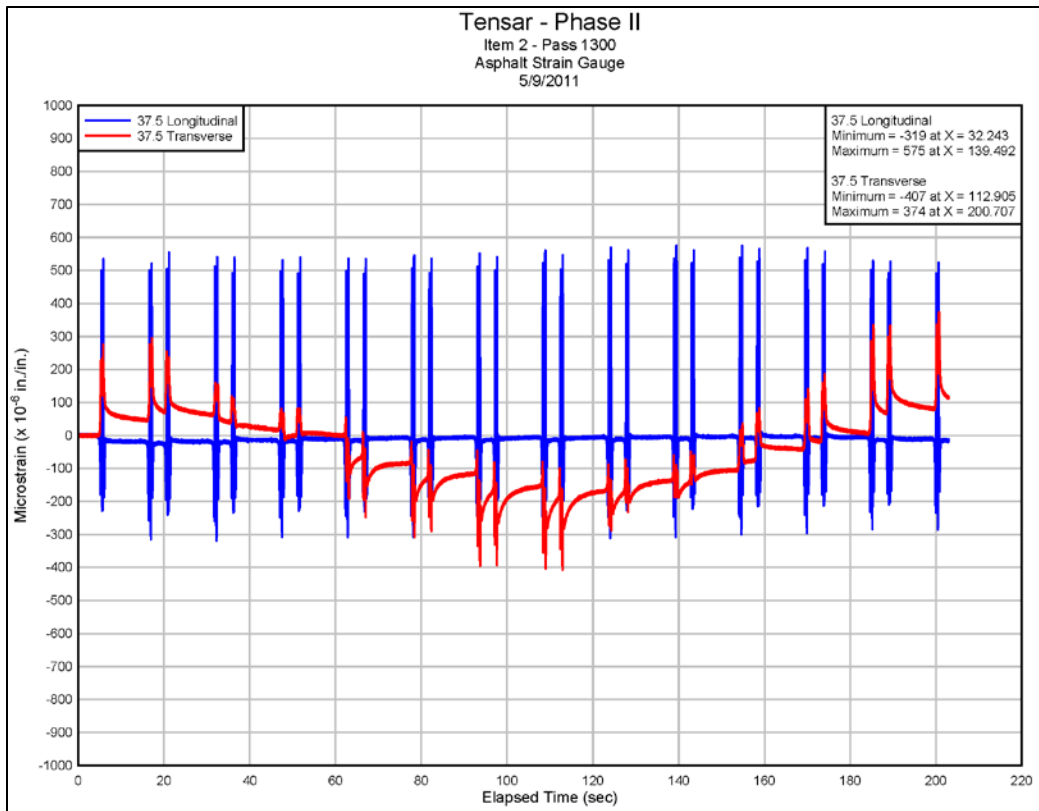


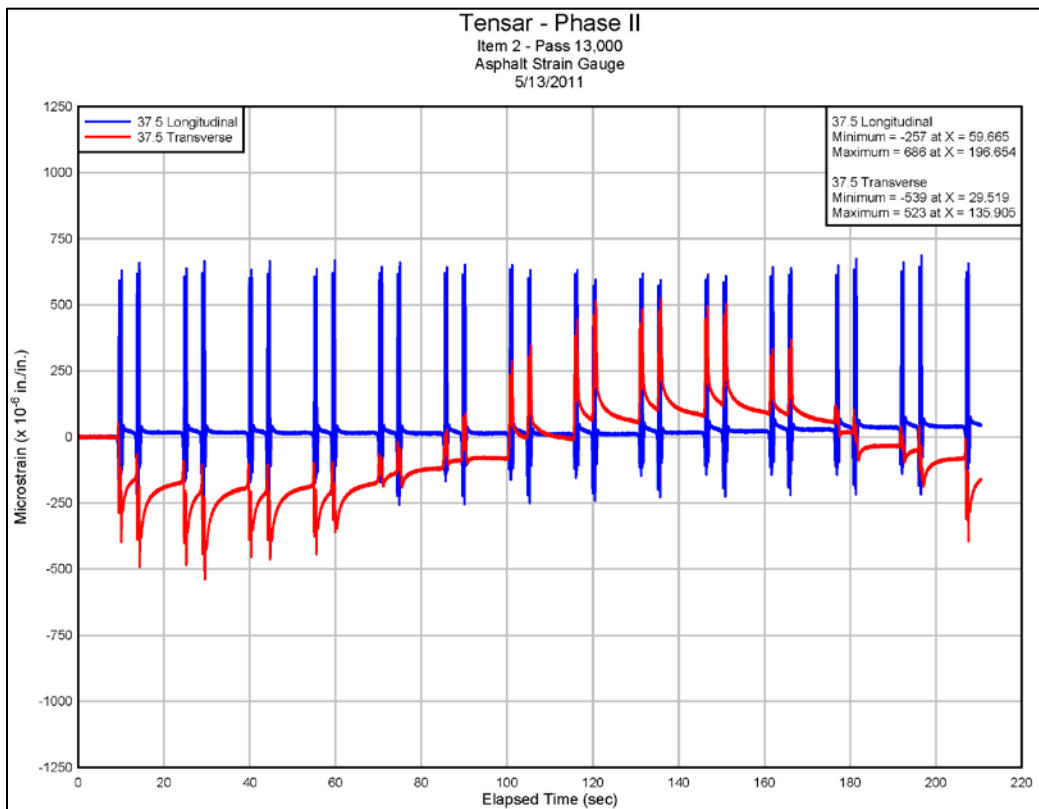
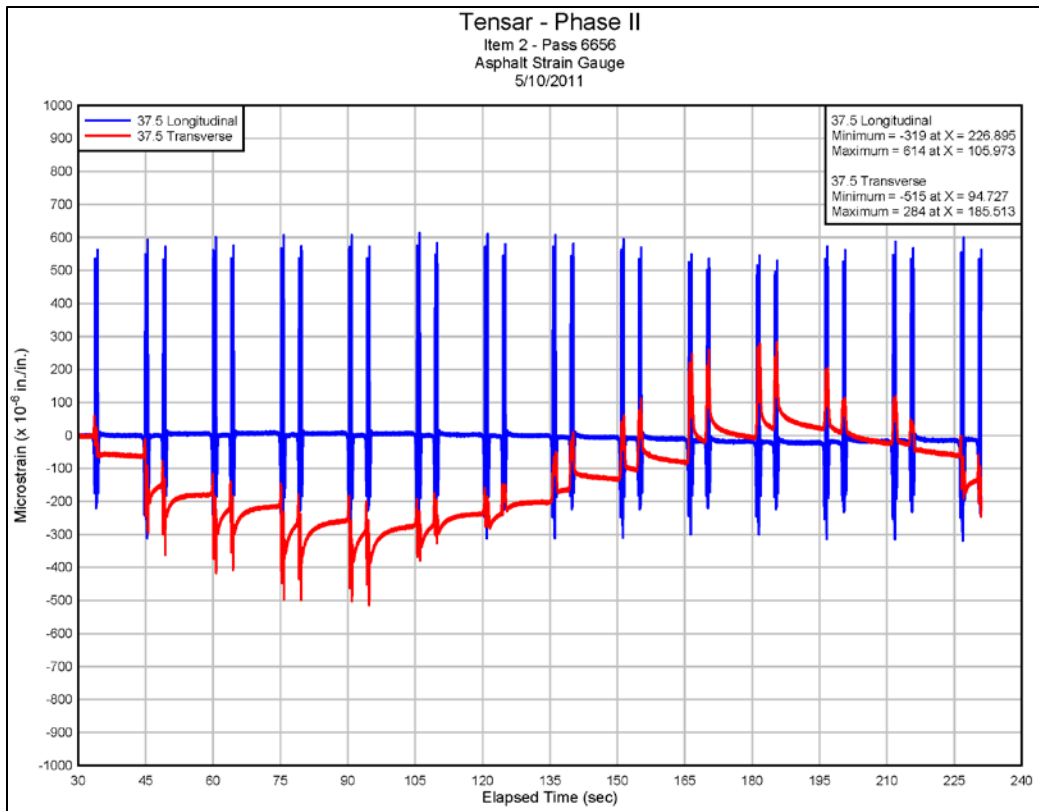


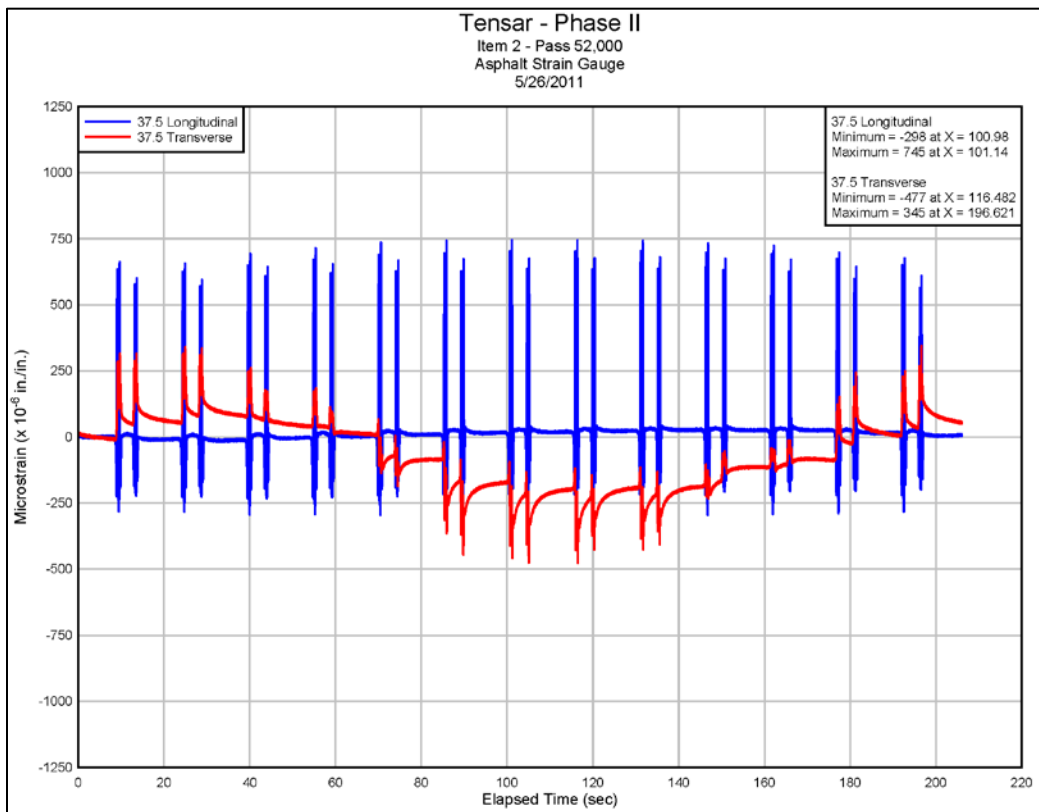
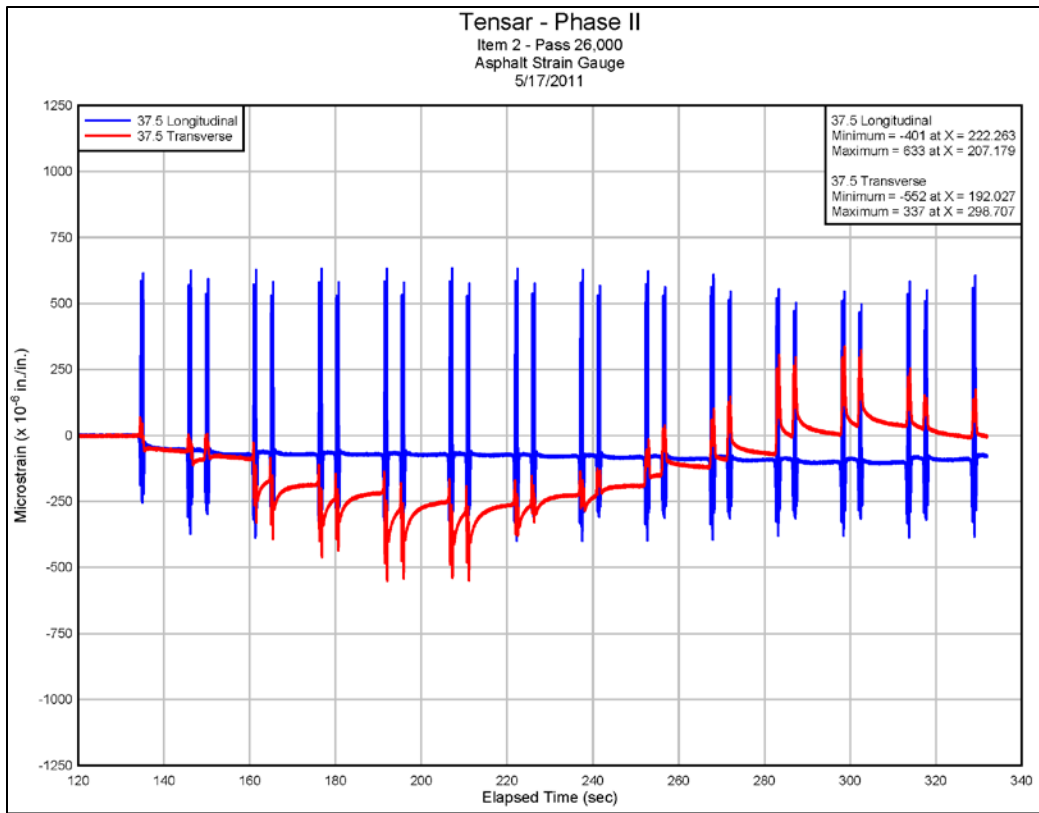


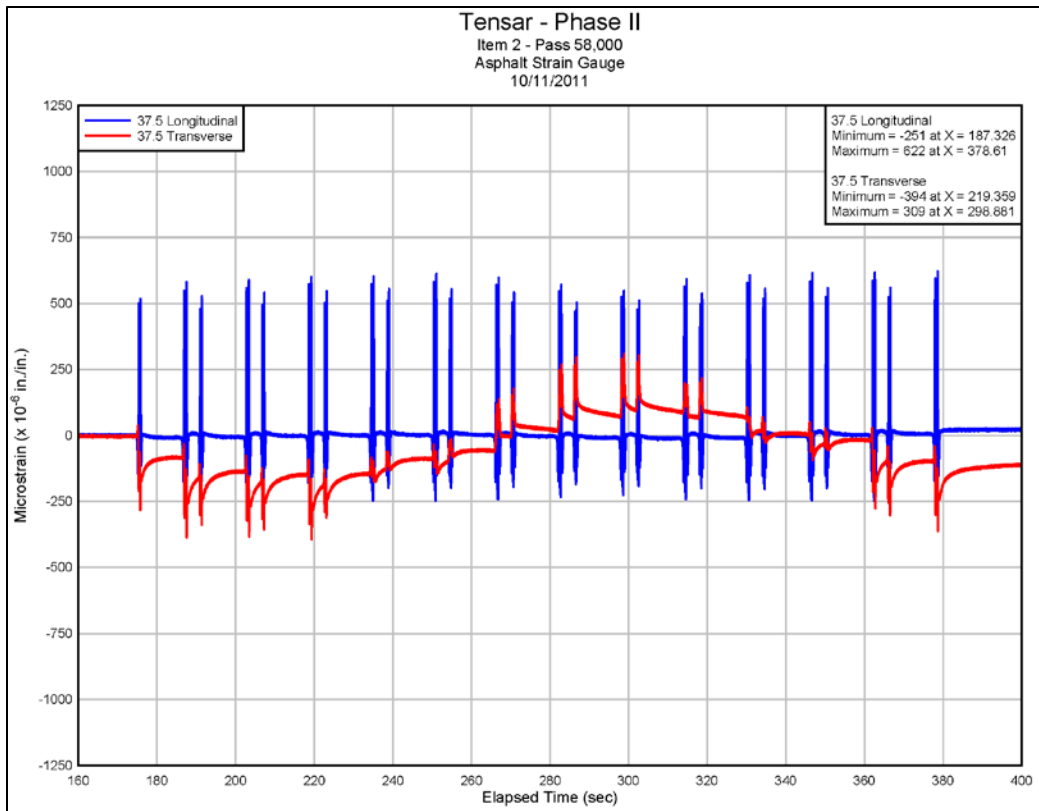












REPORT DOCUMENTATION PAGE

Form Approved
OMB No. 0704-0188

Public reporting burden for this collection of information is estimated to average 1 hour per response, including the time for reviewing instructions, searching existing data sources, gathering and maintaining the data needed, and completing and reviewing this collection of information. Send comments regarding this burden estimate or any other aspect of this collection of information, including suggestions for reducing this burden to Department of Defense, Washington Headquarters Services, Directorate for Information Operations and Reports (0704-0188), 1215 Jefferson Davis Highway, Suite 1204, Arlington, VA 22202-4302. Respondents should be aware that notwithstanding any other provision of law, no person shall be subject to any penalty for failing to comply with a collection of information if it does not display a currently valid OMB control number. **PLEASE DO NOT RETURN YOUR FORM TO THE ABOVE ADDRESS.**

1. REPORT DATE (DD-MM-YYYY) July 2014		2. REPORT TYPE Final		3. DATES COVERED (From - To)	
4. TITLE AND SUBTITLE Performance of Geogrid-Stabilized Flexible Pavements				5a. CONTRACT NUMBER	
				5b. GRANT NUMBER	
				5c. PROGRAM ELEMENT NUMBER	
6. AUTHOR(S) Gregory J. Norwood and Jeb S. Tingle				5d. PROJECT NUMBER	
				5e. TASK NUMBER	
				5f. WORK UNIT NUMBER	
7. PERFORMING ORGANIZATION NAME(S) AND ADDRESS(ES) Geotechnical and Structures Laboratory US Army Engineer Research and Development Center 3909 Halls Ferry Road Vicksburg, MS 39180-6199				8. PERFORMING ORGANIZATION REPORT NUMBER ERDC/GSL TR-14-28	
9. SPONSORING / MONITORING AGENCY NAME(S) AND ADDRESS(ES) Tensar International Corporation Alpharetta, GA 30009				10. SPONSOR/MONITOR'S ACRONYM(S)	
				11. SPONSOR/MONITOR'S REPORT NUMBER(S)	
12. DISTRIBUTION / AVAILABILITY STATEMENT Approved for public release; distribution is unlimited.					
13. SUPPLEMENTARY NOTES					
14. ABSTRACT The US Army Engineer Research and Development Center (ERDC) constructed a full-scale test section to evaluate the performance of geogrid-stabilized thin highway pavements. The test section included two representative highway pavements composed of hot-mix asphalt concrete (HMA) over a base course of crushed limestone and a 6 CBR clay subgrade. One highway lane was surfaced with 3-in. HMA and a 6-in. crushed limestone base course stabilized with geogrid. The second highway lane was surfaced with 4 in. of HMA and an unstabilized, 8-in. crushed limestone base course. Each test lane contained a suite of instrumentation consisting of strain gauges, earth pressure cells, moisture probes, pore water pressure transducers, and temperature probes. The geogrid was also instrumented with strain gauges in an attempt to determine the strain on the geogrid during testing. Each test lane was trafficked with simulated truck traffic to evaluate the rutting performance of the different pavement sections. This report summarizes the material characterization, pavement construction, instrumentation response, and performance response of the two test items.					
15. SUBJECT TERMS Geogrid Geosynthetic		Stabilized Base Course Flexible Pavement Accelerated Pavement Testing			
16. SECURITY CLASSIFICATION OF:			17. LIMITATION OF ABSTRACT	18. NUMBER OF PAGES	19a. NAME OF RESPONSIBLE PERSON Gregory Norwood
a. REPORT Unclassified	b. ABSTRACT Unclassified	c. THIS PAGE Unclassified			19b. TELEPHONE NUMBER (include area code) 601-634-3373